# STUDIES ON ARR GENE EXPRESSION

**Mary Gianniosis**

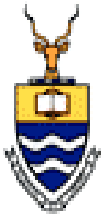

A dissertation submitted to the Faculty of Science, University of the Witwatersrand, Johannesburg, in fulfilment of the requirements for the degree of Master of Science.

Johannesburg, 2006

# ABSTRACT

Rifampicin is a major chemotherapeutic agent used against mycobacterial and nocardial infections. High level resistance is primarily due to mutational alterations in the *rpoB* gene encoding the β subunit of RNA polymerase. When challenged, these bacteria may inactivate rifampicin by one of four mechanisms: decomposition, ADP-ribosylation, glucosylation and phosphorylation. ADP-ribosylation occurs in many mycobacterial pathogens but nothing is known about the properties of the enzyme responsible. Consequently mutational analysis may be used to explore structure-function relationships in this protein.

Three mutants with changes in the open reading frame were selected and studied. The altered *arr* gene in pMG1 was obtained by *in vivo* selection whilst in pMG2 and pMG4 by *in vitro* mutagenesis. The mutated *arr* gene in pMG1 and pMG2 conferred resistance to 50 μg/ml of rifampicin while in pMG4 to 200 μg/ml. This suggested that alterations near the N-terminus resulted in lowered activity because of closer proximity to the active site. This is the first successful report of induced *arr* gene expression. This over-expression of the Arr ADP-ribosyltransferase and its mutants assisted in their later purification by metal affinity chromatography.

# DECLARATION

I declare that this dissertation is my own, unaided work. It is being submitted for the Degree of Master of Science in the University of the Witwatersrand, Johannesburg. It has not been submitted before for any degree or examination at any other university.

_____

Mary Gianniosis

_____ day of December, 2006

# DEDICATION

To my grandmother and parents: **Steliani Savvaides, Evangelos** and **Aikaterini Gianniosis**

# ACKNOWLEDGEMENTS

The following people were kind enough to lend their support, insight and inspiration to this project.

First and foremost I would like to express my sincere gratitude and appreciation to my supervisor, Prof. Eric Dabbs. He gave me encouragement, guidance and advice throughout my project. His contribution was invaluable and I thank him for sharing his knowledge and experience during this challenging process. I would also like to thank Dr Gianfranco Risuleo for his extreme kindness during my stay in his beautiful country. Furthermore, for all of the help you gave me regarding the biophysical measurements. I look forward to working with you in the near future.

A special thank you to my grandmother and parents who provided me with emotional support. Without them, this work might not have been completed. For their endless love, encouragement and belief in me but most of all for their moral and financial support that enabled me to get here. I can only hope that one day I will reciprocate all you have given me. Thank you for believing in me and always pushing me to do my best.

Further thanks to the "Denizens of GH700" (Ana, Youtaro, Melissa, Dorothy and Kobus) for making these two years memorable. I thank you all for your friendship, willingness to help and for making working here so much more interesting and entertaining. Further thanks to the support staff of MCB.

I also graciously acknowledge the University Postgraduate Merit Award and NRF, whose financial support made this work possible

# TABLE OF CONTENTS

ABSTRACT…… i
DECLARATION…… ii
DEDICATION…… iii
ACKNOWLEDGMENTS…… iv
TABLE OF CONTENTS…… v
LIST OF FIGURES…….. ix
LIST OF TABLES……... xiii
FREQUENTLY USED ABBREVIATIONS……... xv

**CHAPTER 1……1**

**Introduction**

1.1 Actinomycetes……..1
1.1.1 Classification……1
1.1.2 Pathogenicity……3
1.2 The ansamycins……5
1.2.1 Origins…….. 5
1.2.2 Rifamycins…… 6
1.3 Rifampicin……... 7
1.3.1 Mode of action…… 8
1.4 Antibiotic resistance mechanisms……11
1.5. Rifampicin resistance……..12
1.5.1.1 Rifampicin resistance through target modifications...12
1.5.1.2 Rifampicin resistance by reduced cell wall permeability……12
1.5.1.3 Rifampicin resistance through active efflux……...13
1.5.1.4 Rifampicin resistance by modification enzymes……13
1.6 ADP-ribosylation……15
1.6.1 Mono ADP-ribosylation……16
1.6.2 Arr ADP-ribosyltransferase……...17

**CHAPTER 2……18**

**Aims of the project**

2.1 Justification……..18
2.2 Aims of the study…… 18

**CHAPTER 3……19**

**Materials and Methods**

3.1 Bacterial strains and plasmids……..19
3.2 Media and growth conditions……...19
3.3 Determination of MIC…….....22
3.4 Cell differentiation by Gram staining…….. 22
3.5 DNA preparations…… 23
3.5.1 *E. coli* bulk plasmid preparation……... 23
3.5.2 *E. coli* mini plasmid preparation……...24
3.6 DNA manipulations and cloning techniques……... 25
3.6.1 DNA precipitation…….25
3.6.1.1 Salt and ethanol precipitation…….....25
3.6.1.2 Isopropanol DNA precipitation……..25
3.6.2 DNA preparation from CsCl density gradients…….....26
3.6.3 Phenol-chloroform extraction……... 26
3.6.4 Restriction enzyme digestion…… 27
3.6.5 Ligation of DNA……...27
3.6.6 Alkaline phosphatase treatment …….... 28
3.7. Gel electrophoresis……. 28
3.7.1 Agarose gel electrophoresis…….. 29
3.7.2 Low gelling agarose gel electrophoresis……...30
3.7.3 The freeze-squeeze method of extracting DNA from agarose gels……....30
3.8 Transformations……... 31
3.8.1 *E. coli* standard $CaCl_2$ transformation……...31
3.8.2 High efficiency transformation protocol……...31
3.9 Mutagenesis……..32
3.9.1 *In vivo* selection for spontaneous mutants…….32
3.9.2 Polymerase chain reaction (PCR)-mediated *in vitro* mutagenesis……33
3.10 Protein Analysis……34
3.10.1 Protein quantification……..34
3.10.2 Protein purification by metal affinity chromatography…… 34
3.10.2.1 Growth of expression cultures……..35
3.10.2.2 Protein purification under native conditions……...35
3.10.3 Sodium dodecyl sulphate-polyacrylamide gel electrophoresis (SDS-PAGE)…….36
3.10.3.1 Preparation of samples for SDS-PAGE…... 36
3.10.3.2 Preparation of gels for SDS-PAGE……. 37
3.10.3.3 Staining and de-staining of SDS-PAGE gels……..37
3.10.3.4 Viewing and photography of gels…… 38
3.11 Assay for enzymatic inactivation of rifampicin…….38

3.11.1 *In vitro* plate inactivation assay by employing the LDR method……..39
3.12 Automated DNA sequencing……40
3.12.1 Preparation of DNA for sequencing……... 40
3.12.2 Sequencing performed by Inqaba Biotechnology Industries (Pty) Ltd…… 41
3.12.3 Internet addresses for sequence analysis and database retrieval…….. 42

**CHAPTER 4…….43**

**Results**

4.1 Mutagenesis Approach A…….43
4.1.1 *In vivo* selection for spontaneous mutants…… 43
4.1.2 Identification of plasmid-borne mutants via marker rescue……. 46
4.1.3 Plasmid copy number determination…… 49
4.1.4 Restriction fragment exchange……. 57
4.2 Mutagenesis Approach B……60
4.2.1 PCR-mediated *in vitro* mutagenesis……..60
4.3 Sequence Analysis of ORF mutants…… 63
4.3.1 Nucleotide sequence analysis……63
4.3.2 Protein sequence analysis……..65
4.3.3 Analysis of protein parameters……..67
4.4 Phenotypic characterisation of ORF mutants……...72
4.4.1 Rifampicin phenotype of *E. coli* MM294-4 and DH5α cells transformed with ORF mutants……..... 72
4.4.2 Effect of temperature on rifampicin resistance……74
4.4.3 Effect of pH on rifampicin resistance……74
4.4.4 Effect of light on rifampicin resistance……77
4.4.5 *In vitro* enzymatic inactivation of rifampicin……85
4.5 Protein expression……87
4.5.1 Investigation of protein expression in pGEM-T-Easy-*Bst*49, pMG1, pMG2 and pMG4…….. 87
4.5.2 Cloning of the *arr* gene and its mutants into pET-28a(+)…….....90
4.5.3 Determination of protein toxicity……..91
4.5.4 Determination of protein solubility……...95
4.5.5 Determination of optimum expression conditions…… 102
4.5.6 Over-expression of the Arr enzyme and its mutants… 104
4.6 Change in *E. coli* cell morphology due to over-expression of the *arr* gene and its mutants…….....109
4.7 Protein purification…….. 113
4.7.1. Protein purification under native conditions……113

**CHAPTER 5…….123**

**Discussion**

5.1 Evaluation of mutagenesis approaches: *in vivo* selection versus PCR-mediated *in vitro* mutagenesis……...123
5.2 Mutational analysis of the Arr ADP-ribosyltransferase……...124
5.2.1 Structural analysis of the *arr* gene in pMG1a……...125
5.2.2 Structural analysis of the *arr* gene in pMG2a……...126
5.2.3 Structural analysis of the *arr* gene in pMG4a……...127
5.2.4 Implications of structural changes on Arr ADP-ribosyltransferase functioning……... 127
5.3 Arr ADP-ribosyltransferase's susceptibility to light……128
5.4 Change in *E. coli* cell morphology due to over-expression of the *arr* gene and its mutants…….....130
5.5. Over-expression, purification and biochemical characterisation of the Arr ADP-ribosyltransferase and its mutants……131

**CHAPTER 6…….133**

**Appendices**

6.1 Appendix A: Media……..133
6.2 Appendix B: Solutions……134
6.3 Appendix C: Antimicrobial agents…….. 141
6.4 Appendix D: Plasmids used in this work……142
6.5 Appendix E: Molecular weight markers…….. 147
6.5.1 DNA molecular weight markers……... 147
6.5.2 Protein molecular weight markers…… 149

**CHAPTER 7…….150**

**References**

# LIST OF FIGURES

**Figure 1**: Chemical structure of mycolic acid……...3

**Figure 2**: The chemical structure of rifampicin…….7

**Figure 3:** Mechanism of RNAP inhibition by rifampicin……10

**Figure 4:** Bacterial defence mechanisms comprising drug inactivation, target alteration, decreased permeability and active extrusion of the antibiotic from the cell…….....11

**Figure 5:** Chemical structure of ADP-ribosylated rifampicin……...16

**Figure 6:** Determination of plasmid copy number of mutants (1-9) obtained after 24 hrs from *in vivo* selection……..50

**Figure 7:** Determination of plasmid copy number of mutants (10-19) obtained after 24 hrs from *in vivo* selection……...51

**Figure 8:** Determination of plasmid copy number of mutants (1-9) obtained after 48 hrs from *in vivo* selection……52

**Figure 9:** Determination of plasmid copy number of mutants (10-18) obtained after 48 hrs from *in vivo* selection……53

**Figure 10:** MIC of (A) mutants (1-9) and (B) mutants (10-19) obtained after 24 hrs from *in vivo* selection in *E. coli* MM294-4 cells…….55

**Figure 11:** MIC of (A) mutants (1-9) and (B) mutants (10-18) obtained after 48 hrs from *in vivo* selection in *E. coli* MM294-4 cells…….56

**Figure 12**: Restriction fragment exchange between the wild type and mutant recombinant plasmids……..58

**Figure 13:** PCR amplification of the *arr* gene under (A) standard and (B) mutagenic conditions…… 61

**Figure 14:** Nucleotide alignment of the known *arr* gene sequence compared to its gene disrupted mutants using the BLASTN search programme……...64

**Figure 15:** Amino acid alignment of the known *arr* translated sequence compared to its gene disrupted mutants using the BLASTP search programme…….... 65

**Figure 16:** Hydropathic characteristics of pMG1……..68

**Figure 17:** Hydropathic characteristics of (A) pMG2 and (B) pMG4…….. 71

**Figure 18:** Rifampicin MIC of ORF mutants obtained from *in vivo* selection and *in vitro* mutagenesis in *E. coli* (A) MM294-4 and (B) DH5α cells……73

**Figure 19:** Rifampicin MIC of ORF mutants at varying temperatures of 25°C, 35°C and 45°C both in (A) the presence and (B) absence of IPTG in *E. coli* MM294-4 cells……75

**Figure 20:** Rifampicin MIC of ORF mutants at varying pH of 5.5, 7.0 & 8.5 both in (A) the presence and (B) absence of IPTG in *E. coli* MM294-4 cells……76

**Figure 21:** Rifampicin MIC of glycosyltransferase, Arr ADP-ribosyltransferase and its mutants in *E. coli* MM294-4 cells in (A) the dark and (B) in the presence of white light at 650 lx……79

**Figure 22:** Rifampicin MIC of glycosyltransferase, Arr ADP-ribosyltransferase & its mutants in *E. coli* MM294-4 cells in (A) blue & (B) red light at 650 lx…80

**Figure 23:** Arr protein expression after being grown in the presence and absence of light……81

**Figure 24:** Calibration curve for determining the molecular weight of the Arr ADP-ribosyltransferase, under varying light conditions……82

**Figure 25:** Glycosyltransferase protein expression after being grown in the presence and absence of light…….83

**Figure 26:** Calibration curve for determining the Mw of the glycosyltransferase that inactivates rifampicin, under varying light conditions……84

**Figure 27:** Initial induction study showing expression levels of the Arr protein, pMG1 and pMG2 both in the presence and absence of IPTG……88

**Figure 28:** Initial induction study showing expression levels of the Arr protein and pMG4, both in the presence and absence of IPTG……..89

**Figure 29:** Growth curve of (A) untransformed *E. coli* Rosetta2(DE3)pLysS cells and (B) *E. coli* Rosetta2(DE3)pLysS cells transformed with pET-28a(+) in LB medium in the presence and absence of IPTG……...92

**Figure 30:** Growth curve of *E. coli* Rosetta2(DE3)pLysS cells transformed with (A) pET28a-*Bst*49 and (B) pMG1a in LB medium in the presence and absence of IPTG……93

**Figure 31:** Growth curve of *E. coli* Rosetta2(DE3)pLysS cells transformed with (A) pMG2a and (B) pMG4a in LB medium in the presence and absence of IPTG……...94

**Figure 32:** Arr solubility determination illustrating the insoluble fraction under varying IPTG concentrations……..96

**Figure 33:** Arr solubility determination illustrating the soluble fraction under varying IPTG concentrations……97

**Figure 34:** Calibration curve for determining the molecular weight of the Arr ADP-ribosyltransferase, under varying IPTG concentrations……98

**Figure 35:** Arr solubility determination illustrating the insoluble fraction under varying induction time……99

**Figure 36:** Arr solubility determination illustrating the soluble fraction under varying induction time……... 100

**Figure 37:** Calibration curve for determining the molecular weight of the Arr ADP-ribosyltransferase, under varying induction time……..101

**Figure 38:** Over-expression of pET28a-*Bst*49, pMG1a and pMG2a…….105

**Figure 39:** Calibration curve for determining the molecular weight of pET28a-*Bst*49, pMG1a and pMG2a…… 106

**Figure 40:** Over-expression of pET28a-*Bst*49 and pMG4a…….. 107

**Figure 41:** Calibration curve for determining the molecular weight of pET28a-*Bst*49 and pMG4a…….. 108

**Figure 42:** Light microscopy of untransformed *E. coli* MM294-4 cells cultured in LB observed under oil immersion (x100)……..110

**Figure 43:** Light microscopy of *E. coli* MM294-4 cells transformed with the vector only cultured in LB observed under oil immersion (x100)…….110

**Figure 44:** Light microscopy of *E. coli* MM294-4 cells transformed with constructs containing the unmutagenised *arr* gene cultured in LB observed under oil immersion (x100)……..111

**Figure 45:** Light microscopy of *E. coli* MM294-4 cells transformed with pMG4a cultured in LB observed under oil immersion (x100)……111

**Figure 46:** Light microscopy of *E. coli* MM294-4 cells transformed with pMG1a cultured in LB observed under oil immersion (x100)……112

**Figure 47:** Light microscopy of *E. coli* MM294-4 cells transformed with pMG2a cultured in LB observed under oil immersion (x100)……112

**Figure 48:** Native purification of heterologously expressed pET28a-*Bst*49.114

**Figure 49:** Calibration curve for determining the molecular weight of purified pET28a-*Bst*49…….115

**Figure 50:** Native purification of heterologously expressed pMG1a……116

**Figure 51:** Calibration curve for determining the molecular weight of purified pMG1a……....117

**Figure 52:** Native purification of heterologously expressed pMG2a……....118

**Figure 53:** Calibration curve for determining the molecular weight of purified pMG2a……119

**Figure 54:** Native purification of heterologously expressed pMG4a…….... 120

**Figure 55:** Calibration curve for determining the molecular weight of purified pMG4a……... 121

**Figure 56:** Chemical structures of (A) proline and (B) threonine…….125

**Figure 57:** Chemical structures of (A) lysine and (B) arginine…….126

**Figure 58:** Chemical structures of (A) valine and (B) tyrosine…….127

# LIST OF TABLES

**Table 1:** Actinomycete cell wall types……..2

**Table 2:** Diseases caused by pathogenic actinomycetes……... 4

**Table 3**: Composition of RNA polymerase……...9

**Table 4:** Rifampicin inactivation genes of mycobacteria and Nocardioforms……13

**Table 5:** Differences between the *arr* encoded enzyme and other mono-ADP-ribosyltransferases……...17

**Table 6:** Bacterial strains used in this work…….. 19

**Table 7:** Plasmids used in this work……. 20

**Table 8**: PCR conditions used to amplify the *arr* ORF…… 34

**Table 9:** Internet addresses for sequence analysis programs & database access……..42

**Table 10:** Rifampicin resistant clones obtained from *in vivo* selection…….43

**Table 11:** Rifampicin resistant clones obtained from *in vivo* selection under optimised conditions……44

**Table 12:** Rifampicin resistant clones with plasmid-borne mutations identified via marker rescue……...47

**Table 13:** Percentage of plasmid-borne mutants obtained from *in vivo* selection……. 48

**Table 14:** Summary of alterations in plasmid copy number in mutants obtained after 24 and 48 hrs from *in vivo* selection……54

**Table 15:** Summary of results obtained from nucleotide (BLASTN) and protein (BLASTP) sequence analyses…….66

**Table 16:** Protein parameters of pMG1 determined by the ProtPar programme……. 67

**Table 17:** Protein parameters of pMG2 determined by the ProtPar programme……..69

**Table 18:** Protein parameters of pMG4 determined by the ProtPar Programme…… 70

**Table 19:** *In vitro* enzymatic inactivation of rifampicin (10 µg/ml) by the ORF mutants……..... 86

**Table 20:** Quantification of induced bands produced by pET28a-*Bst*49 under varying conditions of IPTG concentration and induction time……103

**Table 21:** Quantification of induced bands produced by pET28a-*Bst*49 and its mutants under optimised conditions established for expression……104

**Table 22:** Peak optical density of bands produced from purified pET28a-*Bst*49 and its mutants under native conditions……122

# FREQUENTLY USED ABBREVIATIONS

| | |
|---|---|
| ADP | Adenosine diphosphate |
| AIDS | Acquired Immune Deficiency Syndrome |
| AMP | Adenosine monophosphate |
| Amp | Ampicillin |
| *arr* | ADP-ribosyltransferase |
| ATP | Adenosine triphosphate |
| | |
| Bp | Base pair |
| | |
| C | Carbon |
| $CaCl_2$ | Calcium chloride |
| Cm | Centimetre |
| Cm | Chloroamphenicol |
| CMN | *Corynebacteriaceae*, *Mycobacteriaceae* and *Nocardiaceae* |
| CsCl | Caesium chloride |
| | |
| Da | Daltons |
| $dH_2O$ | Distilled water |
| DNA | Deoxyribonucleic acid |
| DNAP | DNA-dependent-RNA-polymerase |
| DNAse | Deoxyribonuclease |
| dNTP's | Deoxynucleotide triphosphates |
| | |
| EDTA | Ethylenediaminetetraacetic acid |
| EMS | Ethylmethanesulfonate |
| EtBr | Ethidium bromide |
| EtOH | Ethanol |
| | |
| g | Gram |
| | |
| HIV | Human Immune Virus |
| HCl | Hydrogen chloride |
| His-tag | Histidine-tagged |
| hr | Hour |
| | |
| IPTG | Isopropyl-β-D-thiogalactoside |
| *iri* | **I**nactivation of **ri**fampicin |
| | |
| kb | Kilobase |
| kDa | KiloDaltons |

| | |
|---|---|
| LA | Luria-Bertani Agar |
| LB | Luria-Bertani Broth |
| | |
| µg | Microgram |
| µl | Micro litre |
| M | Molar |
| mA | Milliampere |
| MAC | *Mycobacterium avium-intracellulare* complex |
| MCS | Multiple cloning site |
| MDR | Multi-drug resistant |
| mg | Milligram |
| MIC | Minimal inhibitory concentration |
| min | Minute |
| ml | Millilitre |
| mm | Millimetre |
| mM | Millimolar |
| Mw | Molecular weight |
| | |
| NA | Not applicable |
| NaCl | Sodium chloride |
| NAD | Nicotinamide adenine dinucleotide |
| NADH | Nicotinamide adenine dinucleotide, reduced |
| NADPH | Nicotinamide adenine dinucleotide phosphate, reduced |
| nal | Nalidixic acid |
| NaOH | Sodium hydroxide |
| Ni-NTA | Nickel-nitrilotriacetic acid |
| nt | Nucleotide |
| NTG | N-methyl-N'-nitro-N-nitrosoguanidine |
| | |
| Ω | Ohm |
| OD | Optical density |
| OH | Hydroxyl group |
| ORF | Open reading frame |
| | |
| PAGE | Polyacrylamide gel electrophoresis |
| Pers. Comm. | Personal communication |
| | |
| Rif | Rifampicin (rifampin) |
| RNA | Ribonucleic acid |
| RNAP | RNA-dependent-RNA polymerase |
| RNAP/rif | RNA-dependent-RNA polymerase and rifampicin complex |
| RNase | Ribonuclease |
| rpm | Revolutions per minute |
| rRNA | Ribosomal RNA |

| | |
|---|---|
| sd | sterile distilled |
| SDS | Sodium dodecyl sulphate |
| sec | Second |
| srRNA | Small ribosomal RNA |
| TB | Tuberculosis |
| TE | Tris-EDTA |
| Tris | Tris(hydroxymethyl)-aminomethane |
| V | Volt |
| X-Gal | 5-bromo-4-chloro-3-indolyl-β-D-galactopyranoside |

# CHAPTER 1

# INTRODUCTION

*"Actinomycetes are very important from a medical point of view…. They may be a nuisance, as when they decompose rubber products, grow in aviation fuel, produce odorous substances that pollute water supplies, or grow in sewage treatment plants where they form thick clogging foams…. In contrast, actinomycetes are the producers of most of the antibiotics."*

*- H.A. Lechevalier and M.P. Lechevalier*

## 1.1 Actinomycetes

The actinomycetes are aerobic, gram-positive bacteria that form branching filaments and asexual spores. They contain high G+C rich DNA and are ordinarily non-motile. When motility is present, it is confined to flagellated spores. There is extensive morphological variety among these prokaryotes. Several are cocci while others are regular or irregular rods (Goodfellow *et al.*, 1984).

### 1.1.1 Classification

Attempts at categorising these organisms made primary use of morphological criteria such as colour of mycelia and sporangia, surface features and arrangement of conidiospores, percent G+C in DNA, phospholipid composition of cell membranes and spore heat resistance (Embley and Stackebrandt, 1994). Currently, a chemotaxonomic approach that relied on sequence comparisons of 16S ribosomal RNA (rRNA) and on the chemical analysis of cell wall components is used (Zuckerlandl and Pauling, 1965).

Four major cell wall types can be distinguished according to three features of peptidoglycan composition and structure: the amino acid in tetrapeptide side chain position 3, the presence of glycine in interpeptide bridges and peptidoglycan sugar content. Cell wall types II and IV (those with *meso*-diaminopimelic acid) have characteristic sugar patterns that are also useful for identification, (**Table 1**, adapted from Šuput *et al*., 1967).

**Table 1:** Actinomycete cell wall types

| Cell wall type | Diaminopimelic acid isomer | Glycine in interpeptide bridge | Characteristic sugars[a] | Representative genera |
|---|---|---|---|---|
| I | L,L | + | NA | *Streptomyces* |
| II | *meso* | + | Arabinose and xylose | *Actinoplanes* |
| III | *meso* | - | NA | *Microbispora* |
| IV | *meso* | - | Arabinose and galactose | *Mycobacterium* |

[a]NA = either not applicable or no diagnostic sugars

*Mycobacterium* species and their nocardioform relatives belong to a class that produces characteristic lipids known as mycolic acids. These are high molecular weight, long chain 3′-hydroxy fatty acids (**Figure 1**). This mycolic acid-containing group of actinomycetes encompasses the families *Corynebacteriaceae*, *Mycobacteriaceae* and *Nocardiaceae* (CMN) and includes the genera *Rhodococcus*, *Gordona* and *Tsukamurella*. The CMN group is characterised by a type IV cell wall chemotype (**Table 1**). These bacteria have many phenotypic characteristics in common and form a distinct phyletic line.

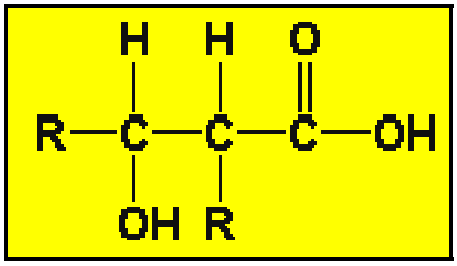


**Figure 1**: **Chemical structure of mycolic acid**. In the diagram above, the R-groups represent long hydrocarbon chains. For *Corynebacteria*, chains of 24-40 carbons (C) are common; for *Nocardia*, $C_{40}$-$C_{56}$ chains are produced and for *Mycobacteria* the chains are $C_{60}$-$C_{90}$ carbons in length (Adapted from Barry *et al.,* 1998).

Phylogenetic classification based on 16S rRNA sequences revealed that all actinomycetes have a unique, homologous insertion (~100 nucleotides) between helix 54 and 55 of the 23S rRNA. Additionally, the molecular sequences of the CMN group differ between fast and slow-growing strains. This supports the concept of an evolutionary dichotomy between them (Embley and Stackebrandt, 1994).

### 1.1.2 Pathogenicity

Most nocardioforms are non-pathogenic. They are primarily soil inhabitants and are widely distributed. These micro-organisms appear to serve three important roles in soil. Firstly, they aid in the bio-deterioration of rubber matter and participate in the degradation of hydrocarbons and waxes. Secondly, their hyphal threads bind clay particles. This imparts a granular viable soil structure that is conducive to crop production. Thirdly, actinomycetes have considerable practical and economical significance as they produce the majority of medically useful natural antibiotics. Several classes of secondary metabolites are isolated from actinomycetes and include: aminoglycosides, ansamycins, β-lactams, macrolides and tetracyclines. In the United States of America and Japan, between 1953 and 1970, it was discovered that over 85% of antibiotics were produced by

streptomycetes with the remaining 11% by fungi and 4.5% by non-actinomycete bacteria (Gottlieb, 1973). Usually nocardioforms are free-living micro-organisms. However, many are pathogens of plants, animals and humans. From a medical and anthropocentric perspective, mycobacteria cause the greatest harm.

*Mycobacterium* species are notable human pathogens responsible for much morbidity and mortality in Southern Africa as well as elsewhere in the developing world (Lucas *et al.,* 1994). This group is accountable for more fatalities worldwide than any other single pathogen as it includes the causative agents of tuberculosis, leprosy and other opportunistic organisms (**Table 2**, adapted from Goodfellow *et al.,* 1984). Tuberculosis (TB) is a primary cause of death among people who are HIV positive. According to the World Health Organisation (WHO) it is responsible for more than 13% of AIDS-related deaths worldwide. It has been acknowledged as a global emergency because of its devastating statistics. TB is accountable for 3 million deaths and results in 10 million new cases each year with a third of the world's population infected. In 1995, Southern Africa registered more tuberculosis cases than any other global region, 2.1 million of which were AIDS-related.

**Table 2:** Diseases caused by pathogenic actinomycetes

| Disease | Causative Agent | Body sites involved |
|---|---|---|
| **Bovine farcy** | *Mycobacterium farcinogenes* | Lymphatic system |
| **Diptheria** | *Corynebacterium diphtheriae* | Throat |
| **Equine pneumonia** | *Rhodococcus equi* | Lung |
| **Leprosy** | *Mycobacterium leprae* | Skin |
| **Mycobacterioses** | Numerous *Mycobacterium* species | Lungs, lymph nodes and skin |
| **Pulmonary nocardiosis** | *Nocardia asteroides,* rarely *Nocardia brasiliensis* | Lung |
| **Tuberculosis** | *Mycobacterium tuberculosis* | Lung |

A number of important opportunistic pathogens exists within this group, for example the *Mycobacterium avium-intracellulare* complex, commonly referred to as MAC. Other examples of opportunistic organisms include *M. bovis*, *M. kansasii*, *M. scrofulaceum*, *M. smegmatis* and *N. asteroids* (**Table 2**). The previously regarded non-pathogenic strains including *R. equi, R. erythropolis, R. rhodochrous, Gordona bronchialis* and *Tsukamurella paurometabolum* are presently described as opportunistic pathogens (Finnerty, 1992).

The most widely used chemotherapeutic agents to combat mycobacterial infections are ethambutol, isoniazid, pyrazinaminde and rifampicin (Grosset, 1989). These four antimicrobial agents are administered in various combinations in order to prevent multi-drug resistant (MDR) forms of the disease from arising. Rifampicin is the focus of this study.

## 1.2 The ansamycins

### 1.2.1 Origins

*Ansamycin* refers to the group of low molecular weight antibiotics that are characterised by the presence of an aliphatic 17-membered ansa bridge connecting two non-adjacent positions of an aromatic nucleus. The name itself derives from the Latin word "ansa", meaning handle (Prelog and Oppolzer, 1973). Most ansamycins are secondary metabolites of actinomycetes. A few have been isolated from plants of the genera *Maytenus, Colubrina, Putterlickia* and *Trewia* (Antosz, 1992).

They are classified into two groups based on the structure of their aromatic moiety. The first group has a naphthalene nucleus and includes the rifamycin antibiotics, which are currently used therapeutically (Antosz, 1992). The second group has a benzene aromatic nucleus and includes ansamitocin, ansatrienin, geldamycin, herbimycin and mycotrienin. The structural differences between the two groups correlate with their specific modes of action (Lancini, 1983).

The naphthoquinoid are bacteriostatic agents, inhibiting DNA-dependent RNA polymerase. The benzoquinoid affect eukaryotic cell replication (Lancini and Zanichelli, 1977). Several exhibit antifungal, antileukemic, antiprotozoal or antiviral activity.

### 1.2.2 Rifamycins

Rifamycins were originally identified in 1957. They are secondary metabolites of the actinomycete *Amycolatopsis mediterranei* (initially classified as *Streptomyces mediterranei* and later reclassified as *Nocardia mediterranei*). Five biologically-active compounds, designated rifamycin A, B, C, D and E, were derived from the fermentation broth of this micro-organism. The only stable crystalline compound, rifamycin B, proved to be the least active antibiotic. The spontaneous expulsion of glycolic acid from rifamycin B yielded rifamycin S. Through subsequent reductions this resulted in the production of rifamycin SV (Sensi *et al.*, 1960).

This compound, also referred to as rifaldehyde, was very active against Gram-positive bacteria such as *M. tuberculosis* and moderately active against several Gram-negative bacteria. However, rifamycin SV is poorly absorbed in the gastrointestinal tract, so oral administration did not give rise to effective levels in the blood stream of patients. Consequently, it was chemically altered to create an antibiotic with improved antimicrobial efficacy by increasing its activity spectrum and absorption characteristics. A semi-synthetic derivative of rifamycin SV called rifampicin was synthesized. It has good oral absorption, with a half-life of ~ 3 hrs in humans, and excellent distribution in body tissues and fluids. Furthermore, there is a low incidence of adverse reactions to daily administration (Sensi, 1983).

### 1.3 Rifampicin

Rifampicin ($C_{43}H_{58}N_4O_{12}$) has a molecular weight of 823.0 $g.mol^{-1}$. This compound is an odourless red-brown crystalline powder which readily dissolves in methanol and chloroform and is slightly soluble in water and acetone. The lipophilic characteristics of rifampicin contribute considerably to its ability to cross the cell wall barrier by passive diffusion. It is an effective broad-spectrum bacteriostatic drug that is utilised predominantly for anti-tuberculosis therapy. It is also employed to treat infections caused by *Neisseria meningitides* (Carter *et al.,* 1994), *Haemophilus influenzae, Staphylococcus aureus* (Kapusnik *et al.,* 1984), *Legionella pneumophila, Streptococcus pneumoniae* and other pathogens (Abadi *et al*., 1996). The major structural difference between rifampicin and rifamycin B is the aromatic structure that occurs on the third carbon of the napthoquinone ring.

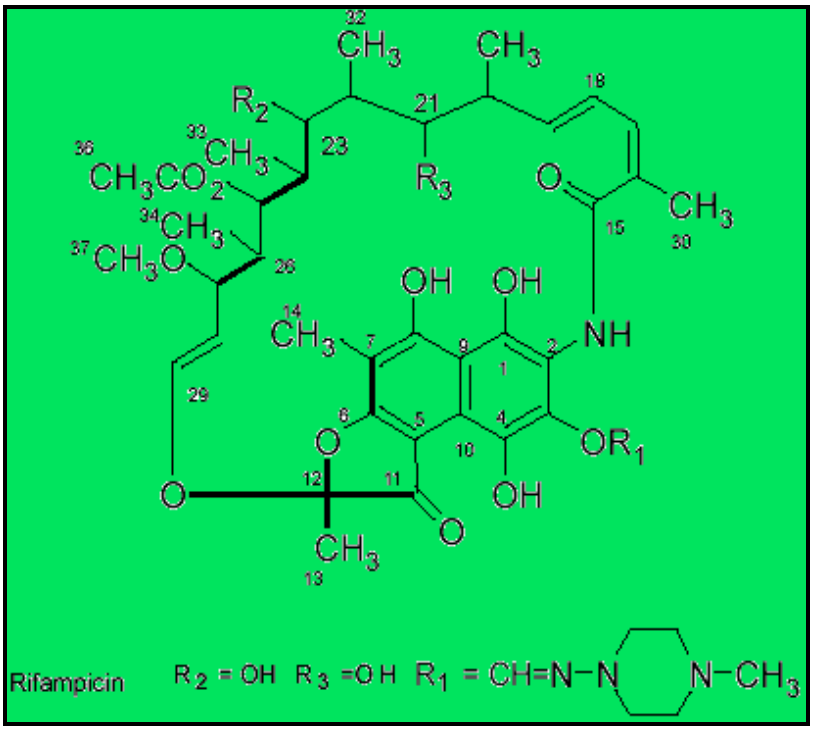


**Figure 2**: **The chemical structure of rifampicin.** Phosphorylative inactivation occurs at the $C_{21}$ position, glucosylation and ADP-ribosylation at the $C_{23}$ position, (Adapted from Campbell *et al.,* 2001).

The most significant functional groups of rifampicin are the two free hydroxyl (OH) groups in positions 21 and 23 of the ansa link and the two polar groups (either hydroxyl or carbonyl) at positions $C_1$ and $C_8$ of the napthoquinone ring (**Figure 2**). These are the minimum requirements for antimicrobial activity as they are involved in the formation of a tight but reversible linkage to DNA-dependent-RNA-polymerase. Any modification involving a substitution, the molecular size of which is not important, or elimination of the 21 or 23 hydroxyl groups results in an inactive compound (Wehrli and Staehelin, 1971).

### 1.3.1 Mode of action

In 1967, Hartmann et al. proposed that the rifamycins might act on RNA synthesis based on the observation that rifampicin inhibited uracil uptake in *Staphylococcus aureus*. *In vitro*, rifampicin concentrations as low as 0.02 µg/ml inhibit the DNA-dependent RNA polymerase (RNAP) of *E .coli*. In contrast, DNA-dependent DNA polymerase (DNAP) remained active even when exposed to rifampicin concentration 5000X higher (Hartmann *et al.,* 1967).

RNAP is responsible for the transcription of DNA into RNA, a process achieved by four enzymatic steps: DNA binding, chain initiation, chain elongation and chain termination. This enzyme consists of five polypeptides: namely, two α subunits, one β subunit, one β′ subunit and one σ subunit (**Table 3**, adapted from Burgess, 1969). In 1970, Zillig et al. showed that the antibiotic binds specifically to the β subunit of RNAP. This stable drug-enzyme (RNAP/rif) complex prevents the elongation of initiated RNA chains beyond a few nucleotides, inhibiting bacterial growth. A sequence comparison in the four distinct regions of the *rpoB* gene showed a low level of conservation between prokaryotes and eukaryotes. This may be the reason why rifampicin is not active against eukaryotic RNAPs (Campbell *et al.,* 2001).

**Table 3**: Composition of RNA polymerase

| Subunit | Molecular weight (Da) | No. of subunits | | Genes encoding the subunits |
|---|---|---|---|---|
| | | In core enzyme | In holoenzyme | |
| **α** | 40 000 | 2 | 2 | *rpoA* |
| **β** | 145 000 | 1 | 1 | *rpoB* |
| **β′** | 160 000 | 1 | 1 | *rpoC* |
| **σ** | 85 000 | - | 1 | *rpoD* |

Structural aspects of rifampicin inhibition of bacterial RNAP were determined by Campbell et al. (2001). This antibacterial agent blocks the pathway of the elongating RNA transcript when it is 2 or 3 nucleotides long. The initiating nucleotide binds the RNAP i-site (i = initiation site at -1 position), the second nucleotide binds at the i+1 site. After a phosphodiester bond has been formed between the two nucleotides, RNAP is translocated. Consequently, the i+1 nucleotide occupies the i-site at the -1 position and the i-site nucleotide moves into the -2 position.

The physical association of rifampicin to the β subunit of RNAP results in a severe steric clash with the 5′ triphosphate of the initiating nucleotide at the -2 position. Owing to the conformational change in the enzyme, the synthesis of the second phosphodiester bond is inhibited (Wehrli and Staehelin, 1971). Consequently, RNAP remains at the same template position, the 2 nucleotide transcript is released and this futile cycle resumes. The mechanism of RNAP inhibition by rifampicin is shown in **Figure 3**. If the third phosphodiester bond of the RNA transcript has been formed the drug is no longer able to exert its effect (Sippel and Hartmann 1970). A possible explanation may be that the complex comprising the DNA template, RNAP and the RNA transcript, has undergone a conformational change, eliminating binding sites for rifampicin.

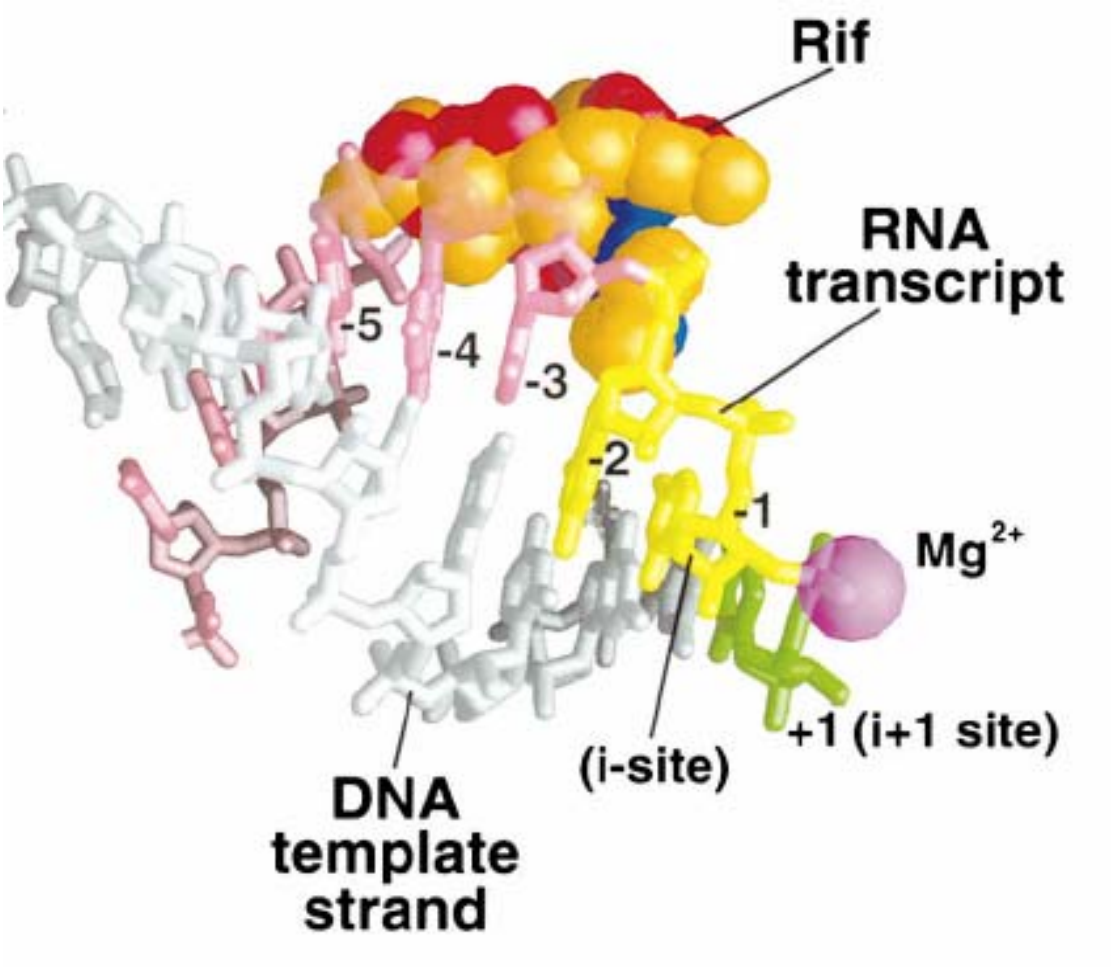


**Figure 3: Mechanism of RNAP inhibition by rifampicin** (Adapted from Campbell *et al.,* 2001). The RNA itself and the rest of the nucleic acids have not been depicted for reasons of clarity. $Mg^{2+}$ is represented by the **magenta** sphere. The incoming nucleotide substrate at the -1 position is shown in **green** and the -1 and -2 positions that can be accommodated in the presence of rifampicin are depicted in **yellow**. The RNA further upstream (-3 to -8) that cannot be accommodated in the presence of rifampicin is coloured **pink.** The DNA template strand is **grey**. Rifampicin is shown positioned in its binding site on the β subunit. The carbon atoms are coloured in **orange** while the oxygen in **red** and nitrogen in **blue**, (Nicholls *et al.,* 1991). The rifampicin is partially transparent, illustrating the RNA nucleotides (at -3 to -5) that sterically clash.

### 1.4 Antibiotic resistance mechanisms

Antibiotics have facilitated the control of infectious diseases. Unfortunately, they also select microbes resistant to these drugs. **Figure 4** illustrates the number of different biochemical resistance mechanisms that have been identified. The first method involves the production of enzymes that inactivate the drug. A second strategy involves alteration of the target moiety. Thirdly, microbes resist antibacterial agents by preventing their entry into the cell. Finally, some bacteria have efflux pumps that actively remove the antibiotic from the cellular cytosol. All four mechanisms have been observed in rifampicin resistance.

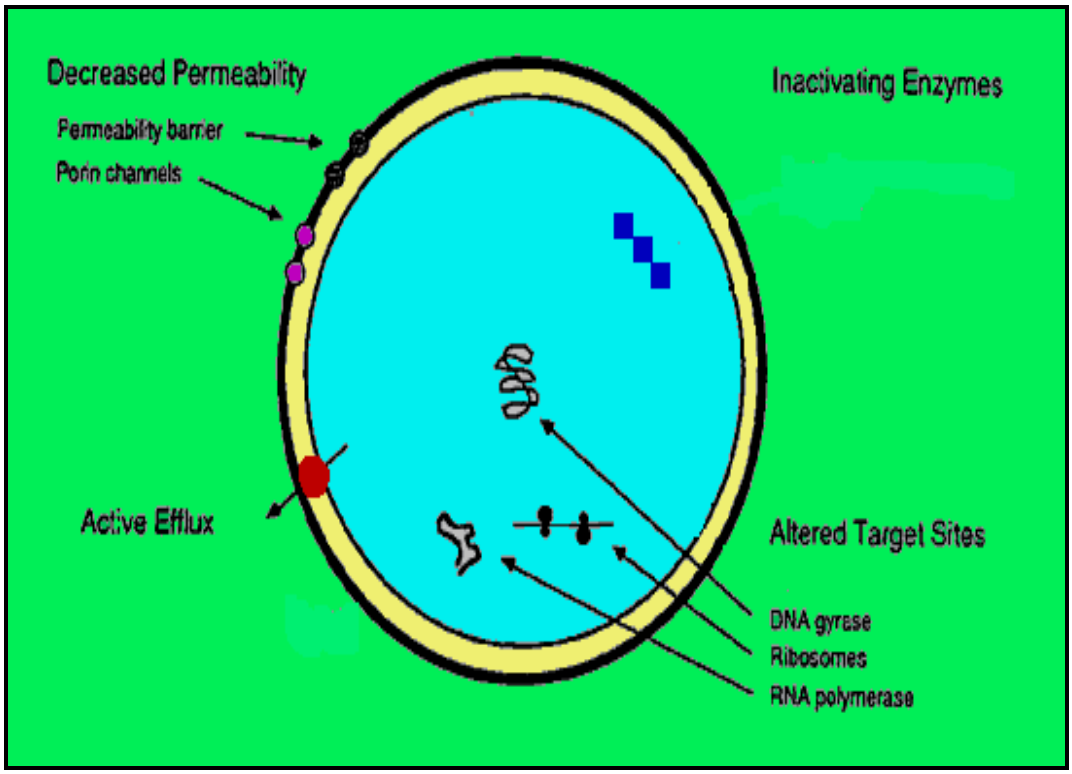


**Figure 4: Bacterial defence mechanisms comprising drug inactivation, target alteration, decreased permeability and active extrusion of the antibiotic from the cell**, (Adapted from Putman *et al.,* 2000).

## 1.5 Rifampicin resistance

### 1.5.1.1 Rifampicin resistance through target modifications

Endogenous rifampicin resistance by mutation of the target moiety is ordinarily the most widespread. Several reports have described mutations in the β subunit, encoded by the *rpoB* gene, of the RNAP that result in alterations of the binding site. These mutations slightly alter the subunit making it unrecognizable to the drug. However, the enzyme maintains its binding properties so that it can still function normally. In *E. coli* most mutations are clustered in a 225 base pair (bp) region of the *rpoB* gene (Jin and Gross, 1988). Similar work done in *M. leprae* (Honore and Cole, 1993) and *M. tuberculosis* (Telenti *et al.,* 1993b) identified the same section as the mutational hotspot for rifampicin resistance. Studies report that these rifampicin resistant as well as multidrug-resistant (MDR) clinical isolates harboured missense mutations. The codons most prone to mutations are 516, 526 and 531 using the *E. coli* system of codon numbering (Ezekiel and Hutchins, 1968). Interestingly, this segment was shown to be conserved among different strains of *M. tuberculosis* (Telenti *et al.,* 1993a) as well as between diverse bacterial species, plants and even some eukaryotes.

### 1.5.1.2 Rifampicin resistance by reduced cell wall permeability

In 1996, Abadi et al. reported rifampicin resistance by alteration of cell wall permeability in *Neisseria meningitides.* In Gram-negative bacteria the cell envelope is effective at restricting permeation by antibiotics and the first barrier in the envelope is the outer membrane. Ordering of water molecules within this membrane is responsible for the extremely slow influx of lipophilic antibiotics. Experiments with Tween 80, a substance that alters membrane permeability, revealed high-level resistance shown by one strain was due to a decrease in membrane permeability. Consequently, the drug was unable to enter the cell. An earlier report also implicated changes in cell wall permeability as being responsible for rifampicin resistance in *Mycobacterium avium* (Hui *et al.,* 1977).

#### 1.5.1.3 Rifampicin resistance through active efflux

In 1997, Sánchez et al. identified efflux pumps as a contributing factor to rifampicin resistance by the pathogen *Haemophilus influenzae*. This study identified a three-gene complex that was homologous to the *acrAB* cluster of *E. coli*. These genes encode an efflux system that is responsible for removing toxic dyes, detergents (Nikaido, 1996) and lipophilic antibiotics (Okusu *et al.,* 1996) from the Gram-negative organism. Gene disruption caused *Haemophilus influenzae* to become more susceptible to rifampicin.

#### 1.5.1.4 Rifampicin resistance by modification enzymes

Analysis of clinical isolates that showed no mutation in the *rpoB* gene allowed for the identification of drug inactivation genes. Four mechanisms have been identified and include decomposition, ADP-ribosylation, glucosylation and phosphorylation (**Table 4**, adapted from Dabbs, 2004).

**Table 4:** Rifampicin inactivation genes of mycobacteria and nocardioforms

| Organism (strain) | Mechanism | Gene | Reference |
|---|---|---|---|
| *R. equi* ATCC 14887 | decomposition | monooxygenase | Andersen and Dabbs, 1991 |
| *M. smegmatis* DSM 43756 | ADP-ribosylation ($C_{23}$) | ADP-ribosyl transferase | Quan *et al.,* 1997 |
| *N. brasiliensis* IFM 0236 | glucosylation ($C_{23}$) | glycosyltransferase | Lephoto, unpublished |
| *N. otitidiscaviarum* IFM0239 | phosphorylation ($C_{21}$) | not known | Rebić, unpublished |

Rifampicin inactivation is species-specific among mycolic acid-containing bacteria. Decomposition is the most widespread of the four mechanisms and is primarily active in *Nocardia, Rhodococcus* and *Mycobacterium,* (Tanaka *et al.,* 1996). Within the genus *Nocardia*, five *N. brasiliensis* strains modify the $C_{23}$-OH group with β-D-glucose and five *N. otitidiscaviarum* strains adjust the $C_{21}$-OH group with phosphate. Phosphorylation is also detected in *R. rhodochrous*. Ribosylation of the antibiotic is observed in the fast-growing *Mycobacterium* species: *M. smegmatis*, *M. avium* and *M. parafortuitum*. Further studies showed it is the only resistance mechanism in the closely related slow-growing genera *Gordona* and *Tsukamurella.* Interestingly, these strains were transferred from the genus *Rhodococcus* only due to differences in their menaquinone (Mk-9 type) compositions (Stackebrandt *et al.,* 1988). Rifampicin inactivation by ribosylation is of particular interest to this study as this is the predominant mechanism in many mycobacterial pathogens, (Tanaka *et al.,* 1996).

A 1.1 *SalI* fragment of DNA, isolated from *M. smegmatis* DSM 43756, was found to contain all the necessary information for the ribosylative inactivation of rifampicin. Biochemical studies showed that the gene encodes for a highly thermostable mono-ADP-ribosyltransferase and was designated *arr* for ADP-ribosylation. The 1 141 bp sequence is 63% GC. It carries a 429 bp open reading frame (ORF), starting at position 356 (GTG start codon) and ending at position 784 with a TAG termination codon. This sequence encodes a 143 amino acid peptide with a predicted molecular weight of 15.9 kDa. A stem structure has been identified further downstream of the stop codon and may function as a transcriptional stop signal. Gene disruption experiments revealed that the presence of the functional *arr* gene product confers a 12-fold increase in rifampicin resistance (>20μg/ml) to *M. smegmatis* DSM 43756 and related organisms. When expressed off the *lac* promoter in *E. coli* MM294-4, the gene confers resistance to >500 μg/ml rifampicin. *In vitro* experiments revealed that nicotinamide adenine dinucleotide (NAD) is the preferred co-factor for inactivation, (Quan *et al.*, 1997).

## 1.6 ADP-ribosylation

ADP-ribosylation is generally a post-translational protein modification. Two classes of ADP-ribosyltransferases exist: mono-ADP-ribosyltransferases found in both prokaryotes and eukaryotes and poly-ADP-ribosyltransferases that occur specifically in eukaryotes (Ueda and Hayaishi, 1985). Many bacterial toxins are mono-ADP-ribosyltransferases and have been found in *Corynebacterium*, *Pseudomonas*, *Staphylococcus*, *Clostridium* and *Bordetella* (Krueger and Barbieri, 1995) causing diseases such as diphtheria, cholera and pertussis. With these toxins, the ADP-ribosylation enzyme is usually a subunit of a larger multimeric enzyme complex. The function of the other subunits is to bind cell receptors to allow transfer of the ADP-ribosylation enzyme within the cell, (Spangler, 1992). Thus, a role in the regulation of protein activity has been suggested.

Rifampicin inactivation by ribosylation is central to this study. Firstly, this mechanism functions in many mycobacterial opportunistic pathogens. Secondly, ADP-ribosylation usually occurs on a nitrogen atom of a protein. Here, the ADP-ribose moiety is attached to the $C_{23}$ of rifampicin via an O-glycosidic bond (**Figure 5**). The initial ADP-ribosylation step is followed by the removal of adenosine monophosphate (AMP) and thereafter dephosphorylation gives rise to ribosylated rifampicin, (Imai *et al.,* 2000). Thirdly, this ribosylation is the first and only known example of it as an antibiotic inactivation mechanism (Dabbs *et al.,* 1995). Finally, it is inhibited by light, even at low levels such as those found in a laboratory (Dabbs and Quan, 2001).

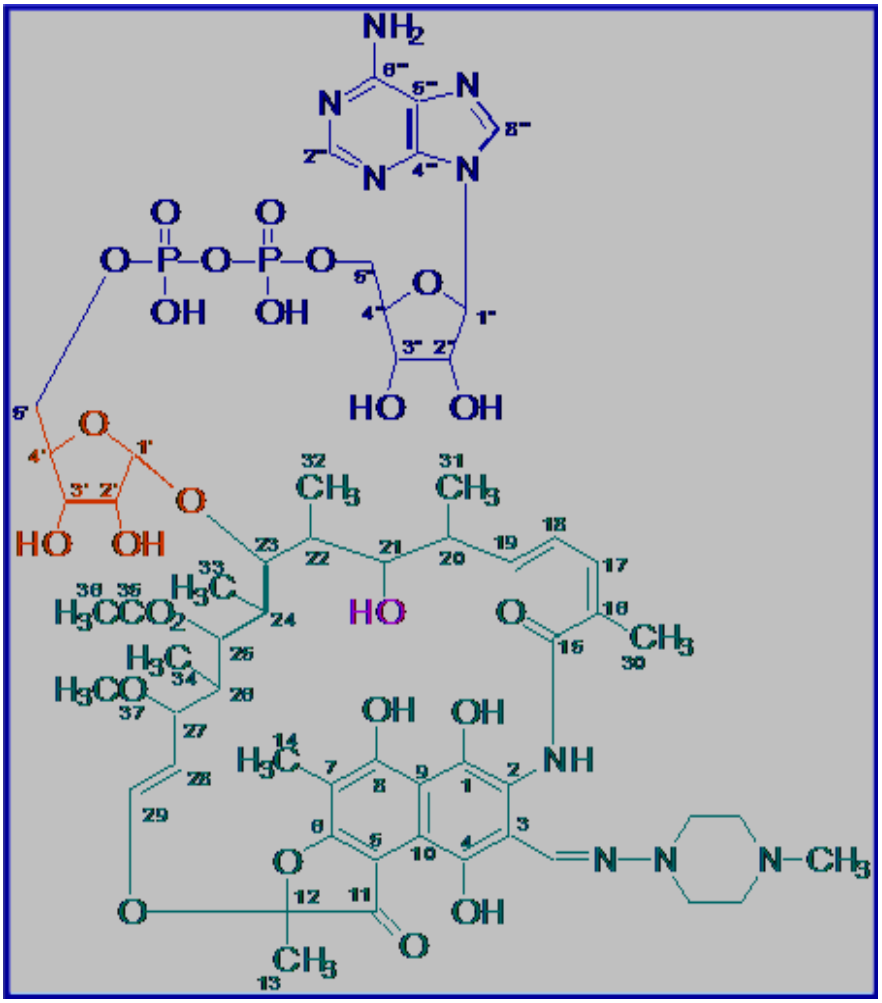

**Figure 5: Chemical structure of ADP-ribosylated rifampicin** (Adapted from Imai *et al.,* 1999). The adenosine diphosphate (ADP) group is shown in **blue** and the ribose sugar in **red**. Ribosylated rifampicin is achieved through two steps. The first involves the removal of adenosine monophosphate (AMP) and the second is dephosphorylation.

### 1.6.1 Mono-ADP-ribosylation

The enzyme encoded by the *arr* gene differs extensively from other mono-ADP-ribosyltransferases (**Table 5**). There is very little sequence similarity between the Arr enzyme and other mono-ADP-ribosyltransferases. This suggests that it may belong to a different class altogether.

**Table 5:** Differences between the *arr* encoded enzyme and other mono-ADP-ribosyltransferases

| Characteristics | Other mono-ADP-ribosyltransferases | *arr* encoded mono- ADP-ribosyltransferase |
|---|---|---|
| **Acceptor molecule** | protein | Antibiotic (rifampicin) |
| **Type of bond** | N-glycoside | O-glycoside |
| **Preferred co-factor** | NADPH | NADH |

Sugawara *et al.* (2002) demonstrated that four proteins isolated from *Streptomyces coelicolor* shared the following consensus sequence Leu(or Ala)-Thr(or Ala)-Ala-Cys-Gly. Here, ribosylation occurred on the sulphur atom of the cysteine residue. Hence, one prediction for the Arr enzyme is that *in vivo* it possibly ribosylates target proteins on the thiol group of a cysteine residue. Additionally, there is another parallel in that these proteins are also extra-cellular (Sugawara *et al.,* 2002).

### 1.6.2 Arr ADP-ribosyltransferase

Several ADP-ribosylation reactions have been described in both eukaryotes and prokaryotes. The *in vivo* function of the Arr ADP-ribosyltransferase is still unknown. It is highly unlikely that it is present to combat rifamycins as it is more active against semi-synthetics than the natural antibiotic (E. Dabbs, Pers. Comm.). More experimentation needs to be performed to elucidate the function of this protein within the cell. I selected and characterised mutants of this gene to provide greater insight into the biochemistry of ribosylative inactivation of rifampicin.

# CHAPTER 2

# AIMS OF THE PROJECT

## 2.1 Justification

Rifampicin remains an important antimicrobial agent for the treatment of mycobacterial diseases. However, the escalating number of infections with opportunistic pathogens belonging to the mycolic acid-containing group of actinomycetes and the development of multi-drug resistant *M. tuberculosis* necessitates the characterisation of all resistance mechanisms to rifampicin. The study of the *arr* gene will contribute to a greater understanding of its significance to clinical rifampicin resistance. Additionally, it will facilitate in the development of more potent antibacterial agents.

## 2.2 Aims of the study

This project continues on the work initiated by Dabbs et al. (1995) in which a novel ribosylation mechanism of rifampicin inactivation by *M. smegmatis* DSM 43756 was described. The broad aim of this project was the further biochemical characterisation, at the molecular level, of the Arr enzyme by mutational analysis. This is a classic way to observe structure-function relationships and to gain a better understanding of a protein of interest.

**Specific experimental objectives:**

1. To obtain Arr mutants with alterations in the open reading frame.
2. To construct a fusion protein comprising the Arr gene product and a purification tag.
3. To optimise heterologous expression of this protein.
4. To purify the Arr gene product by metal chelation chromatography.

# CHAPTER 3

# MATERIALS AND METHODS

## 3.1 Bacterial strains and plasmids

Bacterial strains used in this work are listed in **Table 6**, plasmids in **Table 7**.

**Table 6:** Bacterial strains used in this work

| Strain | Relevant characteristics | Source |
|---|---|---|
| *Escherichia coli* | | |
| BL21(DE3)pLysS | $F^-$, *ompT hsd*$S_B$ with λ prophage carrying the T7 polymerase gene | Novagen |
| DH5α | *rec*A1, *end*A1, *hsd*R17 | Novagen |
| MM294-4 | *end*A1, *hsd*R17, *gyr*A | E. Dabbs |
| Rosetta2(DE3)pLysS | Enhances expression of proteins by supplying tRNAs for seven rare codons | Novagen |
| *Bacillus subtilis* | | |
| 1A3-1 | $Sp^R$ rifampicin assay organism | E. Dabbs |

## 3.2 Media and growth conditions

Luria-Bertani (LB) (Appendix A) media was used for growing *E. coli* and *Bacillus* strains. Liquid cultures were obtained by inoculating single bacterial colonies into 5 ml LB medium and incubating at 37°C overnight. For short-term storage, *E. coli* strains were kept on LB-agar plates at 4°C. For long-term storage, freshly grown strains were kept in 33% glycerol at -70°C. *Bacillus* strains were kept on LB-agar plates at room temperature until they sporulated for long-term storage.

**Table 7:** Plasmids used in this work

| Plasmid | Size (bp) | Relevant characteristics | Source |
|---|---|---|---|
| pCL1 | 10600 | Original rif-R clone isolated from *N.brasiliensis* IFM 0236 *Pst*I library | C. Lephoto |
| pCL2 | 10600 | Reverse orientation of insert in pCL1 | C. Lephoto |
| pDA71 | 8800 | *E. coli-Rhodococcus* shuttle vector | Quan & Dabbs (1993) |
| pDA71* | 8800 | *E. coli-Rhodococcus* shuttle vector with *Eco*RI suicide gene interrupted | E. Dabbs |
| pGEM3Z(f-) | 3199 | *E. coli* high copy number vector, *lacZ′* gene, SP6 and T7 promoters | Promega |
| pGEM3Z-*Bst*49 | 3769 | *Bst*NI fragment of *arr* gene inserted into the *Hind*II site of pGEM3Z(f-) | S. Quan |
| pGEM-T-Easy | 3015 | *E. coli* high copy number vector, *lacZ′* gene, single 3′ thymidine overhangs, SP6 and T7 promoters | Promega |
| pGEM-T-Easy-*Bst*49 | 3450 | *Bst*NI fragment of *arr* gene inserted into pGEM-T-Easy at the *Eco*RV site with single 3′ thymidine overhangs | This work |
| pMG1 | 3450 | pGEM-T-Easy-*Bst*49 except C→A point mutation in *arr* | This work |

| | | | |
|---|---|---|---|
| pMG2 | 3450 | pGEM-T-Easy-*Bst*49 except A→G point mutation in *arr* | This work |
| pMG3 | 3450 | pGEM-T-Easy-*Bst*49 except C→T and T→A double point mutation in *arr* | This work |
| pMG4 | 3450 | pGEM-T-Easy-*Bst*49 except G→T and T→A double point mutation in *arr* | This work |
| pET-28a(+) | 5369 | N-terminal His•Tag/T7 coding sequence, T7 promoter/*lacI* operator element and optional C-terminal His•Tag sequence | Novagen |
| pET28a-*Bst*49 | 5816 | *Nde*I-*Xho*I fragment of *arr* gene inserted into pET28a(+) | This work |
| pMG1a | 5816 | pET28a-*Bst*49 except C→A point mutation in *arr* | This work |
| pMG2a | 5816 | pET28a-*Bst*49 except A→G point mutation in *arr* | This work |
| pMG4a | 5816 | pET28a-*Bst*49 except G→T and T→A double point mutation in *arr* | This work |
| pQE30/31/32 | 3461/3463 | *E. coli* low copy number plasmids, T5 promoter/*lac* operator element | Qiagen |
| pQE31-*Bst*49 | 4023 | *Bst*NI fragment of arr gene inserted into the *Hind*III and *Bam*HI site of pQE31 | This work |

### 3.3 Determination of minimal inhibitory concentration (MIC)

The minimal inhibitory concentration (MIC) of antibiotics was determined on LB-agar plates for *E. coli* strains by the agar dilution method. Freshly grown colonies were inoculated into 200 µl of sterile $dH_2O$ per well. This was replica plated onto LB-agar plates containing the dilutions of antibiotics starting from the lowest concentration. *E. coli* spot tests were analysed after incubation at 37°C for 24 hrs. The antibiotic concentration at which there was no confluent growth was taken as the MIC.

### 3.4 Cell differentiation by Gram staining

The Gram staining method identifies microbial cell wall structural differences. Micro-organisms that retain the crystal violet-iodine complex appear purple under microscopic examination. They are classified as Gram-positive. Conversely, micro-organisms that assume the contrasting colour of the counter stain appear pink and are categorised as Gram-negative (Gregersen, 1978).

A drop of culture was aseptically transferred to the centre of a clean glass slide. The culture was spread to an even thin film, air-dried and heat-fixed over a gentle flame. The smear was flooded with 0.07% crystal violet stain and left to stand at room temperature for 1 minute. The stain was washed off with sterile $dH_20$. Iodine was added (1 minute) as a mordant to form an insoluble crystal violet-iodine complex. The smear was decolourised with 95% ethanol for 10 seconds or until the solvent flowed colourlessly from the slide. The length of the decolouriser treatment is critical in differentiating between the two cell types. Prolonged exposure will cause excess decolourisation in Gram-positive cells. A counter stain of safranin was applied for 30 seconds and rinsed a final time with sterile $dH_20$. The slide was observed directly under oil immersion (100x) using a compound light microscope.

### 3.5 DNA preparations

#### 3.5.1 *E. coli* bulk plasmid preparation

A single colony was used to inoculate 100 ml of LB supplemented with the appropriate selective agent for maintaining the plasmid. The culture was grown with gentle agitation at 37°C overnight. Cells were harvested by spinning in a JA-10 rotor (Beckman) at 6 000 rpm for 10 min and then re-suspended in 5 ml of solution I (50 mM glucose, 25 mM Tris-HCl, 10 mM EDTA, pH 8.0). 10 ml of solution II (0.2 M NaOH, 1% SDS) was then added to the cell suspension, mixed gently by inversion and left at room temperature for 15 min. Afterwards, 7.5 ml of chilled solution III (5 M KAc, pH 6.0) was added and the tube was shaken vigorously and then left on an ice-water slurry for 15 min.

The cellular debris was removed by spinning in a pre-chilled (4°C) JA-20 rotor at 15 000 rpm for 10 min. The supernatant was transferred to a clean Beckman centrifuge tube and the DNA was precipitated with 0.6 volumes of isopropanol. The precipitation process was allowed to proceed for 15 min on the bench followed by centrifugation in a warm (25°C) JA-20 rotor at 15 000 rpm for 15 min.

The supernatant was decanted off and the DNA pellet was rehydrated with 2 ml of ethanol. The ethanol was gently poured off and the DNA pellet was vacuum-dried for 20 min. The DNA was then re-suspended in 4 ml TE buffer (Appendix B) for 2 hrs at 42°C. Thereafter, 400 µl of a 1% ethidium bromide (EtBr) solution and 4.1 g of caesium chloride (CsCl) were added and the refractive index adjusted to between 1.387 and 1.389 (0.001 units = 100 mg CsCl if the index was below or 0.001 units = 100 µl TE if the index was over). The mixture was loaded into a Beckman Quick-seal tube using a Pasteur pipette. The tube was sealed, balanced and ultra-centrifuged overnight at 45 000 rpm in a Beckman vertical VTi 65.2 rotor. The DNA was purified from the CsCl gradient as described in section 2.6.2 below.

### 3.5.2 *E. coli* mini plasmid preparation

The mini plasmid preparation is based on the alkaline-lysis method of Birnboim and Doly (1979). The yield of plasmid will vary depending on several factors. These include the plasmid copy number, cell density of the bacterial culture, type of culture medium and bacterial strain used. Plasmid DNA is isolated by disrupting the integrity of the bacterial cell wall, cell membrane and denaturing the cellular proteins. This is achieved with the ionic detergent SDS (sodium dodecyl sulphate). The DNA is renatured in the presence of sodium hydroxide. The addition of acetic acid, which leads to the rapid neutralisation of the solution, allows for the quick renaturation of the plasmid DNA, which remains in the soluble phase. Chromosomal DNA also begins to renature, as it is much larger, the renaturation step is interrupted. It therefore does not renature completely. Instead, it remains in the insoluble precipitate.

Individual bacterial colonies were inoculated into 2 ml of LB containing the appropriate selective agent for maintaining the plasmid. This was incubated at 37°C on a shaker, overnight. The culture was transferred to a sterile Eppendorf tube and the cells were harvested by microfuging for 1 minute at room temperature. The supernatant was decanted off and the cell pellet re-suspended in 80 µl of solution I (50 mM glucose, 25 mM Tris-HCl, 10 mM EDTA, pH 8.0) by vortexing. Then, 160 µl of solution II (0.2 M NaOH, 1% SDS) was added, mixed gently by inversion and left to stand on the bench for 15 min. Thereafter, 120 µl of chilled solution III (5 M KAc, pH 6.0) was added. The mixture was shaken vigorously and placed on ice for 5 min. Cellular debris was removed by microfuging at 4°C for 10 min. The supernatant was transferred to a clean sterile Eppendorf tube and warmed in a 42°C water bath for 2 min.

Isopropanol (220 µl) was added and the precipitation process allowed to proceed for 5 min at room temperature. This was followed by centrifugation for a further 5 min. The pellet was washed with 150 µl of 96% ethanol and dried in a speed vacuum for 20 min. The DNA was usually re-suspended in 150 µl of sterile $dH_2O$

or 4 mM Tris-HCl (pH 8.0) containing freshly boiled ribonuclease (RNAse) (10 mg/ml). A small aliquot was then analysed on an agarose gel. If the plasmid was of low copy number, such as pQE, the volumes of solutions were increased twofold and the volume of sterile $dH_2O$ used to re-suspend the DNA was halved.

### 3.6 DNA manipulations and cloning techniques

This work dealt exclusively with manipulation of DNA. Extracts prepared by steps outlined in section 2.5 above as well as DNA samples obtained from commercial suppliers, *e.g*., pGEM-T-Easy were subjected to several manipulation protocols: precipitation, preparation from CsCl gradients, phenol-chloroform extraction, restriction enzyme digestion, ligations, alkaline phosphatase treatment and agarose gel electrophoresis.

#### 3.6.1 DNA precipitation

##### 3.6.1.1 Salt and ethanol precipitation

DNA was precipitated from aqueous solution using a 0.1 volume of 1 M NaCl and 2 volumes of 96% ethanol. The mixture was microfuged at 4°C for 20 min. The supernatant was decanted and the remaining liquid removed by blotting on a paper towel. The DNA pellet was vacuum dried for 10-20 min and re-suspended in the appropriate volume of sterile $dH_2O$ or 4 mM Tris-HCl. Contamination with RNA was removed by incubating the plasmid DNA solution containing freshly boiled RNAse (10 mg/ml).

##### 3.6.1.2 Isopropanol DNA precipitation

Following addition of 220 µl isopropanol, the solution was mixed by inversion and left to stand at room temperature for 5 min. This was followed by centrifugation at room temperature for a further 5 min. The pellet was washed briefly with 150 µl of 96% ethanol and dried under vacuum for 20 min. Finally,

the plasmid DNA was re-suspended in 150-200 µl of sterile $dH_2O$ or the same volume of 4 mM Tris-HCl (pH 8.0). Contamination with RNA was removed by incubating the plasmid DNA solution containing freshly boiled RNAse (10 mg/ml).

### 3.6.2 DNA preparation from CsCl density gradients

Ethidium bromide (EtBr) was removed from the DNA by thorough mixing with a 0.1 volume of butanol. The procedure had to be repeated at least 3 times before all traces of EtBr were removed. This left the DNA in a CsCl solution. The DNA was stored at -20°C until required. The salt was removed by adding 2 volumes of sterile $dH_2O$ and 2.5 volumes of 96% ethanol and precipitated by centrifugation for 20 min at 4°C. The DNA pellet was dried under vacuum and re-suspended either in the appropriate buffer or sterile $dH_2O$.

### 3.6.3 Phenol-chloroform extraction

DNA was extracted from aqueous solution by phenol and chloroform. The phenol removes a complex mixture of molecules such as restriction enzymes and other proteins. The chloroform then removes the phenol. Both phenol and chloroform denature the proteins which can be removed easily as proteins partition into the organic phase, leaving the DNA behind in the aqueous phase.

Small volumes of DNA samples to be subjected to phenol-chloroform extraction were adjusted to 300 µl with TE buffer. 35% of TE-saturated phenol was added, mixed by inversion and microfuged at room temperature for 5 min to separate the organic and aqueous phases. The upper aqueous layer was then transferred to a sterile Eppendorf tube and where necessary, as in the case of extracting DNA from low gelling agarose, a further phenol step was performed until there was no visible protein at the interface. Then, a 35% volume of chloroform was added to the aqueous layer and mixed thoroughly by inversion. The organic and aqueous layers were separated by microfuging for 30 seconds at room temperature. The

upper aqueous layer was removed to a fresh Eppendorf tube and the DNA precipitated with a 0.1 volume of NaCl as outlined above in section 2.6.1.1.

### 3.6.4 Restriction enzyme digestion

Enzymes were obtained from Boehringer Mannheim, New England Biolabs, Amersham or Promega and used according to the manufacturer's instructions. The total volume of a digestion reaction was 15 µl (13.5 µl DNA and 1.5 µl 10x buffer) or a multiple thereof. The mixture was tapped briefly to ensure even buffer distribution and spun down for 1 second. 0.3-1 µl of restriction endonuclease was added and the contents mixed and briefly re-spun. Digestions were incubated at the appropriate temperature for maximal enzyme activity for at least 4 hrs. For double digestions an appropriate buffer in which both enzymes showed suitable activity was selected, otherwise the digestions were performed sequentially starting with the enzyme that required the lower pH buffer. For enzymes that exhibit sensitivity to DNA methylation, restriction digestion was carried out on DNA isolated from strains that lack *dam* and *dcm* methylating ability.

### 3.6.5 Ligation of DNA

DNA ligases catalyze the formation of phosphodiester bonds by joining 3′-hydroxyl and 5′-phosphate ends of double stranded DNA (dsDNA). The *E. coli* enzyme uses nicotinamide adenine dinucleotide (NAD) as an energy source whilst the more commonly used bacteriophage T4 ligase uses the energy of adenosine triphosphate (ATP) hydrolysis. The latter is more useful because it ligates not only sticky ends like its *E. coli* counterpart, but also blunt ends. T4 DNA ligase (Boehringer Mannheim) was used in all ligation procedures. The total volume for ligation was kept minimal at 20 µl. Ligation buffer and the appropriate volume of sterile $dH_2O$ were added to the DNA sample, mixed by tapping and microfuged for 1 second. Subsequently, 1 µl of ligase was added, remixed and re-spun. Ligation was performed in a water bath at 16°C for 16-22 hrs.

### 3.6.6 Alkaline phosphatase treatment

Calf intestinal alkaline phosphatase (Boehringer Mannheim) was used to prevent the vector from ligating to itself. The alkaline phosphatase removes the 5′-phosphates that are necessary for ligation by DNA ligase. Without these phosphates the vector cannot ligate on its own but can still ligate to the insert that retains its 5′-phosphates (Weaver, 1999). Following digestion of the vector, 1 µl of calf intestinal alkaline phosphatase was added to the reaction mixture. Addition of 10x dephosphorylation buffer was not necessary since the enzyme functions equally well in the digestion buffer. The reaction mixture was incubated further at 37°C overnight. Immediately after incubation, the enzymes were removed by a phenol-chloroform DNA extraction as previously described in section 2.6.3.

## 3.7 Gel electrophoresis

Gel electrophoresis is a method of analysing nucleic acids and proteins for various purposes, *e.g.*, determining fragment size, ensuring successful PCR amplification or searching for single base changes in DNA. The term *electrophoresis* refers to the movement of small ions and charged macro-molecules in solution under the influence of an electric field. Electrophoresis is used extensively in nucleic acid and protein analysis. The rate of migration depends on the size and shape of the molecule, the charge carried, the applied current and the resistance of the medium. Gel electrophoresis is commonly used to separate duplex DNA fragments at neutral pH values. At these conditions, DNA is negatively charged so that fragments loaded in sample wells at the cathode end of a gel move through the gel towards the anode. The electrophoretic mobility of the DNA fragments is dependant on fragment size and is fairly independent of base composition or sequence (Sealey and Southern, 1982). The larger the molecule, the more friction there is on a fragment as it attempts to move through the pores of the agarose gel slab. Hence, the more slowly it will migrate. The conformation of DNA also affects its migration. A super-coiled plasmid will migrate faster than its nicked or linear forms as it adopts a tighter conformation and therefore occupies less space.

Agarose gels are used to analyse double stranded DNA fragments ranging from 70 bp (3% agarose) to 800 000 bp (0.1% agarose). For much smaller fragments (6-1000 bp) and for protein analysis, polyacrylamide gels are used.

### 3.7.1 Agarose gel electrophoresis

Agarose (FMC, SeaKem®) stock solutions were prepared in 0.5x TBE (0.089 M Tris, 0.089 M boric acid, 0.002 M EDTA, pH 8.5) buffer at concentrations of 0.4%, 0.8% or 1.2% depending on the size of the fragments to be separated. The solutions were sterilised by autoclaving (121°C, 20 min). Fragment sizes ≥ 10 kb were analysed on 0.4% agarose gel, 2-10 kb on 0.8% agarose gel and ≤3 kb on 1.2% agarose gel. Gels were prepared by melting the agarose stock in a microwave oven. 20 ml of the melted agarose was then mixed with 2 µl of a 10 mg/ml EtBr solution. The mixture was poured in a gel tray with a 12-tooth well former and allowed to polymerise at 4°C for ≥ 30 min. Combs were removed when the gel had completely set.

The electrophoresis buffer was 0.5x TBE (0.089 M Tris, 0.089 M boric acid, 0.002 M EDTA, pH 8.5) mixed with 15 µl of a 10 mg/ml EtBr solution. DNA samples were loaded with 2 µl of bromophenol blue tracking dye. Molecular weight markers λII or λIII (Fermentas, SM0101 and SM0193) or GeneRuler™ DNA ladder mix (Fermentas, SM0333) were used in all electrophoretic runs using a Hoefer PS 500xdc power supply. The process was carried out at room temperature, at 80 V and a current of 21-28 mA, until the dye front reached the bottom of the gel. DNA sizes were determined from a standard curve generated from migration distances of known molecular weight size markers run on the same gel. The concentrations were estimated by comparing the intensity of the bands to bands of similar intensity and known concentration. Additionally, the DNA was quantified using the LabWorks Software Version 4.5. Gels were documented using the UVP BioDoc-It™ system. The gels recorded with the UVP BioDoc-It™ system were in no way digitally enhanced and the pictures in this dissertation are presented as they were recorded.

### 3.7.2 Low gelling agarose gel electrophoresis

Low gelling temperature agarose (FMC, Seaplaque®) was prepared in the same manner as normal agarose. Gels were run at 4°C at 80 V until the tracking dye reached the bottom edge of the gel. Successful separation of DNA bands was confirmed by viewing the gel under long wavelength ultraviolet (UV) light (366 nm) to prevent nicking of the DNA. The band of interest was excised from the gel with a scalpel blade and transferred to a sterile Eppendorf tube. The DNA was extracted from the agarose by melting at 65°C for 1 hr and then performing a phenol extraction (section 2.6.3) at room temperature. A further three phenol extractions were performed at 4°C followed by a chloroform extraction at room temperature. DNA was precipitated with salt and ethanol as described in section 2.6.1.1. Alternatively, if the DNA did not require purification, digestion was completed in the low gelling agarose.

### 3.7.3 The freeze-squeeze method of extracting DNA from agarose gels

(Adapted from Tautz and Renz, 1983)

DNA was digested with the appropriate restriction endonuclease and the fragments were then separated on a 0.8% agarose gel. The relevant fragment was excised from the gel with a scalpel while viewed under long wavelength UV light (366 nm). The gel slice was equilibrated in the dark with 10 volumes of 0.3 M sodium acetate (pH 7.0) containing 0.1 mM EDTA. The equilibration process was allowed 45 min with occasional shaking. The gel slice was then transferred to a 0.6 ml Eppendorf tube which had been punctured in the bottom and plugged with sterile glass wool. Prior to transfer, the tube had been washed by placing it in a 1.5 ml Eppendorf tube together with 150 µl of sterile $dH_2O$ and microfuging for 1 minute. The tube containing the gel slice was then placed in a fresh 1.5 ml Eppendorf tube and frozen at -20°C for 1 hr. The tubes were then centrifuged immediately at 4°C for 5 min. The DNA could be found in the 1.5 ml Eppendorf following this process and was purified with a phenol-chloroform extraction step,

precipitated, dried and re-suspended for further use as described in section 2.6.1 and 2.6.3 above.

### 3.8 Transformations

#### 3.8.1 *E. coli* standard $CaCl_2$ transformation

A 20 ml volume of pre-warmed LB supplemented with 0.5% glucose was inoculated with a 0.01 volume of an overnight culture of *E. coli*. The culture was incubated, shaking, at 37°C until an $O.D._{600}$ of 0.2-0.4 had been reached (generally 2 hrs). The flask was chilled in an ice-water slurry for 5 min and the cells were harvested in a pre-chilled Beckman JA-20 rotor at 10 000 rpm for 5 min at 4°C. The supernatant was discarded and the cells re-suspended in 10 ml of ice cold transformation buffer. The cell suspension was placed on ice for 15 min and re-centrifuged at 10 000 rpm for 5 min. The supernatant was decanted and the cells re-suspended in one-fifteenth of the original volume of transformation buffer. The cells were left on ice for 2-24 hrs in the cold room (4°C).

Aliquots of the cells were placed into sterile Eppendorf tubes and plasmid DNA was added and mixed with the cells by bubbling air through. The DNA-cell mixture was left on ice for 15 min to allow for diffusion. The cells were then heat-shocked at 42°C for 90 seconds. Pre-warmed LB (1.0 ml) was added to each tube followed by incubation at 37°C for 90 min to allow for phenotypic expression of the resistance genes. The cells were then spread onto LB-agar plates containing the appropriate selective agent and further incubated at 37°C overnight. Colonies were visible the following day for *E. coli* strains.

**3.8.2 High efficiency transformation protocol** (Adapted from Inoue *et al.,* 1990)

An overnight pre-culture of *E. coli* MM294-4 was used to inoculate 50 ml SOB with 500 µl. The culture was incubated at 37°C with vigorous shaking until an $0.D._{600}$ of between 0.6 and 0.7 was reached. The culture was placed on ice for 5

min and the cells were then collected by centrifuging at 6 000 rpm for 10 min at 4°C. The supernatant was decanted and the cells re-suspended in 8 ml of ice-cold TB buffer (Appendix B). After incubating for a further 10 min on ice, the cells were once again collected by centrifugation. The supernatant was decanted and the cells re-suspended in 4 ml of TB buffer. Dimethyl sulphoxide (DMSO) was added to a concentration of 7% and mixed by gentle swirling. The cells were incubated in an ice-water slurry for 10 min. Aliquots of 200 µl of cells were dispensed into Eppendorfs containing a small volume of DNA usually between 1 to 5 µl. The Eppendorfs were incubated on ice for 30 min and then transferred to a 42°C water bath for a 30 second heat shock. After adding 0.8 ml of SOC the cells were incubated at 37°C for 1 hr to allow for phenotypic expression of the resistance genes. The cells were then spread on selective LB-agar plates and incubated at 37°C overnight. Colonies were visible by morning.

### 3.9 Mutagenesis

Two approaches were utilised to identify and characterise Arr mutants with an altered MIC. The first was an *in vivo* approach that employed selective pressure. The second was an *in vitro* technique that was mediated by the polymerase chain reaction.

#### 3.9.1 *In vivo* selection for spontaneous mutants

*E. coli* transformants containing the original *arr* insert ligated to pQE31 (pQE31-*Bst*49) were inoculated in 5 ml LB supplemented with 100 µg/ml of ampicillin. They were left to grow overnight at 37°C. Ten separate transformants were utilised to obtain mutants of an independent origin. 0.1 ml of each pre-culture was spread onto two LB-agar plates. One LB-agar plate was supplemented with 100 µg/ml of ampicillin whereas the other with 100 µg/ml of ampicillin and rifampicin. Ampicillin was always included to maintain the plasmid. These LB-agar plates were incubated at 37°C for three days in a dark box. A pool of rifampicin resistant colonies was observed.

### 3.9.2 Polymerase chain reaction (PCR)-mediated *in vitro* mutagenesis

**(**Adapted from Leung *et al.,* 1989 and Cadwell and Joyce, 1991)

PCR was performed in a MJ MINI$^{TM}$ personal thermal cycler (Bio-Rad). The *arr* ORF, cloned into pGEM3Z(f-) (Promega), was used as a template. PCR reactions were carried out in a total volume of 50 µl as follows:

| **Component** | **Volume per reaction (µl)** | **Final Concentration** |
|---|---|---|
| 10x *Taq* buffer | 5.0 | 1x |
| 50 mM $MgCl_2$ | 1.5 | 1.5 mM |
| 10 mM dNTP mix | 1.0 | 200 µM each |
| *Taq* DNA polymerase | 0.25 | 1.25 Units |
| DMSO | 2.0 | 4 % |
| Forward primer | 2.0 | 100-500 nM |
| Reverse primer | 2.0 | 100-500 nM |
| Sterile water | 34.25 | |
| DNA template | 2.0 | |
| **TOTAL** | **50 µl** | |

Mutagenic PCR was utilised to introduce random point mutations into the *arr* ORF. It exploits the elevated error rate of *Taq* polymerase in the presence of high $MgCl_2$ (10 mM) without significantly decreasing the level of amplification achieved in the PCR. Additionally, 0.5 mM $MnCl_2$ was added to the reaction mixture. Error-prone PCR is similar to random chemical mutagenesis with the added advantage that the chosen primer pair provides a convenient way to target the random base pair mutations to a defined segment of DNA.

The PCR reaction was performed under the conditions indicated in **Table 8**. Thirty amplification cycles were carried out. DMSO was included when the wild-type recombinant plasmid was being amplified because it increases the specificity of the reaction. This resulted in the amplification of a region of the *arr* gene

constituting 432 bp. The reaction utilised 5′-GTGGTGGCGAATCCGCCGAAA-3′ and 5′-CTAGTCATAGATGACCGCGAG-3′ as the forward and reverse primers respectively. Following PCR, the PCR product was subject to agarose gel electrophoresis to verify the amplification of the fragment of interest and to separate the amplified product from the reaction mixture.

**Table 8**: PCR conditions used to amplify the *arr* ORF

| Cycle | Temperature (°C) | Time (seconds) |
|---|---|---|
| **Cycle 1** | | |
| ▪ *Taq* polymerase activation | 95 | 180 |
| **Cycle 2** | | |
| ▪ Denaturation | 95 | 30 |
| ▪ Annealing | 60 | 40 |
| ▪ Extension | 72 | 30 |
| **Cycle 3** | 4 | ∞ |

### 3.10 Protein Analysis

#### 3.10.1 Protein quantification

Protein quantification was executed according to the Bradford method (1976). When Coomassie dye binds protein in an acidic medium, an immediate shift in absorption maximum occurs from 465 nm to 595 nm with a concomitant colour change from brown to blue. To a protein sample of 10 µl, 1 ml of the assay reagent was added. This was mixed and incubated at room temperature for 10 min. After incubation, the absorbance at $O.D._{595}$ was measured. Protein concentrations were determined from a standard curve generated with varying amounts of bovine serum albumin (BSA) to produce a linear curve, usually between 100-1 500 µg/ml.

### 3.10.2 Protein purification by metal affinity chromatography

This protein purification system is based on the selectivity of nickel-nitrilotriacetic acid (Ni-NTA) resin for recombinant proteins carrying a small affinity tag consisting of 6 consecutive histidine residues, the 6xHis tag.

#### 3.10.2.1 Growth of expression cultures

A fresh bacterial colony was used to inoculate 10 ml of LB supplemented with the appropriate selective agent (20 µg/ml kanamycin) for maintaining the plasmid. The culture was grown with gentle agitation at 37°C overnight. The non-induced overnight culture was diluted 1:60 with DYT medium supplemented with 20 µg/ml of kanamycin. This was incubated, shaking, at 37°C until the $O.D._{600}$ reached 0.6. Then, expression was induced by adding isopropyl-β-D-thiogalactoside (IPTG) to a final concentration of 0.9 mM. The culture was grown at 37°C for a further 3 hrs. Cells were harvested by spinning in a JA-10 rotor (Beckman) at 10 000 rpm for 15 min. For purification under native conditions, the minimum cell culture volume processed was 100 ml resulting in a 100x concentrated cell lysate.

#### 3.10.2.2 Protein purification under native conditions

The pellet was re-suspended in 1 ml lysis buffer. Lysozyme was added to 1 mg/ml and incubated on ice for 30 min. Sonication was conducted using the micro tip of a Vibra Cell (Sonics and Materials, Inc.) for 10 seconds repeating 6 times with 5 second pauses between each cycle. The sonication was performed over ice to prevent enzyme denaturation. The cell lysate was centrifuged at 20 000 rpm for 25 min at 4°C. The supernatant was collected. The Ni-NTA spin columns were equilibrated with 600 µl of lysis buffer. The spin columns were centrifuged with an open lid for 2 min at 2 000 rpm. 600 µl of the cleared lysate containing the 6xHis-tagged protein of interest was loaded onto the pre-equilibrated spin columns. These were centrifuged with a closed lid for 4 min at 2 000 rpm. The flow through was collected. The spin columns were washed three times with 600

µl of wash buffer (Appendix B). The wash fractions were also collected for analysis by SDS-PAGE to ascertain the stringency of the wash conditions. The fusion protein was then eluted twice with 100 µl of elution buffer (Appendix B). The eluate was collected after centrifugation at 2 000 rpm for 2 min.

### 3.10.3 Sodium dodecyl sulphate-polyacrylamide gel electrophoresis (SDS-PAGE)

This method is used to determine both the molecular weight and quantity of proteins. The molecular weight is determined by comparing the migration distances of the protein bands to standards of known molecular weight run on the same gel. Similarly, the intensity of the protein bands reveals the protein quantities when compared to standard bands of known quantity on the same gel. As shape affects the mobility of macro-molecules through sieving-gels, macro-molecules of arbitrary structures, such as proteins, must be denatured to assume similar random coil shapes before any conclusive comparisons can be made from polyacrylamide gels. Sodium dodecyl sulphate (SDS) was used to denature the protein forming a stable, negatively charged complex. The amount of SDS in the complex depends only on the size of the protein, neither the charge nor sequence. Thus, using SDS gives an accurate size of the protein based on the migration distance when compared to those of standards of known size run on the same gel. Additionally, the protein was quantified using the Quantity One® Software Version 4.6. Gels were documented using the GS-800 calibrated densitometer (BioRad). The gels recorded with this system were in no way digitally enhanced and the pictures in this dissertation are presented as they were recorded.

#### 3.10.3.1 Preparation of samples for SDS-PAGE

*E. coli* protein extracts were prepared from 1.5 ml stationary phase cultures grown in 100 µg/ml ampicillin. The cells were harvested by centrifugation for 1 minute and washed twice with 1.0 ml sterile $dH_2O$. Then, they were re-suspended in 40 µl of $dH_2O$ and mixed with 40 µl 2x sample loading buffer (Appendix B) containing bromophenol blue as the dye marker. The samples were boiled for 10 min to lyse

the cells. Insoluble material was removed by centrifuging at room temperature for 2 min. 20 µl of each sample was loaded onto a 15% SDS-PAGE gel. Samples were electrophoresed at room temperature, at 80 V, until the dye front reached the bottom of the gel. The run time was ~ 60 min.

### 3.10.3.2 Preparation of gels for SDS-PAGE

Gels were prepared according to the method of Laemmli (1970). Resolving gels were 15% acrylamide and the stacking gels were 4% acrylamide prepared from an acrylamide: bis-acrylamide (30:0.8%) stock (Appendix B). 15 ml of the resolving gel mixture (6 ml acrylamide: bis stock solution, 5.04 ml deionised $H_2O$, 3.75 ml 1.5 M Tris-HCl (pH 8.8), 150 µl 10% SDS, 100 µl 10% APS and 10 µl TEMED) was poured into the gel cast, leaving a space of 3-4 cm from the top end of the glass plates, and overlaid with water-saturated-*n*-butanol to prevent gel exposure to oxygen. The gel was allowed to polymerise for 1 hr at room temperature. The overlay was poured off once the gel had polymerized. 10 ml of the stacking gel mixture (1.3 ml acrylamide: bis stock solution, 6.1 ml deionised $H_2O$, 2.5 ml 1.5 M Tris-HCl (pH 8.8), 100 µl 10% SDS, 50 µl 10% APS and 10 µl TEMED) was then prepared and added to the top of the resolving gel. A ten-tooth comb was inserted and the gel allowed to polymerize at room temperature. Once set, the comb was removed and the wells were rinsed and then filled with electrophoresis buffer before the samples were loaded. Electrophoresis was conducted using a BioRad® Mini-PROTEAN™ Vertical Electrophoresis Unit.

### 3.10.3.3 Staining and de-staining of SDS-PAGE gels

Following electrophoresis the gels were covered with 200 ml isopropanol fixing solution (Appendix B) and allowed to shake gently at room temperature for 30 min. The fixing solution was then discarded and the gel covered with Coomassie blue staining solution (10% (v/v) acetic acid; 0.006% (w/v) Coomassie brilliant blue G-250 (BioRad)). This fixes the proteins in the gel by denaturing them and binding the dye to the proteins. Staining was allowed to occur while the gel was shaken gently until the desired intensity was reached (≈ 2hrs). The staining

solution was then poured off and the gel destained in water: acetic acid: methanol (17:1.5:20) solution. The gel was left to destain overnight with gentle agitation. The gels were considered ready for photography when the background was clear.

### 3.10.3.4 Viewing and photography of gels

The gels were viewed with the UVP BioDoc-It$^{TM}$ system where UV light was used for agarose gels and white light was used for viewing of polyacrylamide gels. Attached to the UVP BioDoc-It$^{TM}$ is a Mitsubishi Thermal Printer (115/230V) which was used to photograph the gels. Polyacrylamide gels were also dried by placing the gel on two sheets of Whatman 3 MM filter paper and covering the top with saran wrap. The gel was dried by vacuum in a Bio-Rad Model 583 gel dryer for 1-2 hrs at 80°C. Dried gels could then be scanned for documentation. For protein size determinations, low molecular weight protein markers (Fermentas, SM1811) were run together with the samples. The size of the unknown protein was determined from a standard curve obtained by plotting the logarithm of the protein size against its $R_f$. Lines were fitted by linear regression analysis and molecular weights were obtained from the formula for the linear regression line.

## 3.11 Assay for enzymatic inactivation of rifampicin

Antibiotic resistance by bacteria result from the presence of inactivating enzymes, efflux pumps ejecting the antibiotics from the cytoplasm or the acquisition of extra-chromosomal genetic material in the form of plasmids or transposons. Antibiotic inactivation by enzymes can be easily assayed by the lysozyme-DNAse-RNAse (LDR) method of O'Hara et al, (1997). This method was developed to determine the activity of inactivating enzymes in intact cells. The lysozyme lyses the cell while the DNAse and RNAse digest the nucleic acids released from the cell. The advantage of the LDR method over others is its simplicity and time conservation. The method can be applied easily in clinical practice and may contribute to the selection of appropriate drugs for the treatment of a given bacterial infection.

### 3.11.1 *In vitro* plate inactivation assay by employing the LDR method

The assay for *in vitro* inactivation of rifampicin *E. coli* cultures was conducted with a plate inactivation assay technique. *E. coli* cultures were grown in 10 ml LB to which ampicillin (100 µg/ml) and rifampicin (5-10 µg/ml) had been added. The culture was incubated, shaking, at 37°C overnight. The cells were pelleted by centrifugation in a JA-20 rotor at 15 000 rpm for 5 min. The antibiotics were removed from the cells by washing twice with 2 ml sonication buffer (Appendix B). Each time the cells were pelleted by centrifugation at 15 000 rpm. After the final wash step, the pellet was re-suspended in 1 ml sonication buffer and the suspension was transferred to an Eppendorf tube. The micro tip of a Vibra Cell was used for sonication (Sonics and Materials, Inc.), for 10 seconds repeating 3-4 times. The sonication was performed over ice to prevent enzyme denaturation. The cell debris was removed by centrifugation for 1 minute at 15 000 rpm.

The clarified supernatant was transferred to a sterile Eppendorf tube, to which rifampicin and the appropriate co-factor required for enzyme activity was added. The preferred ADP-ribose donor substrate of the Arr enzyme is nicotinamide adenine dinucleotide (NAD), and nicotinamide adenine dinucleotide, reduced (NADH). Each inactivation assay included only rifampicin, only co-factor and neither rifampicin nor co-factor controls. The reaction was stopped after the desired incubation time of 24 hrs at 37°C by denaturing the thermostable enzyme with Proteinase K (300 µg/ml) at 56°C for 15 min.

Inactivation reactions were set up with the *E. coli* homogenate in µl as follows:

| | |
|---|---|
| Rifampicin (1 mg/ml) | 2.5 |
| NAD/NADH Co-factor | 25 |
| LDR solution (1 µg/ml each) | 5 |
| Cell homogenate | 235 |
| **TOTAL** | **267 µl** |

A rifampicin sensitive assay organism, *B. subtilis* 1A3-1, was diluted 1:100 and spread on a LB plate solidified with half the normal amount of agar containing 200 μg/ml of spectinomycin. Wells were made in the plate using the broad end of an ethanol-flamed sterilized Pasteur pipette. 65 μl of the rifampicin-containing reaction mixture (for the *in vitro* inactivation assays) or culture (for the *in vivo* inactivation assays) was then added to the wells (after appropriate labelling) and the plate was incubated at 4°C for 4 hrs to allow for diffusion of the antibiotic. Following this, the plate was incubated for a further 4-5 hrs at 42°C or until the zones were clearly defined. Alternatively, the plate was incubated overnight at 32°C as soon as the cultures had been added to the wells. A measure of rifampicin inactivation was obtained from the size of the zones of inactivation that were visible on the plate when compared to the control (no cell lysate in the reaction mixture).

### 3.12 Automated DNA sequencing

Automated DNA sequencing is based on the Sanger chain-termination sequencing method (1977). The primary difference between this and the manual sequencing method is that each of the four dideoxynucleotides (ddATP, ddCTP, ddGTP and ddTTP) is tagged with a different fluorescent molecule. Thus, each will emit a different colour fluorescent when excited by light. Sequencing was performed using the automated DNA sequencer ABI Prism$^{TM}$ 310 Genetic Analyser (PE Biosystems). The computer in this system converts the colours emitted by the ddNTPs to black, red, blue and green corresponding to the bases guanine, thymine, cytosine and adenine respectively.

#### 3.12.1 Preparation of DNA for sequencing

DNA was prepared using the GFX$^{TM}$ Micro Plasmid Prep Kit (Amersham Biosciences). This plasmid purification protocol is based on a modified alkaline-lysis procedure, followed by the binding of plasmid DNA to a glass fibre matrix under appropriate pH conditions. RNA, protein, dyes and low molecular weight impurities are removed by a medium-salt wash. Plasmid DNA is eluted in a low

ionic strength buffer, and then concentrated and desalted by isopropanol precipitation (Section 2.6.1.2).

*E. coli* colonies carrying the appropriate plasmid were inoculated into 1.5 ml LB medium and incubated for 16 hrs at 37°C. The cells were harvested by centrifugation at 16 000 rpm for 1 minute at room temperature. The bacterial pellet was re-suspended in 150 µl of solution I (100 mM Tris-HCl, pH 7.5; 10 mM EDTA) containing 400 µg/ml RNAse A. Then, 150 µl of solution II (1 M NaOH, 1% SDS) was added. The solution was mixed gently by inversion and incubated at room temperature for 5 min. 300 µl of chilled solution III (3.0 M KAc, pH 5.5) was then added. The mixture was incubated on ice for 5 min. The cellular debris was separated from the supernatant by centrifuging at 16 000 rpm for 10 min. While the tube was spinning, a GFX column was prepared by placing it in a collection tube. The clear supernatant was transferred to the column and incubated at room temperature for 1 minute. The column was centrifuged for 30 seconds and the flow-through was discarded. The DNA was retained in the fibre matrix of the column and washed with 400 µl of washing buffer (Tris-EDTA) to remove all contaminants. The DNA was subsequently eluted with 100 µl TE buffer (Appendix B) and collected in a sterile 1.5 ml Eppendorf tube. The DNA was precipitated by the addition of 2 volumes of ethanol followed by centrifugation for 20 min at 4°C. The supernatant was decanted, the pellet air-dried for 15 min and re-dissolved in 100 µl sterile $dH_20$. After plasmid preparations, DNA concentration and purity were determined using quantitative analysis on a 0.8% agarose gel.

### 3.12.2 Sequencing performed by Inqaba Biotechnology Industries (Pty) Ltd

*E. coli* MM294-4 cells were transformed with pGEM-T-Easy carrying the appropriate insert. Plasmid DNA was prepared using the GFX™ Micro Plasmid Prep Kit (Amersham Biosciences). Then, digestions were performed to ensure the presence of the insert within a polylinker of the cloning vector. Transformants were streaked to single colonies on LB-agar plates supplemented with 100 µg/ml ampicillin. Plates were posted to Inqaba Biotechnology Industries (Pty) Ltd.

There, the purification of DNA template, sequencing reaction, sequence analysis and editing was completed. The sequencing included the Full Economic Sequencing Service.

### 3.12.3 Internet addresses for sequence analysis and database retrieval

Sequence analysis, ORF prediction and protein prediction were carried out with the help of the Internet programs listed in **Table 9** below.

**Table 9:** Internet addresses for sequence analysis programs and database access

| Program | World wide web site |
|---|---|
| **Sequence Analysis** | |
| BLAST | http://www.ncbi.nlm.nih.gov/BLAST/ |
| ExPASy | http://www.expasy.org |
| FASTA | http://www.ebi.ac.uk |
| FRAMEPLOT | http://www.nih.go.jp/~jun/research/frameplot/ |
| PROSITE | http://www.expasy.ch/ |
| WEBCUTTER | http://www.firstmarket.com/cutter/cut2.html |
| **Databases** | |
| EMBL | http://www.ebi.ac.uk |
| GENEBANK | http://www.ncbi.nlm.nih.gov/Genbank/ |
| SWISSPROT | http://www.expasy.ch/ |

# CHAPTER 4

# RESULTS

## 4.1 Mutagenesis Approach A

The first approach utilised to identify Arr mutants with an altered MIC was an *in vivo* technique that employed selective pressure.

### 4.1.1 *In vivo* selection for spontaneous mutants

A construct consisting of the *Bst*NI fragment of the *arr* gene cloned into the *Hind*III and *Bam*HI site of pQE31 (hereafter referred to as pQE31-*Bst*49) was developed. A double digestion of this construct was performed with *Hind*III and *Bam*HI. A 0.8% agarose gel confirmed the presence of the 560 bp insert. An *E. coli* MM294-4 transformant containing the intact construct was exposed to two environments: one where selective pressure was absent (100 µg/ml ampicillin) and the other where selective pressure was present (50 µg/ml rifampicin and 100 µg/ml ampicillin). The results are indicated in **Table 10** below.

**Table 10:** Rifampicin resistant clones obtained from *in vivo* selection

| Constructs | LB-agar supplement (µg/ml) | Number of rif resistant clones | | |
|---|---|---|---|---|
| | | 24 hrs | 48 hrs | 72 hrs |
| No DNA | ▪ 100 amp | 0 | 0 | 0 |
| control | ▪ 50 rif & 100 amp | 0 | 0 | 0 |
| pQE31 only | ▪ 100 amp | 602 | 604 | 605 |
| | ▪ 50 rif & 100 amp | 0 | 1 | 2 |
| pQE31-*Bst*49 | ▪ 100 amp | 600 | 601 | 606 |
| | ▪ 50 rif & 100 amp | 43 | 67 | 80 |

A few resistant clones, in the case of the vector only, were anticipated. This was owing to mutations in the chromosomal DNA of the host. The number of rifampicin resistant clones obtained from pQE31-*Bst*49 was due to leaky transcription from the T5 promoter of pQE31. This implied that mutations in the *arr* gene had not occurred. The conditions were manipulated to obtain such mutants. Two factors were varied: rifampicin concentration and number of cells. Firstly, the rifampicin concentration was increased to 100, 200 and 400 µg/ml. Secondly, the number of cells was decreased from 0.1 ml to 0.01 ml. After numerous trials, empirically-determined optimum conditions were established. Furthermore, mutants of an independent origin were required. Thus, ten separate *E. coli* MM294-4 colonies transformed with pQE31-*Bst*49 were utilised. This ensured phenotypic variation. The results are indicated in **Table 11** below.

**Table 11:** Rifampicin resistant clones obtained from *in vivo* selection under optimised conditions

| ***E. coli* colonies** | **Constructs** | **LB-agar plate environments (100 µg/ml amp) with varying rif** | **Number of rif resistant clones (mean % ± SD)[a]** | | |
|---|---|---|---|---|---|
| | | | **24 hrs** | **48 hrs** | **72 hrs** |
| **Clone 1** | pQE31-*Bst*49 | ▪ 100 | 80 ± 1.5 | 88 ± 2.1 | 88 ± 2.6 |
| | | ▪ 200 | 10 ± 0.6 | 12 ± 0.6 | 12 ± 0.7 |
| | pQE31 only | ▪ 100 | 0 | 1 ± 0.6 | 2 ± 0.6 |
| | | ▪ 200 | 0 | 0 | 1 ± 0.6 |
| **Clone 2** | pQE31-*Bst*49 | ▪ 100 | 79 ± 2.1 | 86 ± 1.1 | 86 ± 1.2 |
| | | ▪ 200 | 8 ± 0.6 | 8 ± 0.6 | 8 ± 0.6 |
| | pQE31 only | ▪ 100 | 0 | 0 | 1 ± 0.5 |
| | | ▪ 200 | 0 | 0 | 0 |
| **Clone 3** | pQE31-*Bst*49 | ▪ 100 | 78 ± 2.7 | 84 ± 2.1 | 85 ± 0.8 |
| | | ▪ 200 | 9 ± 0.6 | 10 ± 0.6 | 10 ± 0.6 |
| | pQE31 only | ▪ 100 | 0 | 2 ± 0.6 | 2 ± 0.6 |
| | | ▪ 200 | 0 | 1 ± 0.6 | 1 ± 0.6 |

| | | | | | |
|---|---|---|---|---|---|
| **Clone 4** | pQE31-*Bst*49 | ▪ 100 | 81 ± 1.5 | 88 ± 2.7 | 90 ± 2.1 |
| | | ▪ 200 | 5 ± 0.6 | 6 ± 0.6 | 6 ± 0.6 |
| | pQE31 only | ▪ 100 | 0 | 1 ± 0.6 | 3 ± 0.8 |
| | | ▪ 200 | 0 | 0 | 1 ± 0.6 |
| **Clone 5** | pQE31-*Bst*49 | ▪ 100 | 84 ± 3.8 | 90 ± 3.2 | 90 ± 0.8 |
| | | ▪ 200 | 5 ± 0.8 | 7 ± 0.8 | 7 ± 0.6 |
| | pQE31 only | ▪ 100 | 1 ± 0.6 | 1 ± 0.6 | 2 ± 0.6 |
| | | ▪ 200 | 0 | 0 | 1 ± 0.6 |
| **Clone 6** | pQE31-*Bst*49 | ▪ 100 | 79 ± 1.5 | 85 ± 2.1 | 85 ± 1.5 |
| | | ▪ 200 | 6 ± 0.8 | 8 ± 0.6 | 8 ± 0.6 |
| | pQE31 only | ▪ 100 | 1 ± 0.6 | 1 ± 0.6 | 1 ± 0.6 |
| | | ▪ 200 | 0 | 0 | 1 ± 0.6 |
| **Clone 7** | pQE31-*Bst*49 | ▪ 100 | 81 ± 1.5 | 89 ± 2.1 | 89 ± 4.4 |
| | | ▪ 200 | 10 ± 0.8 | 10 ± 1.0 | 10 ± 1.0 |
| | pQE31 only | ▪ 100 | 0 | 0 | 1 ± 0.6 |
| | | ▪ 200 | 1 ± 0.6 | 1 ± 0.6 | 1 ± 0.6 |
| **Clone 8** | pQE31-*Bst*49 | ▪ 100 | 82 ± 0.6 | 88 ± 1.5 | 89 ± 0.6 |
| | | ▪ 200 | 9 ± 0.6 | 10 ± 0.8 | 10 ± 0.6 |
| | pQE31 only | ▪ 100 | 0 | 0 | 1 ± 0.6 |
| | | ▪ 200 | 0 | 0 | 0 |
| **Clone 9** | pQE31-*Bst*49 | ▪ 100 | 79 ± 2.7 | 82 ± 0.6 | 84 ± 1.5 |
| | | ▪ 200 | 5 ± 0.8 | 5 ± 0.6 | 5 ± 0.6 |
| | pQE31 only | ▪ 100 | 0 | 0 | 3 ± 0.6 |
| | | ▪ 200 | 0 | 0 | 0 |
| **Clone 10** | pQE31-*Bst*49 | ▪ 100 | 85 ± 4.4 | 86 ± 1.5 | 86 ± 2.7 |
| | | ▪ 200 | 4 ± 0.6 | 5 ± 0.8 | 5 ± 0.6 |
| | pQE31 only | ▪ 100 | 0 | 1 ± 0.6 | 3 ± 0.6 |
| | | ▪ 200 | 0 | 0 | 1 ± 0.6 |

[a] Values are the means ± the standard deviation of data from duplicates of four sets of independent experiments.

The no DNA control for each clone was omitted from **Table 11** to prevent repetition as the result was consistent. No transformants were obtained as untransformed *E. coli* MM294-4 cells are susceptible to these antibiotics. Two environments were excluded for the same reasons. The ampicillin 100 μg/ml plates were not indicated as they all had on average 600 colonies. The rifampicin (400 μg/ml) and ampicillin (100 μg/ml) plates were excluded as no colonies were observed, even after 72 hrs. **Table 11** indicated that more mutants were obtained on the lower rifampicin concentration of 100 μg/ml. Furthermore, this environment had a higher ratio of additional colonies over the 72 hr time period than the 200 μg/ml rifampicin LB-agar plate. The resistant clones from both sets of LB-agar plates were pooled together and re-selected at 100 μg/ml rifampicin. A few resistant colonies were observed with the vector only control. This was due to chromosomal mutations in the host's DNA. Interestingly, more vector mutants also appeared on LB-agar plate supplemented with 100 μg/ml of rifampicin.

The mutants obtained may have been due to several factors: chromosomal mutations in the host cell, mutations in the *rpo*B gene, reduced antimicrobial permeability or mutations associated with the plasmid. The marker rescue technique was then performed to identify colonies that had arisen owing to plasmid-borne mutations.

### 4.1.2 Identification of plasmid-borne mutants via marker rescue

The marker rescue technique involved the following steps: the pool of rifampicin resistant clones was washed off and left to grow overnight at 37°C in 2 ml LB supplemented with 100 μg/ml ampicillin. A mini plasmid preparation of these clones was executed according to the alkaline-lysis method of Birnboim and Doly (1979). The DNA obtained was utilised to transform *E. coli* MM294-4 cells via the calcium chloride technique. A negative control consisting only of the vector, pQE31, was included. Colonies with plasmid-borne mutations were re-selected for on LB-agar plates supplemented with 100 μg/ml ampicillin and rifampicin. These LB-agar plates were incubated at 37°C for two days in a light-proof container. Growth was monitored every 24 hrs.

**Table 12:** Rifampicin resistant clones with plasmid-borne mutations identified via marker rescue

| *E. coli* colonies | Constructs selected for on LB-agar plates (100 µg/ml amp and rif)[a] | Average number of rif resistant clones (mean % ± SD)[b] | | | |
|---|---|---|---|---|---|
| | | Before marker rescue | | After marker rescue | |
| | | 24 hrs | 48 hrs | 24 hrs | 48 hrs |
| **Clone 1** | pQE31-*Bst*49 | 80 ± 1.5 | 88 ± 2.1 | 15 ± 0.6 | 18 ± 0.6 |
| | pQE31 only | 0 | 1 ± 0.6 | 0 | 0 |
| **Clone 2** | pQE31-*Bst*49 | 79 ± 2.1 | 86 ± 1.0 | 30 ± 0.8 | 32 ± 0.6 |
| | pQE31 only | 0 | 0 | 0 | 1 ± 0.6 |
| **Clone 3** | pQE31-*Bst*49 | 78 ± 2.7 | 84 ± 2.1 | 25 ± 1.5 | 28 ± 0.6 |
| | pQE31 only | 0 | 2 ± 0.6 | 0 | 1 ± 0.6 |
| **Clone 4** | pQE31-*Bst*49 | 81 ± 3.2 | 88 ± 2.7 | 23 ± 2.08 | 25 ± 0.6 |
| | pQE31 only | 0 | 1 ± 0.6 | 1 ± 0.6 | 1 ± 0.6 |
| **Clone 5** | pQE31-*Bst*49 | 84 ± 3.8 | 90 ± 3.2 | 18 ± 0.6 | 24 ± 0.6 |
| | pQE31 only | 1 ± 0.6 | 1 ± 0.6 | 0 | 0 |
| **Clone 6** | pQE31-*Bst*49 | 79 ± 1.5 | 85 ± 2.1 | 22 ± 2.7 | 28 ± 0.8 |
| | pQE31 only | 1 ± 0.6 | 1 ± 0.6 | 0 | 1 ± 0.6 |
| **Clone 7** | pQE31-*Bst*49 | 81 ± 1.5 | 89 ± 2.1 | 28 ± 0.6 | 30 ± 2.1 |
| | pQE31 only | 0 | 0 | 1 ± 0.6 | 0 |
| **Clone 8** | pQE31-*Bst*49 | 82 ± 0.6 | 88 ± 1.5 | 16 ± 1.5 | 21 ± 0.6 |
| | pQE31 only | 0 | 0 | 0 | 0 |
| **Clone 9** | pQE31-*Bst*49 | 79 ± 2.7 | 82 ± 0.6 | 18 ± 0.6 | 20 ± 0.8 |
| | pQE31 only | 0 | 0 | 0 | 1 ± 0.6 |
| **Clone 10** | pQE31-*Bst*49 | 85 ± 4.4 | 86 ± 1.5 | 23 ± 0.6 | 30 ± 1.0 |
| | pQE31 only | 0 | 1 ± 0.6 | 0 | 1 ± 0.6 |

[a] The ampicillin 100 µg/ml control plates were not indicated as they all had on average 600 colonies.
[b] Values are the means ± the standard deviation of data from duplicates of four sets of independent experiments.

The results obtained (**Table 12**) were utilised to establish the percentage of plasmid-borne mutants from the pool of rifampicin resistant clones acquired from *in vivo* selection. This was achieved by dividing the number of pQE31-*Bst*49 rifampicin resistant clones on the 100 µg/ml ampicillin and rifampicin LB-agar plate by all the pQE31-*Bst*49 transformants (600) on the control plate supplemented with only 100 µg/ml ampicillin. The results are indicated in the **Table 13** below.

**Table 13:** Percentage of plasmid-borne mutants obtained from *in vivo* selection

| ***E. coli* colonies (transformed with only the pQE31-*Bst*49 construct)** | **Average number of plasmid-borne rif resistant mutants (mean % ± SD)[a]** | |
|---|---|---|
| | **After marker rescue** | |
| | **24 hrs** | **48 hrs** |
| **Clone 1** | 2.5 ± 0.6 | 3.0 ± 0.6 |
| **Clone 2** | 5.0 ± 0.8 | 5.3 ± 0.6 |
| **Clone 3** | 4.2 ± 1.5 | 4.6 ± 0.6 |
| **Clone 4** | 3.8 ± 2.1 | 4.2 ± 0.6 |
| **Clone 5** | 3.0 ± 0.6 | 4.0 ± 0.6 |
| **Clone 6** | 3.6 ± 2.7 | 4.6 ± 0.8 |
| **Clone 7** | 4.6 ± 0.6 | 5.0 ± 2.1 |
| **Clone 8** | 2.6 ± 1.5 | 3.5 ± 0.6 |
| **Clone 9** | 3.0 ± 0.6 | 3.3 ± 0.8 |
| **Clone 10** | 3.8 ± 0.6 | 5.0 ± 1.0 |

[a] Values are the means ± the standard deviation of data from duplicates of four sets of independent experiments.

**Table 13** demonstrated that ≈4% of the original pool of rifampicin resistant mutations were plasmid-borne. This relatively small selection suggested a limited number of original clones. This percentile was significantly lower than a previous one obtained two years ago (data not shown). Roughly one quarter (23%) were plasmid-borne mutants and the remaining three quarters were *rpoB* or uptake mutants. The reason for this discrepancy remains unclear. However, the conditions were not manipulated during the latter experiment. Another possibility was the time at which the pre-culture was spread on the LB-agar plates. An active cell culture would have produced more rifampicin resistant clones than one at stationery phase. Although the marker rescue technique identified clones with plasmid-borne mutations, it was necessary to differentiate among the three types of mutations that occurred.

### 4.1.3 Plasmid copy number determination

The first type of mutation entailed alterations of the *copy number*, defined as the number of plasmids per cell. A high plasmid copy number, i.e. a high gene dosage, typically leads to high expression of plasmid-coded genes and to overproduction of recombinant proteins. Thus, the level of antibiotic resistance may be directly correlated to the vector copy number. As pQE31 is a low copy number plasmid, an increase in copy number may explain an increased level of resistance.

Clones from both 24 and 48 hr selection periods were chosen and streaked to single colonies. A mini plasmid preparation of each clone was performed according to the alkaline-lysis method of Birnboim and Doly (1979). The DNA was linearised overnight with *Bam*HI at 37°C. This digestion was performed to obtain an improved indication of the quantity of plasmid DNA as uncut DNA did not provide high resolution bands. The DNA was quantified using the LabWorks Software Version 4.5. The results are visible in **Figures 6, 7, 8** and **9**.

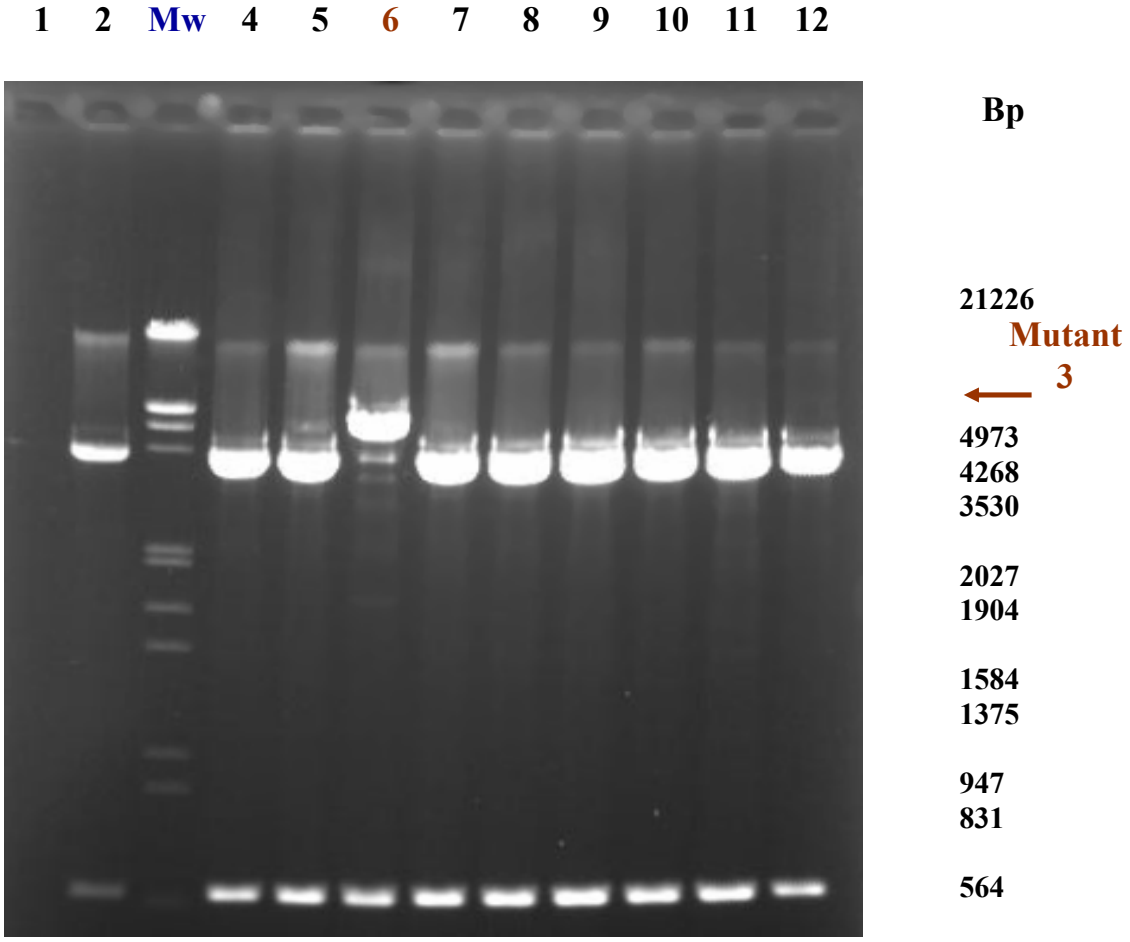


**Figure 6: Determination of plasmid copy number of mutants (1-9) obtained after 24 hrs from *in vivo* selection.** 0.8% agarose gel showing *E. coli* MM294-4 mutants after digestion with *Bam*HI. 20 µl of each sample was loaded in each lane in the following order: unmutagenised pQE31-*Bst*49 (2), mutant 1 (4), mutant 2 (5), mutant 3 (6), mutant 4 (7), mutant 5 (8), mutant 6 (9), mutant 7 (10), mutant 8 (11) and mutant 9 (12). **Mutant 3** showed a rearrangement of the plasmid resulting in a larger plasmid. It was excluded from further testing. The remaining 8 clones displayed an increase (≈4-fold) in copy number in comparison to the unmutagenised clone, pQE31-*Bst*49 (lane 2).

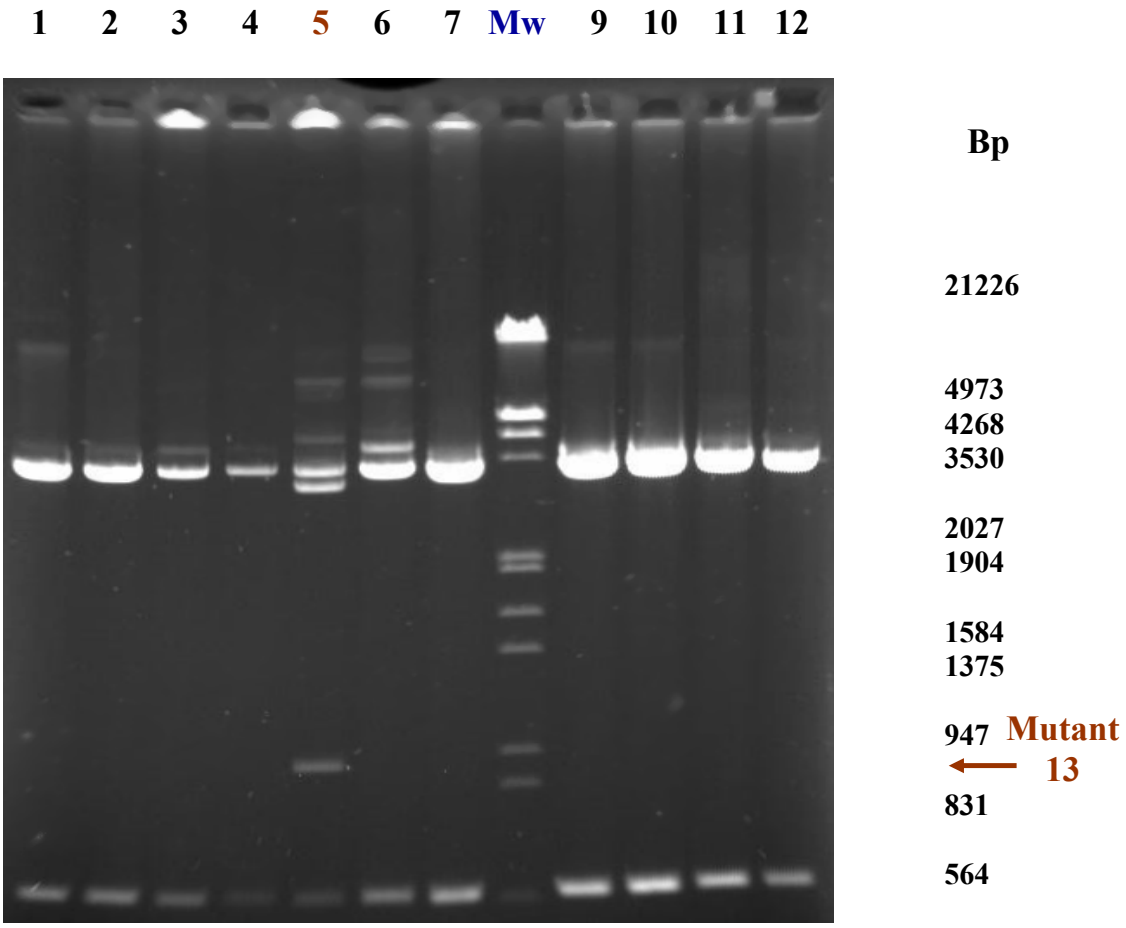


**Figure 7: Determination of plasmid copy number of mutants (10-19) obtained after 24 hrs from *in vivo* selection.** 0.8% agarose gel showing *E. coli* MM294-4 mutants after digestion with *Bam*HI. 20 µl of each sample was loaded in each lane in the following order: unmutagenised pQE31-*Bst*49 (1), mutant 10 (2), mutant 11 (3), mutant 12 (4), mutant 13 (5), mutant 14 (6), mutant 15 (7), mutant 16 (9), mutant 17 (10), mutant 18 (11) and mutant 19 (12). **Mutant 13** showed a rearrangement of the plasmid resulting in an additional fragment. It was excluded from further testing. Mutants 11 and 12 displayed a decrease (≈2-fold) whilst mutants 16-18 exhibited an increase (≈4-fold) in copy number in comparison to the unmutagenised clone, pQE31-*Bst*49.

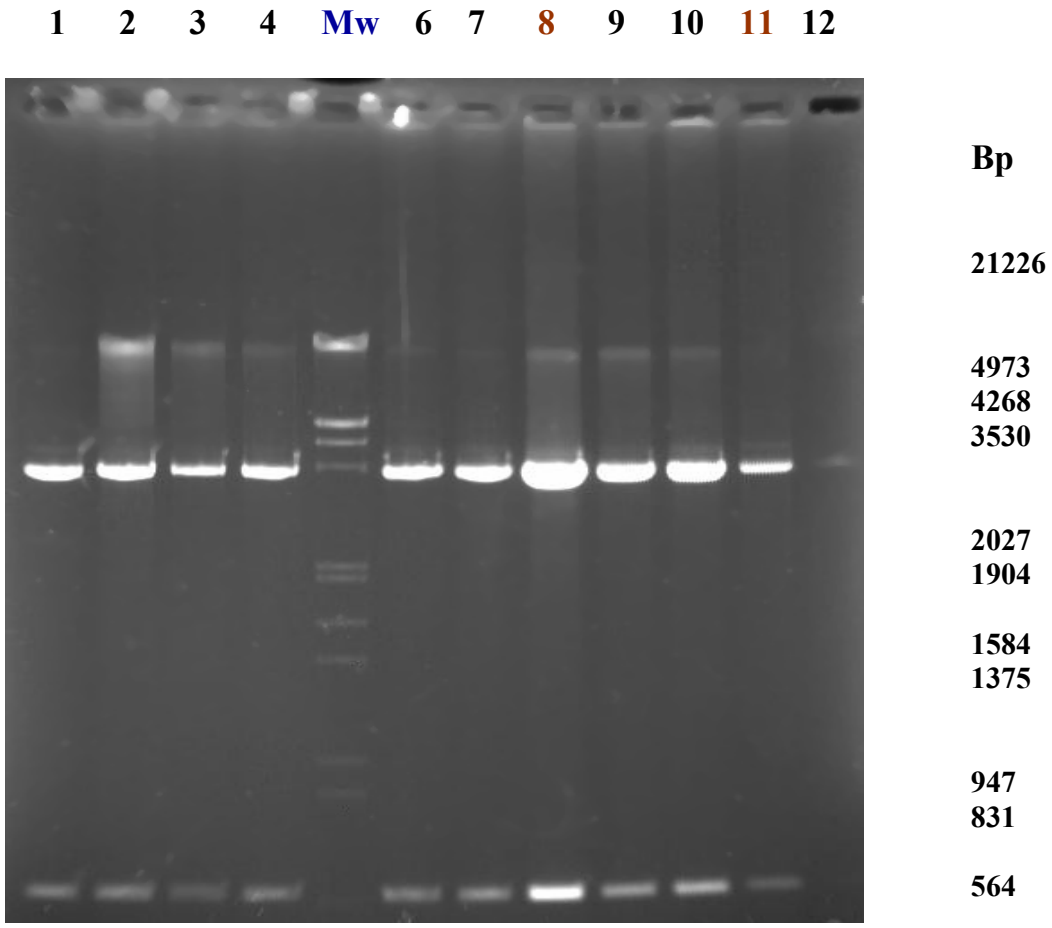


**Figure 8: Determination of plasmid copy number of mutants (1-9) obtained after 48 hrs from *in vivo* selection.** 0.8% agarose gel showing *E. coli* MM294-4 mutants after digestion with *Bam*HI. 20 µl of each sample was loaded in each lane in the following order: unmutagenised pQE31-*Bst*49 (1), mutant 1 (2), mutant 2 (3), mutant 3 (4), mutant 4 (6), mutant 5 (7), mutant 6 (8), mutant 7 (9), mutant 8 (10) and mutant 9 (11). No alteration in copy number was observed with the exception of mutants 6 (≈4-fold increase) and 9 (≈1-fold decrease) when compared to the unmutagenised clone, pQE31-*Bst*49.

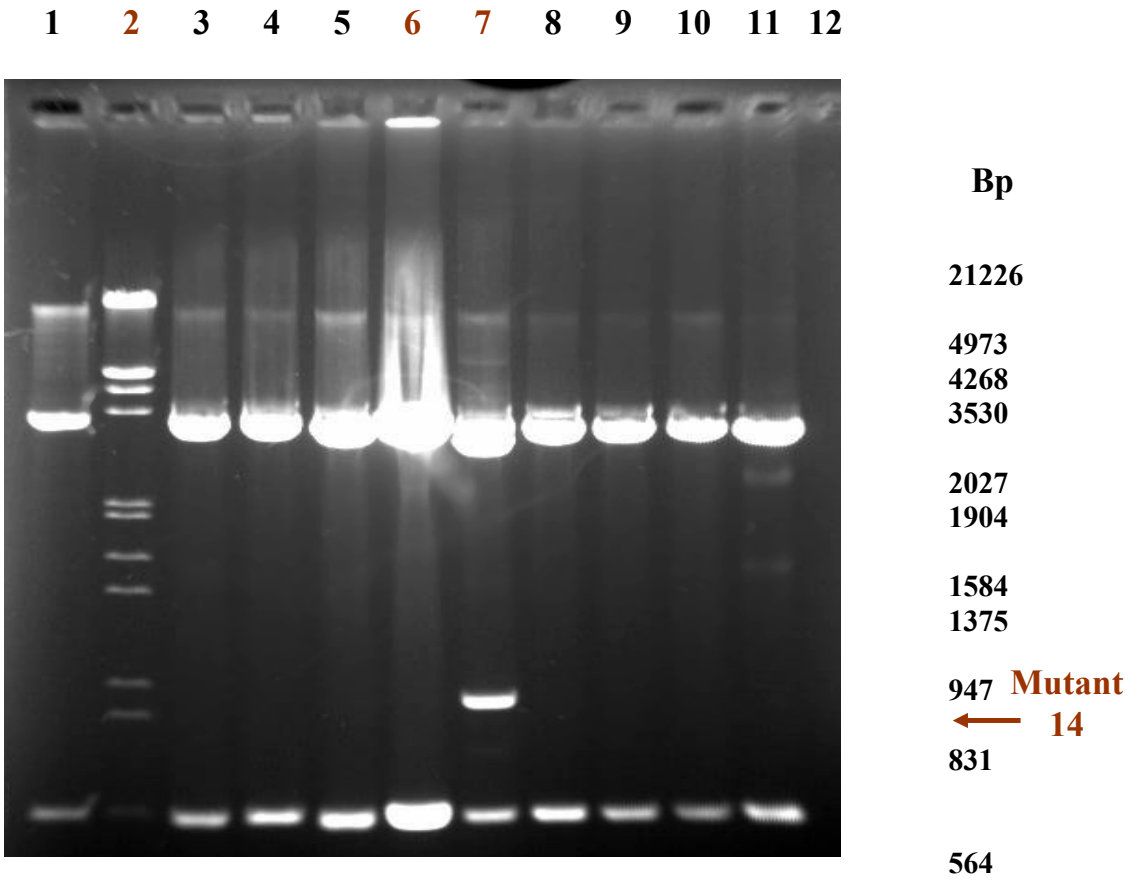


**Figure 9: Determination of plasmid copy number of mutants (10-18) obtained after 48 hrs from *in vivo* selection.** 0.8% agarose gel showing *E. coli* MM294-4 mutants after digestion with *Bam*HI. 20 µl of each sample was loaded in each lane in the following order: unmutagenised pQE31-*Bst*49 (1), mutant 10 (3), mutant 11 (4), mutant 12 (5), mutant 13 (6), mutant 14 (7), mutant 15 (8), mutant 16 (9), mutant 17 (10) and mutant 18 (11). **Mutant 14** showed a rearrangement of the plasmid resulting in an additional fragment. This clone was found to be identical to mutant 13 (**Figure 7**). This implied that *in vivo* selection may have represented a single mutational event. It was excluded from further testing. Mutant 13 displayed a considerable increase in copy number (≈6-fold) whereas the remaining mutants (with the exception of #17) showed ≈4-fold increase.

**Table 14:** Summary of alterations in plasmid copy number in mutants obtained after 24 and 48 hrs from *in vivo* selection

| Type of alteration in plasmid copy number | Mutants (#) that exhibited these alterations | | % of mutants with these alterations |
|---|---|---|---|
| | 24 hrs | 48 hrs | |
| No change | 10, 14, 15, 19 | 1, 3, 4, 5, 7, 8, 17 | 30 |
| Plasmid Rearrangement | 3, 13 | 14 | 8 |
| Lower copy number | 11, 12 | 2, 9 | 11 |
| Higher copy number | 1, 2, 4, 5, 6, 7, 8, 9, 16, 17, 18 | 6, 10, 11, 12, 13, 15, 16, 18 | 51 |

The majority of mutants displayed an increase (≈4-fold) in copy number. This was not as dramatic when compared to mutants obtained in my Honours work (data not shown), where the increase was 1000-fold. This was not due to variations in laboratory techniques as standard conditions were maintained throughout the experiments. Gel electrophoresis quantification is the most consistent assay for determining copy number. Other methods are characterised by the function of a gene product (usually an enzyme) coded by the plasmid. These are prone to errors due to production kinetics, turnover rate and protein denaturation.

To verify that the level of antibiotic resistance may be directly correlated to the vector copy number, the MIC of each mutant was determined. A spot test, with concentrations of rifampicin ranging from 0 to 400 µg/ml, was performed. Plates were incubated at 37°C for 24 hrs and the results are shown in **Figure 10** and **11**.

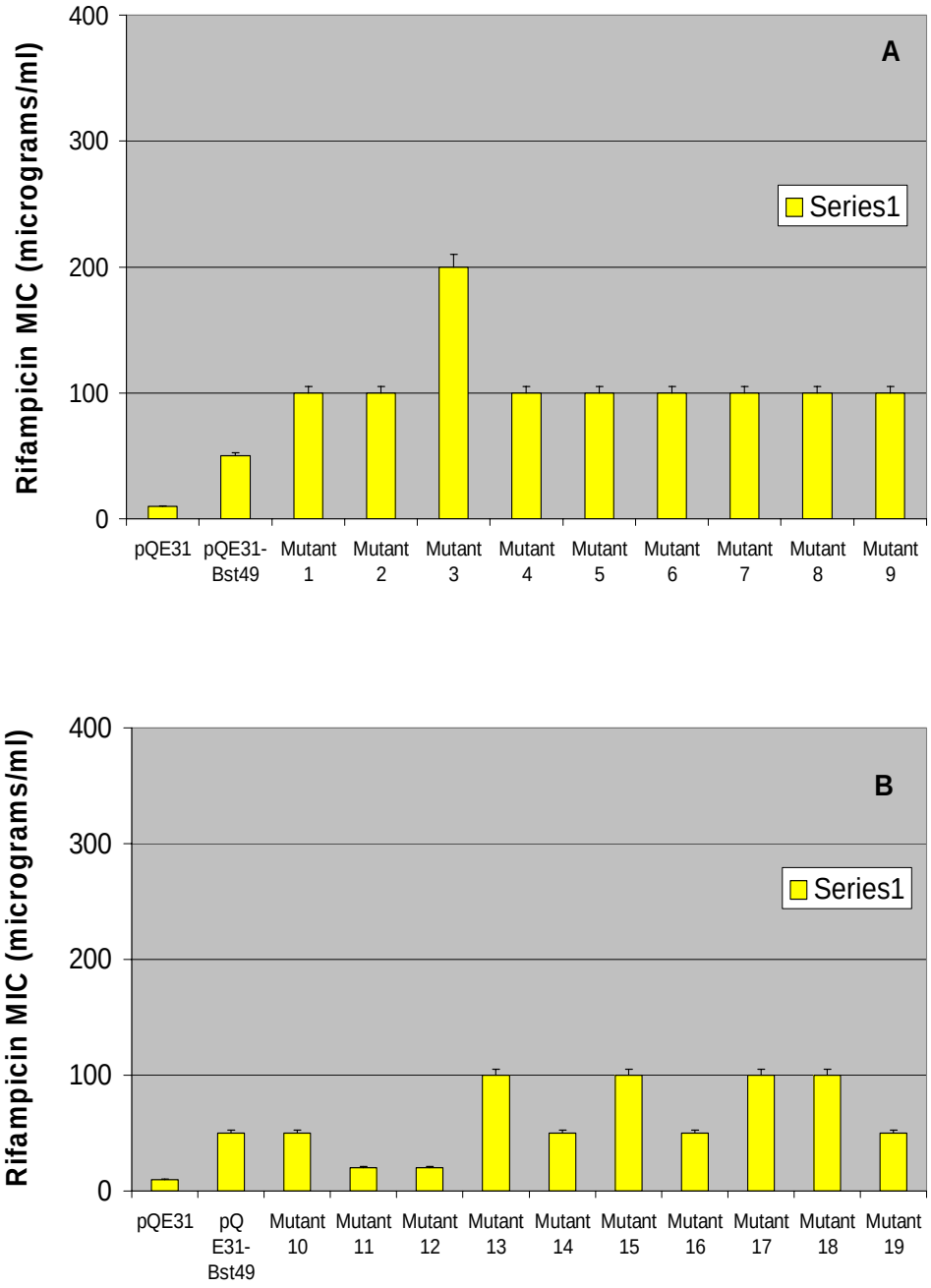


**Figure 10: MIC of (A) mutants (1-9) and (B) mutants (10-19) obtained after 24 hrs from *in vivo* selection in *E. coli* MM294-4 cells**. Each set of experiments was repeated three times. The columns represent the means of results from all four experiments. Standard deviations of the means are indicated by error bars.

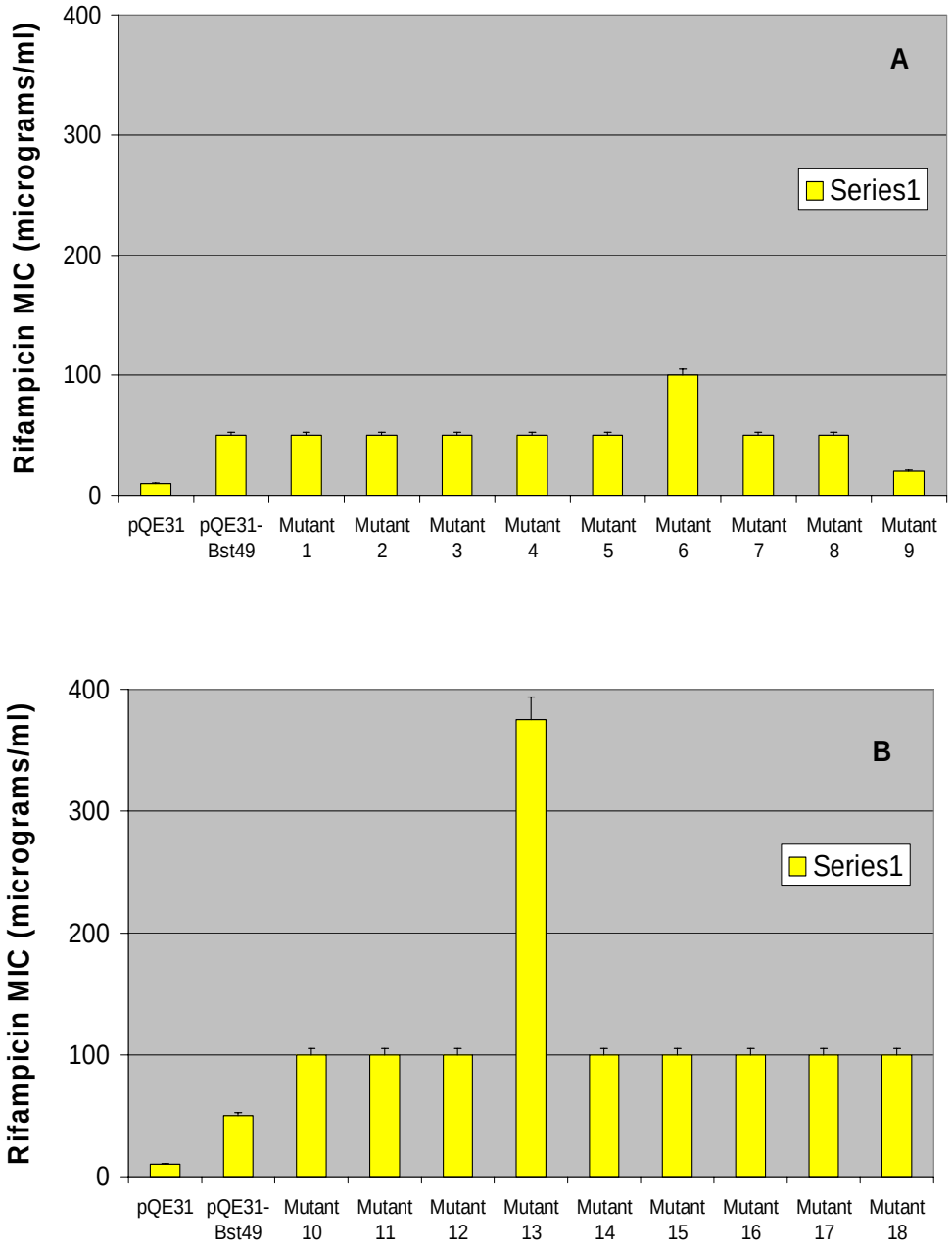


**Figure 11: MIC of (A) mutants (1-9) and (B) mutants (10-18) obtained after 48 hrs from *in vivo* selection in *E. coli* MM294-4 cells.** Each set of experiments was repeated three times. The columns represent the means of results from all four experiments. Standard deviations of the means are indicated by error bars.

An extremely high level of resistance (400 µg/ml) was displayed by mutant 13 that had a considerable increase in copy number (≈6-fold) (**Figure 9**). An intermediate level of resistance (100 µg/ml) was observed in all clones that had an increase in copy number of ≈4-fold. As pQE31 is a low copy number vector, a mutation in the plasmid resulted in an increase in copy number and consequently a higher resistance to the antibiotic. pQE31-*Bst*49 and the eleven mutants that showed no change in copy number conferred resistance up to 50 µg/ml of rifampicin. Four mutants with a lowered copy number had a maximum rifampicin resistance of 25 µg/ml. These results support the correlation of antibiotic resistance with vector copy number. These copy number mutants were not of interest because they related to plasmid replication. They were excluded from further testing.

### 4.1.4 Restriction fragment exchange

The mutants obtained from *in vivo* selection were further characterised to differentiate between the two remaining types of plasmid mutations. These included mutations associated with the promoter or the ORF. Promoter mutations are quite common and a large number have been well characterised. Rare ORF mutations would provide more valuable information about the active site of this enzyme. A technique known as restriction fragment exchange was performed to isolate clones with mutations in the ORF (**Figure 12**).

Large scale plasmid preparations of the pool of rifampicin resistant clones and that of pQE31-*Bst*49 were executed. Then, both constructs were digested overnight with *Bam*HI at 37°C. The smaller fragments, containing the *arr* ORF, were separated from the larger plasmid fragments of pQE31 by purification from a 1% low-melting agarose gel. After alkaline phosphatase treatment, the inserts were ligated to the relevant vectors and thus the fragments were exchanged. The DNA obtained was utilised to transform *E. coli* MM294-4 cells via the calcium chloride method. Selection occurred on LB-agar plates supplemented with 100 µg/ml ampicillin and rifampicin.

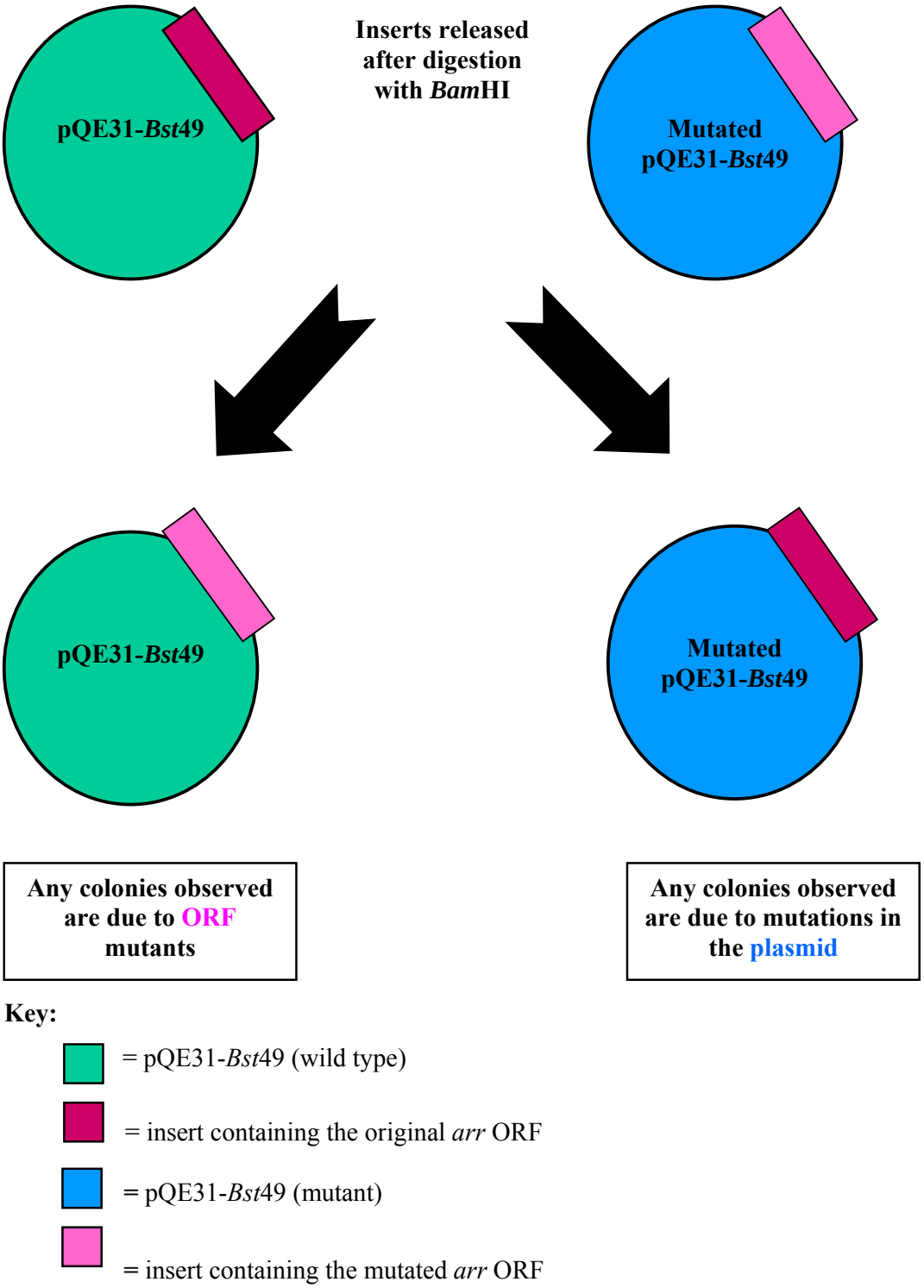


**Figure 12**: **Restriction fragment exchange between the wild type and mutant recombinant plasmids**

Transformants were analysed for the presence of inserts. This ensured that a confident representation had been attained. Numerous colonies containing the mutagenised plasmid ligated to the original *arr* insert were observed. They were classified as plasmid mutations possibly associated with the promoter. These were not of interest in terms of this project and were not investigated further. One colony containing the mutagenised *arr* insert ligated to pQE31 was identified as an ORF mutant. It was designated pMG. This clone was further characterised in order to analyse its enzyme characteristics in comparison to the wild-type, pQE31-*Bst*49. Later, DNA of both the mutated and wild-type *arr* ORFs was cloned into vector pGEM-T-Easy. These constructs were designated pMG1 and pGEM-T-Easy-*Bst*49.

## 4.2 Mutagenesis Approach B

The second approach utilised to identify and characterise Arr mutants with an altered MIC was an *in vitro* technique that was mediated by the polymerase chain reaction. *Taq* DNA polymerase lacks a 3′→5′ exonucleolytic editing activity. Consequently, it is an error-prone DNA polymerase with a measured error rate of $10^{-5}$ to $10^{-4}$ errors per nucleotide synthesized. Mutagenic PCR was utilised to introduce random point mutations into the *arr* ORF. It exploited the elevated error rate of *Taq* DNA polymerase by imposing imperfect reaction conditions.

### 4.2.1 PCR-mediated *in vitro* mutagenesis

The template DNA, pQE31-*Bst*49, was linearised with *Not*I. It was then amplified under standard as well as mutagenic PCR conditions. The PCR reactions were run on 0.8% agarose gels (**Figure 13**). Relevant controls comprising no template DNA, only the forward (Fw) primer and only the reverse (Rv) primer were included. The amplified *arr* inserts (both unmutagenised and mutagenised) were excised and purified. These PCR products had a single 3′-A overhang on each end because of the terminal transferase activity of the *Taq* DNA polymerase. Consequently, they were directly cloned into a linearised cloning vector, pGEM-T-Easy. This vector had single base 3′-T overhangs on each end. Thus, the complementary overhangs of the vector and the PCR products were hybridised by TA cloning. The recombinants were transformed into *E. coli* DH5α cells.

Selection occurred on LB-agar plates supplemented with 100 μg/ml ampicillin. Thirty minutes prior to use, 0.5 mM isopropyl-β-D-thiogalactoside or IPTG (induces *lac* repressor to disengage) and 80 μg/ml X-gal (chromogenic substrate that yields blue precipitate when hydrolysed by β-galactosidase) were spread on the LB-agar plates. The selection plates were left at 37°C for absorption to occur. White colonies indicated successful cloning because the inserted *arr* gene interrupted the coding sequence of β-galactosidase. Conversely, unsuccessful cloning was indicated by blue colonies that expressed functional β-galactosidase. Thus, α-complementation was utilised to identify recombinants by colour screening on indicator plates.

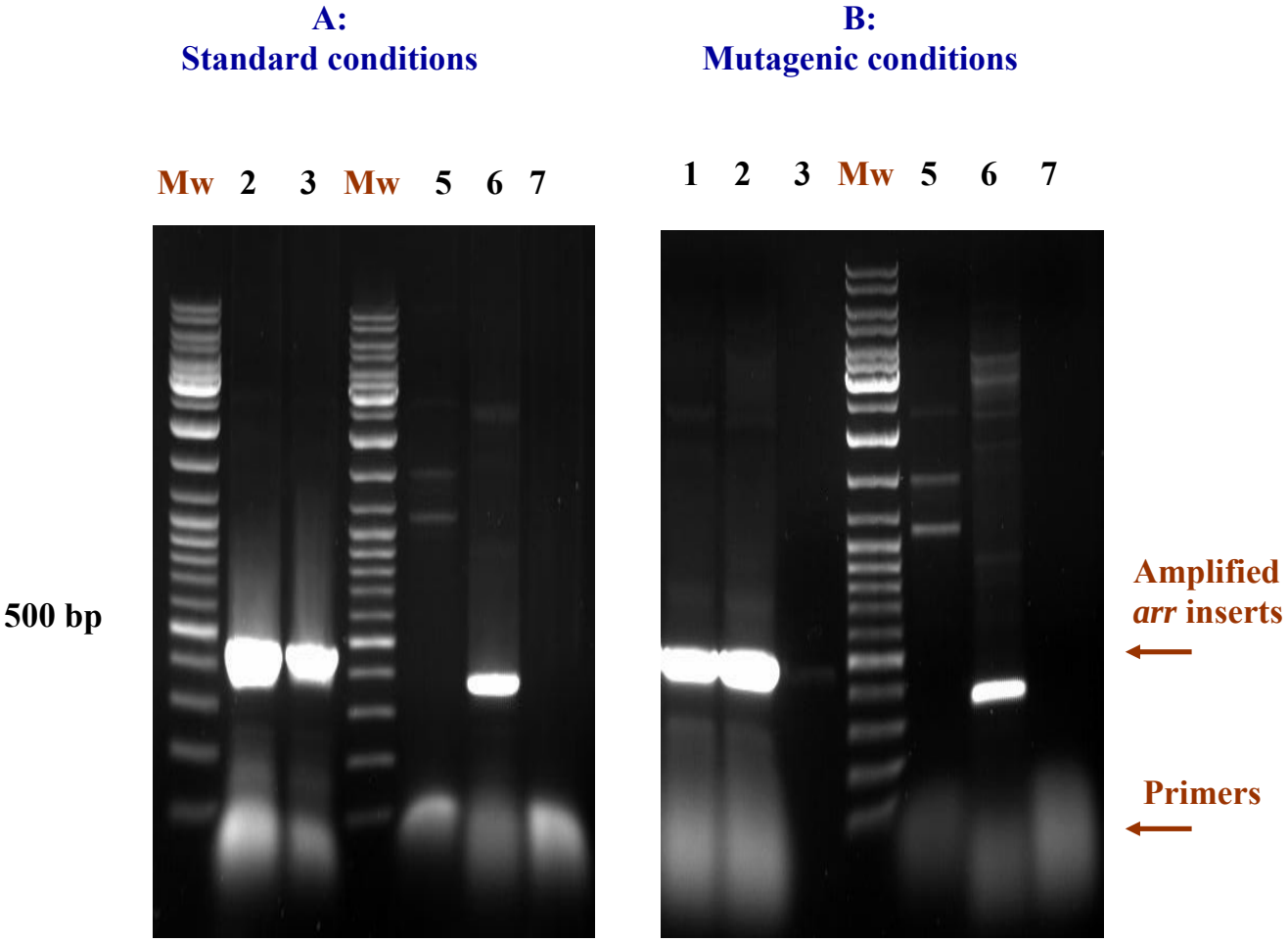


**Figure 13: PCR amplification of the *arr* gene under (A) standard and (B) mutagenic conditions.** 0.8% agarose gel showing (A): amplified *arr* inserts (2 and 3), only the Fw primer control (5), only the Rv primer control with non-specific amplification (6) and the no template DNA control (7). 0.8% agarose gel showing (B): amplified *arr* inserts containing random mutations (1 and 2), only the Fw primer control (5), only the Rv primer control with non-specific amplification (6) and the no template DNA control (7). The amplified *arr* inserts (both unmutagenised and mutagenised) were detectable at the 500 bp marker. The band indicating the vector pQE31 was not visible when recorded with the UVP BioDoc-It™ system.

The combined white colonies represented a mutant library. Here, random mutations within the *arr* gene were present. The difference in size observed with the transformants may have been a result of the orientation of the insert or of a particular mutation. Ten colonies were randomly selected. The presence of the insert within the polylinker of the cloning vector was confirmed by restriction digestion. After digestion with *Eco*RI, they were run on a 0.8% agarose gel. No false positives were obtained as each colony released an insert. These ten transformants were re-streaked to single colonies on LB-agar plates supplemented with 100 µg/ml ampicillin. Plates were posted to Inqaba Biotechnology Industries (Pty) Ltd. There, the purification of DNA template, sequencing reaction, sequence analysis and editing was completed. The sequencing included the Full Economic Sequencing Service. Following sequence analysis, three colonies containing mutated *arr* ORFs cloned into pGEM-T-Easy were identified. These constructs were designated pMG2, pMG3 and pMG4. These clones were further characterised to analyse their enzyme characteristics in comparison to the wild-type, pGEM-T-Easy-*Bst*49.

### 4.3 Sequence Analysis of ORF mutants

#### 4.3.1 Nucleotide sequence analysis

The *arr* gene sequences of pMG1 (obtained from *in vivo* selection), pMG2, pMG3 and pMG4 (obtained from PCR-mediated *in vitro* mutagenesis) were analysed by internet databases. All four were compared to the wild-type *arr* gene sequence using the **B**asic **L**ocal **A**lignment **S**earch **T**ools for nucleotide alignments (BLASTN) (Altschul *et al.,* 1990). The edited sequences of 432 bps were used as the input sequences for the BLASTN program. The default settings of the program were used to screen the November 7, 2006 non-redundant GeneBank database.

The BLASTN search results detected base substitutions for each mutant (**Figure 14**). The *arr* gene in pMG1 had a single base pair change from cytosine to adenine at position 16 on the direct strand. This transversion resulted in a codon change from CCG to ACG. Four base pairs downstream, a transition was detected in the *arr* gene in pMG2. Consequently, a codon change from AAA to AGA at position 20 on the direct strand or 412 on the reverse strand was observed. Two base pair changes were identified in the *arr* gene in pMG3. The first substitution was located at the same position (16 on the direct strand) as the base change detected in pMG1. Thus, it was not illustrated in **Figure 14**. However, the single base pair change was from cytosine to thymine. This transition resulted in a codon change from CCG to TCG. This first base change was not represented in **Figure 14** because it occurred at the same nucleotide as the mutation in pMG1. The second substitution was further downstream at position 317 on the direct strand or 155 on the reverse strand. Here, a thymine to adenine change resulted in a codon change from GTG to GAG. Two base pair changes were also discovered in the *arr* gene in pMG4. However, they were isolated to one codon. Both were transversions and resulted in a codon change from GTC to TAC.

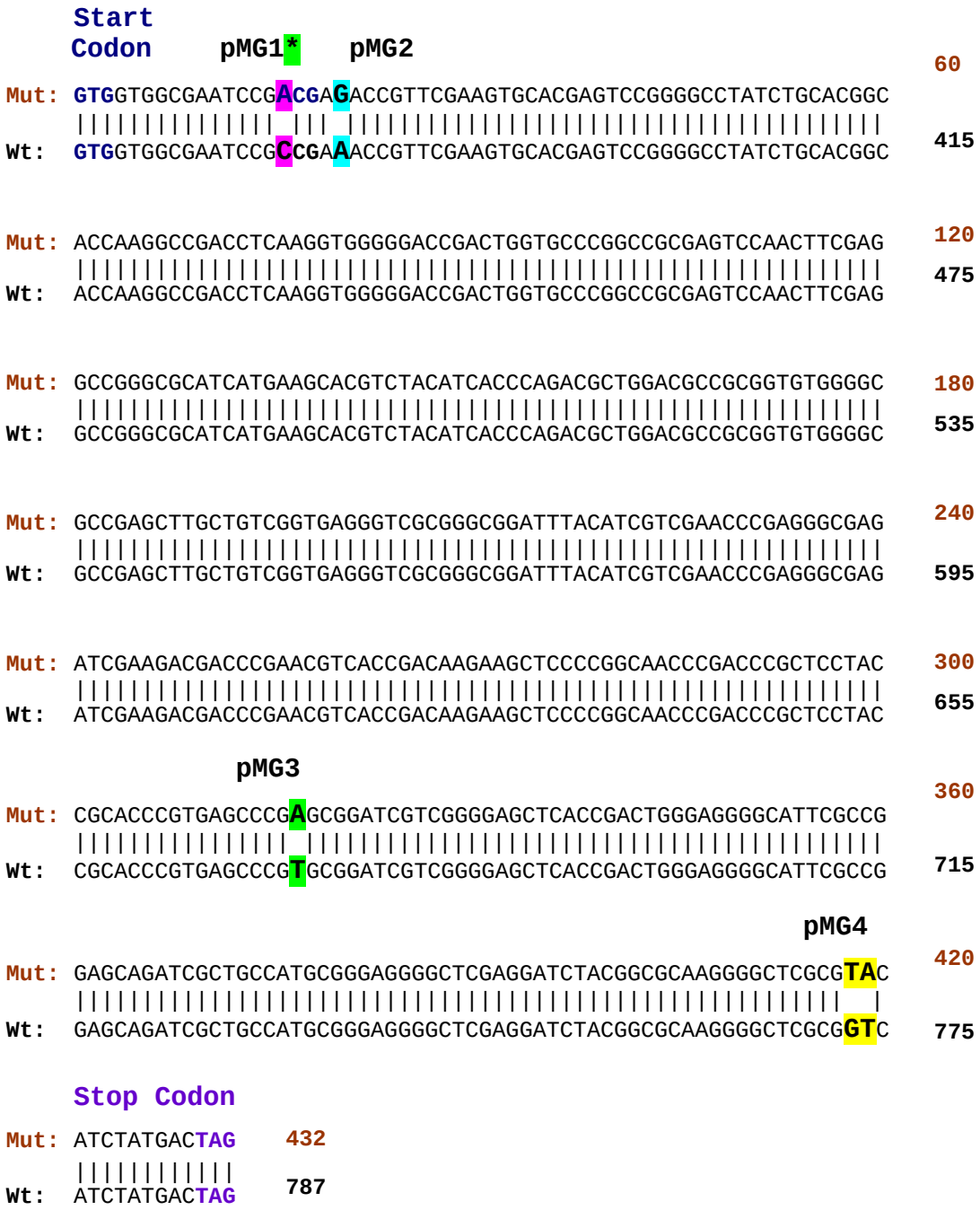


**Figure 14: Nucleotide alignment of the known *arr* gene sequence (wt) compared to its gene disrupted mutants using the BLASTN search programme.** *The first base pair change in pMG3, located at position 16 on the direct strand, was not illustrated. Here, cytosine changed to thymine.

### 4.3.2 Protein sequence analysis

All four mutant *arr* sequences were translated into proteins and then compared to the wild-type *arr* sequence using the **B**asic **L**ocal **A**lignment **S**earch **T**ools for protein data (BLASTP). The translated sequences were used as the input sequences for the BLASTP program. The default settings of the program were used to screen the November 8, 2006 non-redundant GeneBank database.

The BLASTP search results predicted amino acid substitutions for each mutant in the *arr* ORF (**Figure 15**). pMG1 had a predicted amino acid change of proline (P) to threonine (T). An alteration from lysine (K) to arginine (R) was observed in pMG2. Two amino acid changes were identified in pMG3. The first substitution was located at the same position as the amino acid change detected in pMG1. However, proline (P) was replaced by serine (S). The second substitution was further downstream, where a valine (V) was altered to a glutamic acid (E). pMG4 had a predicted amino acid change of valine (V) to tyrosine (Y).

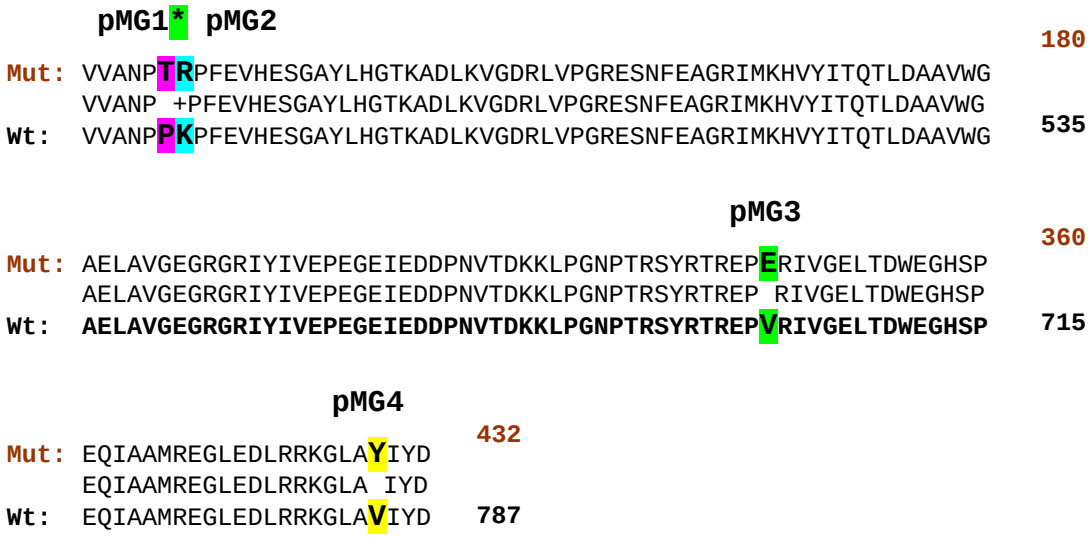


**Figure 15: Amino acid alignment of the known *arr* translated gene sequence (wt) compared to its gene disrupted mutants using the BLASTP search programme.** *The first amino acid change in pMG3 was not illustrated. Here, proline changed to serine.

pMG3 was excluded from further testing since two nucleotide alterations within the structural gene resulted in two predicted amino acid changes. This was indicated in **Figures 14** and **15**. Thus, one would be unable to distinguish which of the two mutations was responsible for the mutant phenotype. pMG4 also had two nucleotide alterations in the *arr* gene. However, these were located in one codon. Thus, the mutant phenotype would be as a result of this mutation and it was kept for further analysis. The results obtained from the nucleotide and protein sequence analyses are summarised in **Table 15** below.

**Table 15:** Summary of results obtained from nucleotide (BLASTN) and protein (BLASTP) sequence analyses

| **Mutant (size kDa)** | **Codon change** | **Type of mutation** | **Position (Fw strand)** | **Amino acid change** | | ***In vivo/in vitro* identification** |
|---|---|---|---|---|---|---|
| | | | | **Before mutation** | **After mutation** | |
| **pMG1** (15.89) | CCG→ACG | Transversion | 16 | Proline | Threonine | *In vivo* |
| **pMG2** (15.92) | AAA→AGA | Transition | 20 | Lysine | Arginine | *In vitro* |
| **pMG3*** (15.91) | CCG →TCG | Transition | 16 | Proline | Serine | *In vitro* |
| | GTG→GAG | Transversion | 317 | Valine | Glutamic acid | |
| **pMG4** (15.96) | GTC →TAC | Transversion | 418 | Valine | Tyrosine | *In vitro* |

* pMG3 was excluded from further testing.

### 4.3.3 Analysis of protein parameters

The translated sequences were used as the input sequences to conduct an analysis of the protein parameters using the ProtPar and ProtScale programmes from the **E**xpert **P**rotein **A**nalysis **S**ystem (ExPasy) engine.

**Table 16:** Protein parameters of pMG1 determined by the ProtPar programme

| | | | | |
|---|---|---|---|---|
| **Theoretical pI** | 5.29 | | | |
| **Instability index** | 26.35 → This classified the protein as stable | | | |
| **Aliphatic index** | 83.15 | | | |
| **Amino acid** | **Amino Acid** | **Symbol** | **Number** | **% composition** |
| **composition** | Alanine | A | 11 | 7.7 |
| | Arginine | R | 12 | 8.4 |
| | Asparagine | N | 4 | 2.8 |
| | Aspartic Acid | D | 9 | 6.3 |
| | Cysteine | C | 0 | 0.0 |
| | Glutamine | Q | 2 | 1.4 |
| | Glutamic Acid | E | 16 | 11.2 |
| | Glycine | G | 15 | 10.5 |
| | Histidine | H | 4 | 2.8 |
| | Isoleucine | I | 8 | 5.6 |
| | Leucine | L | 10 | 7.0 |
| | Lysine | K | 7 | 4.9 |
| | Methionine | M | 2 | 1.4 |
| | Phenylalanine | F | 2 | 1.4 |
| | Proline | P | 9 | 6.3 |
| | Serine | S | 4 | 2.8 |
| | Threonine | T | 8 | 5.6 |
| | Tryptophan | W | 2 | 1.4 |
| | Tyrosine | Y | 5 | 3.5 |
| | Valine | V | 13 | 9.1 |

From the data shown in **Table 16**, the total number of negatively charged residues, i.e. aspartic acid and glutamic acid was determined to be 25 (17.5%) while that of positively charged residues, arginine and lysine was 19 (13.3%). The above protein parameters were utilised to investigate the protein's hydrophobic/hydrophilic properties. This information may be useful for determining the cellular localisation of this protein. The Kyte and Doolittle (1982) scale of hydropathic characteristics of the twenty amino acids was used to plot a hydrophobicity plot. In this scale, hydrophobic amino acids are assigned a positive value while hydrophilic ones are assigned negative values. Thus, the most hydrophobic amino acid is isoleucine scoring 4.5 while arginine is the most hydrophilic with a score of -4.5. An amino acid window of 20 was taken to plot the graph shown in **Figure 16**. According to this graph, the protein is primarily hydrophilic with one major hydrophobic region spanning amino acids 52 to 65.

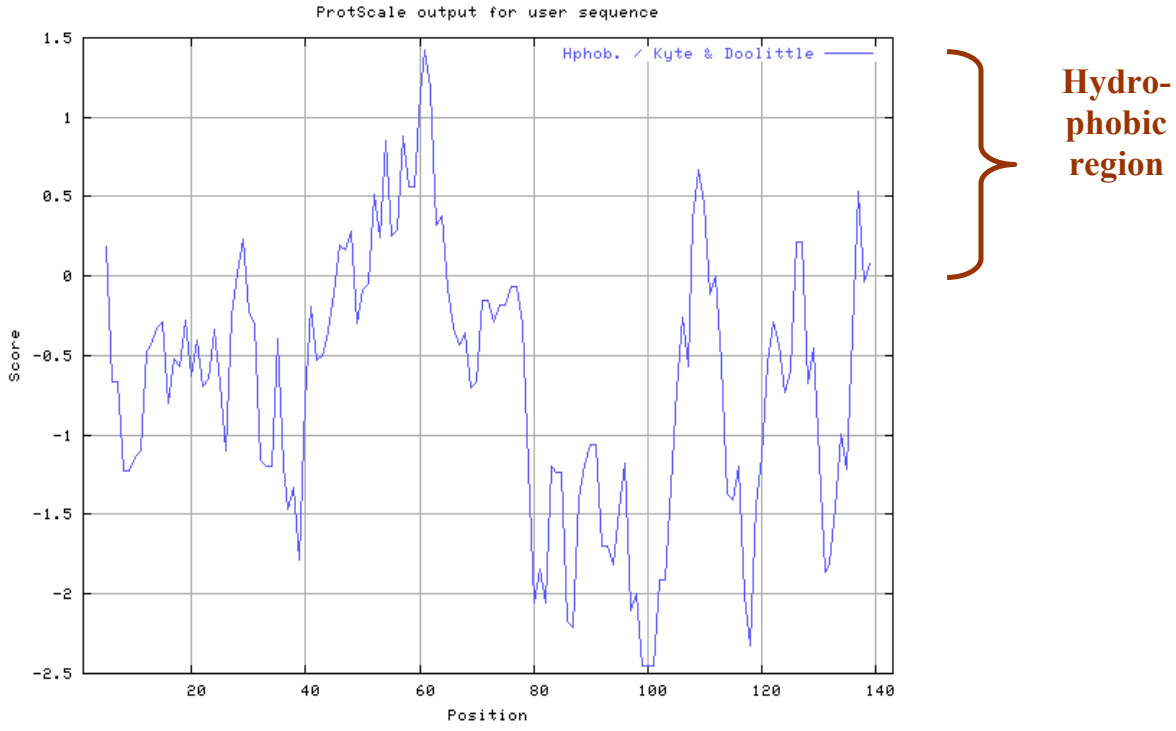


**Figure 16: Hydropathic characteristics of pMG1.** Kyte-Doolittle hydrophobicity plot showing a minimum hydrophilic amino acid of -2.46 at position 100 and a maximum hydrophobic amino acid of 1.42 at position 60.

**Table 17:** Protein parameters of pMG2 determined by the ProtPar programme

| | | | | |
|---|---|---|---|---|
| **Theoretical pI** | 5.29 | | | |
| **Instability index** | 29.05 → This classified the protein as stable | | | |
| **Aliphatic index** | 83.15 | | | |
| **Amino acid composition** | **Amino Acid** | **Symbol** | **Number** | **% composition** |
| | Alanine | A | 11 | 7.7 |
| | Arginine | R | 13 | 9.1 |
| | Asparagine | N | 4 | 2.8 |
| | Aspartic Acid | D | 9 | 6.3 |
| | Cysteine | C | 0 | 0.0 |
| | Glutamine | Q | 2 | 1.4 |
| | Glutamic Acid | E | 16 | 11.2 |
| | Glycine | G | 15 | 10.5 |
| | Histidine | H | 4 | 2.8 |
| | Isoleucine | I | 8 | 5.6 |
| | Leucine | L | 10 | 7.0 |
| | Lysine | K | 6 | 4.2 |
| | Methionine | M | 2 | 1.4 |
| | Phenylalanine | F | 2 | 1.4 |
| | Proline | P | 10 | 7.0 |
| | Serine | S | 4 | 2.8 |
| | Threonine | T | 7 | 4.9 |
| | Tryptophan | W | 2 | 1.4 |
| | Tyrosine | Y | 5 | 3.5 |
| | Valine | V | 13 | 9.1 |

From the data shown in **Table 17**, the total number of negatively charged residues, i.e. aspartic acid and glutamic acid was determined to be 25 (17.5%) while that of positively charged residues, arginine and lysine was 19 (13.3%). The above protein parameters were utilised to plot a hydrophobicity plot (**Figure 17A**).

**Table 18:** Protein parameters of pMG4 determined by the ProtPar programme

| | | | | |
|---|---|---|---|---|
| **Theoretical pI** | 5.29 | | | |
| **Instability index** | 27.70 → This classified the protein as stable | | | |
| **Aliphatic index** | 81.12 | | | |
| **Amino acid composition** | **Amino Acid** | **Symbol** | **Number** | **% composition** |
| | Alanine | A | 11 | 7.7 |
| | Arginine | R | 12 | 8.4 |
| | Asparagine | N | 4 | 2.8 |
| | Aspartic Acid | D | 9 | 6.3 |
| | Cysteine | C | 0 | 0.0 |
| | Glutamine | Q | 2 | 1.4 |
| | Glutamic Acid | E | 16 | 11.2 |
| | Glycine | G | 15 | 10.5 |
| | Histidine | H | 4 | 2.8 |
| | Isoleucine | I | 8 | 5.6 |
| | Leucine | L | 10 | 7.0 |
| | Lysine | K | 7 | 4.9 |
| | Methionine | M | 2 | 1.4 |
| | Phenylalanine | F | 2 | 1.4 |
| | Proline | P | 10 | 7.0 |
| | Serine | S | 4 | 2.8 |
| | Threonine | T | 7 | 4.9 |
| | Tryptophan | W | 2 | 1.4 |
| | Tyrosine | Y | 6 | 4.2 |
| | Valine | V | 12 | 8.4 |

From the data shown in **Table 18**, the total number of negatively charged residues, i.e. aspartic acid and glutamic acid was determined to be 25 (17.5%) while that of positively charged residues, arginine and lysine was 19 (13.3%). The above protein parameters were utilised to plot a hydrophobicity plot (**Figure 17B**).

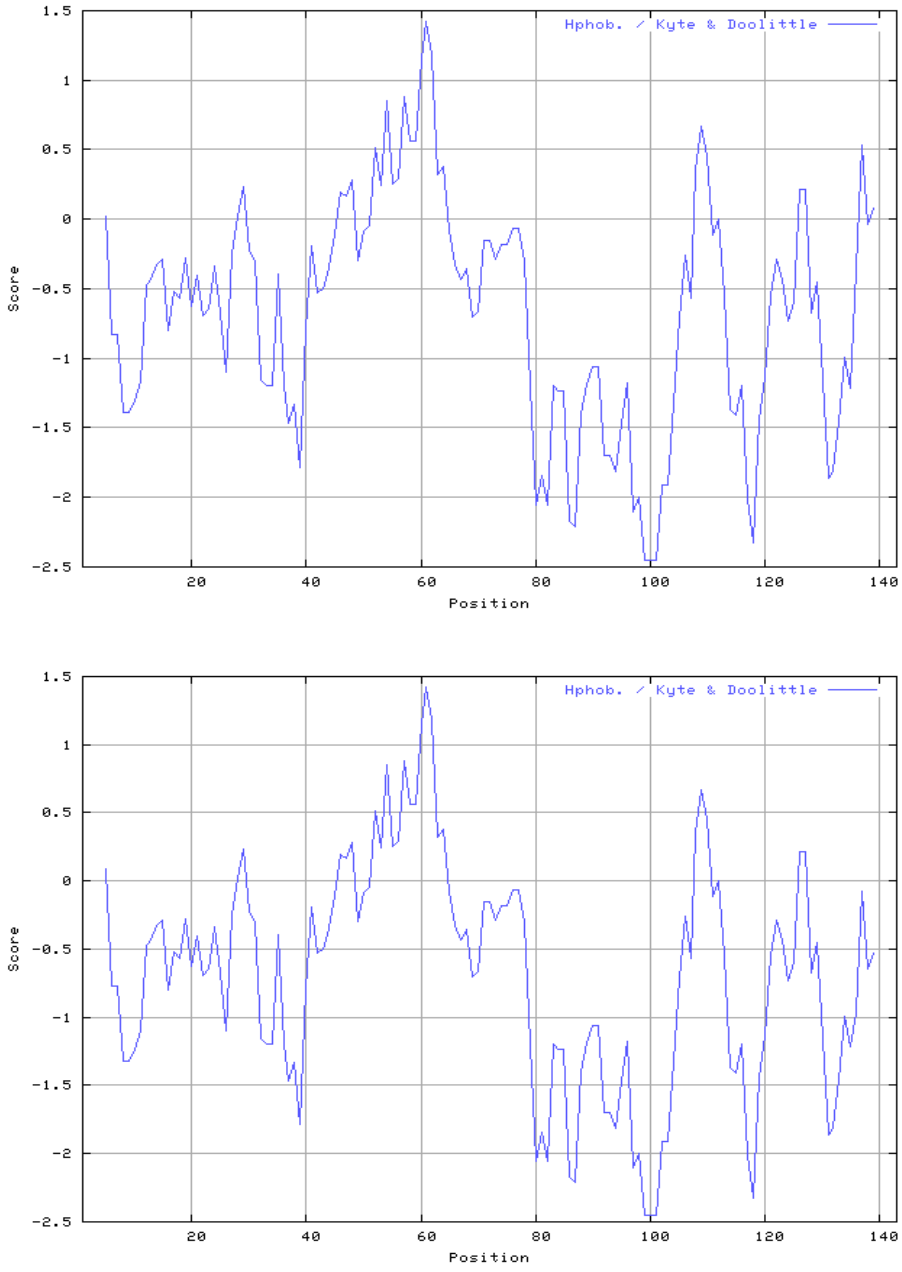


**Figure 17: Hydropathic characteristics of (A) pMG2 and (B) pMG4.** Kyte-Doolittle hydrophobicity plot showing a minimum hydrophilic amino acid of -2.5 at position 100 and a maximum hydrophobic amino acid of 1.42 at position 60. An amino acid window of 20 was taken to plot the above graphs. According to this graph, the proteins are primarily hydrophilic with one major hydrophobic region spanning amino acids 45 to 65. A change in hydropathicity caused by an alteration in amino acid composition is indicated by the red arrows.

## 4.4 Phenotypic characterisation of ORF mutants

### 4.4.1 Rifampicin phenotype of *E. coli* MM294-4 and DH5α cells transformed with ORF mutants

The MIC of each mutant was determined via a spot test with concentrations of rifampicin ranging from 0 to 400 µg/ml. Plates were incubated at 37°C for 24 hrs and the results are shown in **Figures 18A** and **18B**. In *E. coli* MM294-4 cells, pMG4 conferred resistance up to 200 µg/ml of rifampicin as opposed to 10 µg/ml for the vector only control. This indicated a 20-fold increase in resistance. pMG1 and pMG2 displayed a 2.5-fold increase in rifampicin resistance.

In *E. coli* DH5α cells, pMG4 conferred resistance up to 30 µg/ml of rifampicin as opposed to 5 µg/ml for the vector only control. This indicated a 6-fold increase in resistance whereas pMG1 and pMG2 displayed a 2-fold increase in rifampicin resistance. These phenotypes were established to determine the effect of the host strain on the level of antibiotic resistance. However, the results obtained did not provide a clear representation of this relationship because DH5α is a *rec*A- strain. RecA is a protein that is involved in the inactivation of the LexA repressor, making it essential for DNA repair and recombination. Consequently, DH5α cells grew too slowly for a comparison to be drawn between the two strains after 24 hrs. This comparison was abandoned and all future phenotypic characterisation occurred in *E. coli* MM294-4 cells. The effects of physical factors such as temperature and pH were investigated, both in the presence and absence of IPTG.

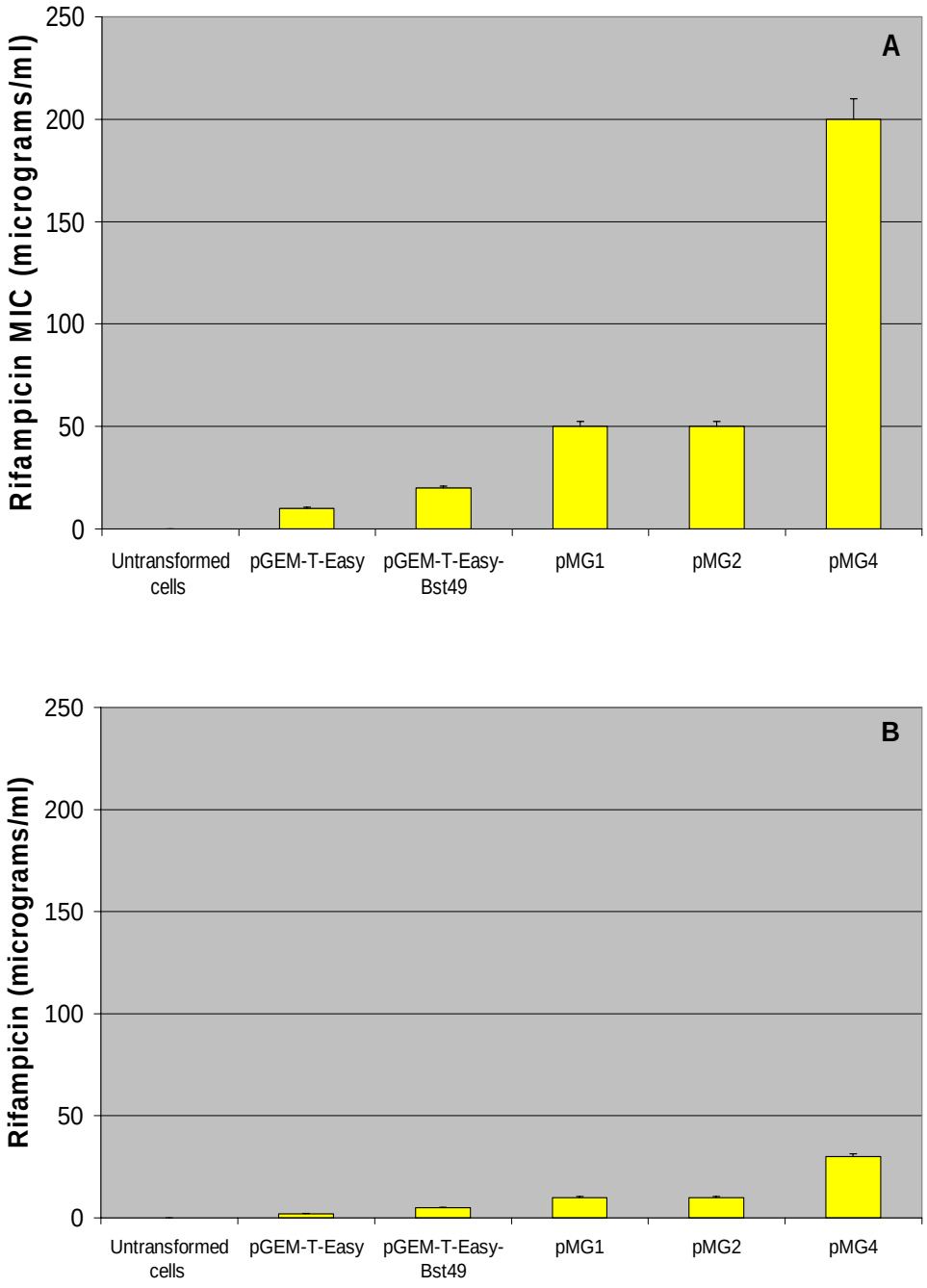


**Figure 18: Rifampicin MIC of ORF mutants obtained from *in vivo* selection and *in vitro* mutagenesis in *E. coli* (A) MM294-4 and (B) DH5α cells.** Each set of experiments was repeated three times. The columns represent the means of results from all four experiments. Standard deviations of the means are indicated by error bars.

### 4.4.2 Effect of temperature on rifampicin resistance

*E. coli* MM294-4 cells, transformed with the ORF mutants, were spotted onto increasing concentrations of rifampicin ranging from 0 to 400 µg/ml. The plates were incubated at 25°C, 35°C and 45°C for 24 hrs. The MIC of each mutant at varying temperatures was determined both in the presence (**Figure 19A**) and absence (**Figure 19B)** of IPTG. However, rifampicin resistance proved not to be IPTG inducible. The results indicated that at low temperature, the resistance was reduced. However, resistance by pMG4 was more sensitive to temperature change. This construct dropped by a factor of twenty whereas resistance conferred by pMG1 and pMG2 displayed a 5-fold decrease at 25°C, both in the presence and absence of IPTG. At 25°C, enzyme activity was inhibited probably due to problems with protein folding and protein stability. Thus, the rifampicin resistance phenotype in *E. coli* MM294-4 was determined to be cold-sensitive. At 45°C, a slight decrease in rifampicin resistance was observed by all three mutants when compared to 35°C.

### 4.4.3 Effect of pH on rifampicin resistance

The MIC of each mutant was determined via a spot test with concentrations of rifampicin ranging from 0 to 400 µg/ml. Plates used in these tests were made from LA whose pH had been adjusted to 5.5 using HCl or 8.5 using NaOH from the usual 7.0. The MIC of each mutant at varying pH was determined both in the presence (**Figure 20A**) and absence (**Figure 20B)** of IPTG. The results indicated that resistance was highest at neutral pH and lowest at acidic pH. pMG4 displayed a 1-fold increase in resistance at acidic pH, a 40-fold increase at neutral pH and a 24-fold increase at basic pH. The results for pMG1 and pMG2 were comparable at a 2-fold, 10-fold and 8-fold increase at pH 5.5., 7.0 and 8.5 respectively. At basic pH, the vector only control grew at higher concentrations of rifampicin than it did at acidic or neutral pH. For both temperature and pH, a 1.5-fold increase in resistance was observed with the vector only control in the presence of IPTG. No difference was displayed by the ORF mutants.

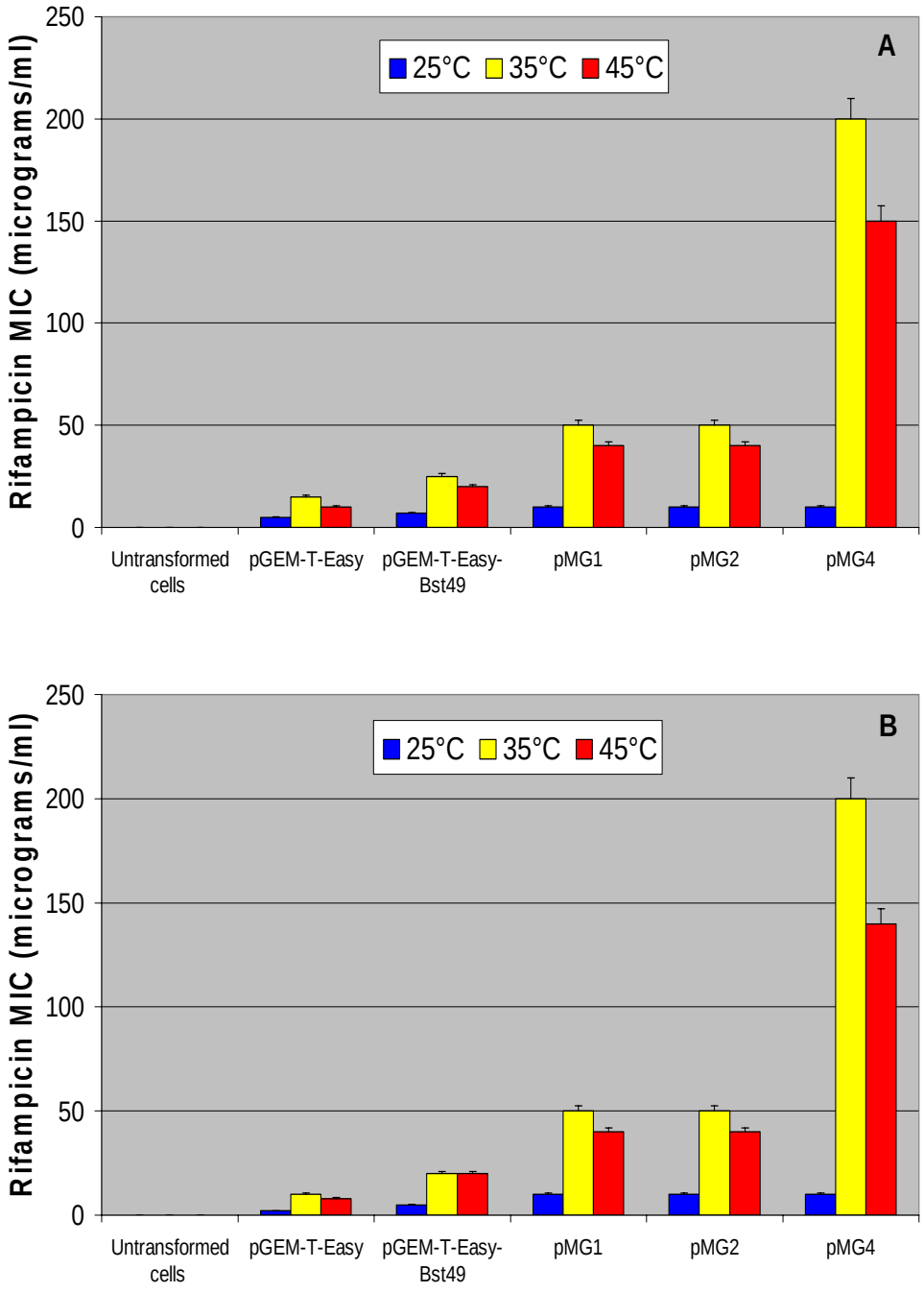


**Figure 19: Rifampicin MIC of ORF mutants at varying temperatures of 25°C, 35°C and 45°C both in (A) the presence and (B) absence of IPTG in *E. coli* MM294-4 cells.** Each set of experiments was repeated three times. The columns represent the means of results from all four experiments. Standard deviations of the means are indicated by error bars.

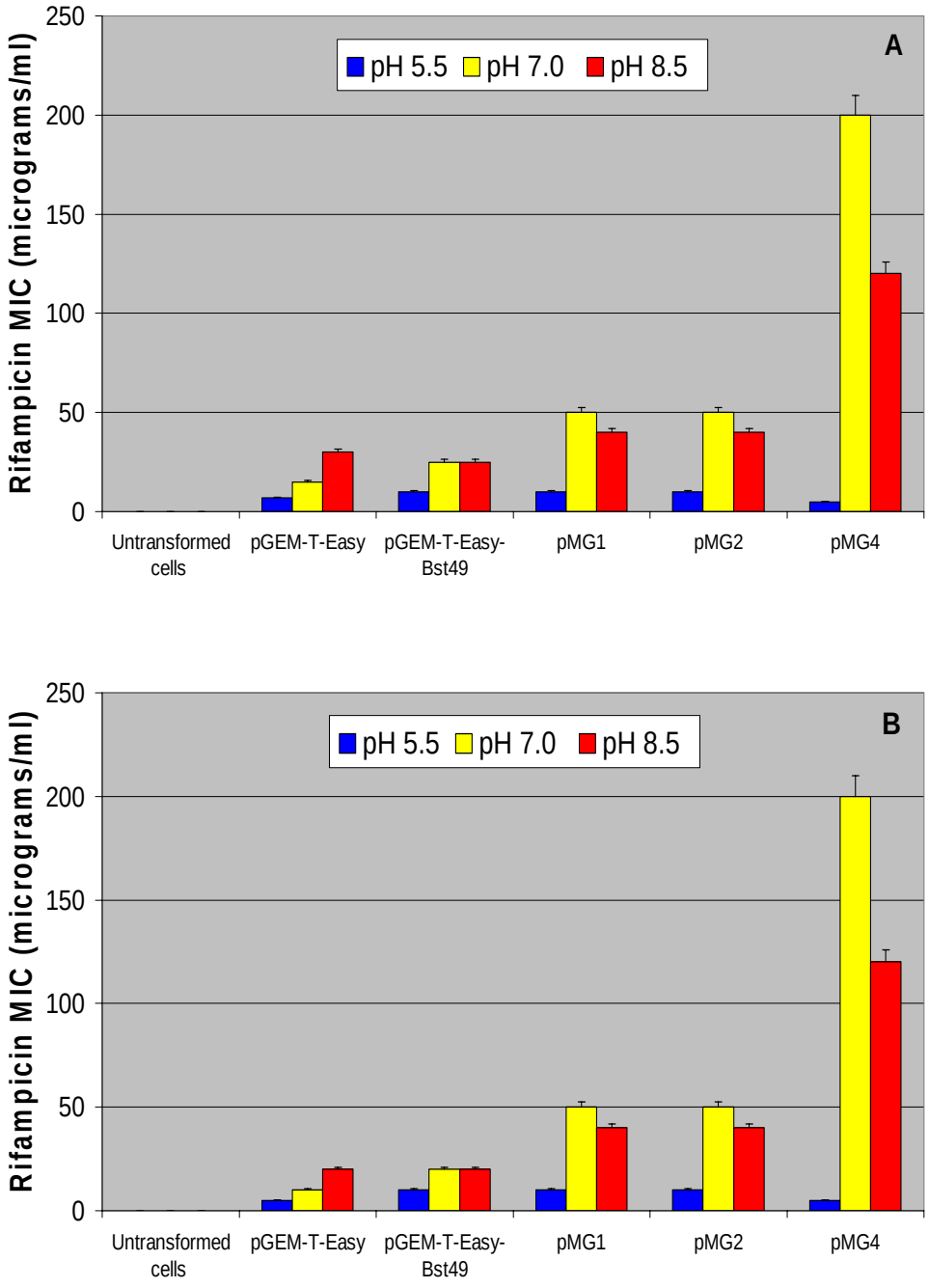


**Figure 20: Rifampicin MIC of ORF mutants at varying pH of 5.5, 7.0 and 8.5 both in (A) the presence and (B) absence of IPTG in *E. coli* MM294-4 cells.** Each set of experiments was repeated three times. The columns represent the means of results from all four experiments. Standard deviations of the means are indicated by error bars.

### 4.4.4 Effect of light on rifampicin resistance

The Arr ADP-ribosyltransferase is inhibited by white light. However, the effect of red and blue light was investigated, through the use of monochromatic light filters, and compared to the inhibition displayed when exposed to white light. The effect of light on the glycosyltransferase gene cloned from *N. brasiliensis* IFM 0236 was also examined.

*E. coli* MM294-4 cells, transformed with the relevant constructs, were spotted onto increasing concentrations of rifampicin ranging from 0 to 400 µg/ml. An LB-agar plate supplemented only with 100 µg/ml of ampicillin was included as a control. This verified that differences in MIC were due to the cloned inactivation genes as *E. coli* MM294-4 cell growth remains unaffected in the presence or absence of light. The plates were incubated at 37°C for 24 hrs. The MIC of each construct was determined in the absence of light (**Figure 21A**) and under white (**Figure 21B**), blue (**Figure 22A**) and red light (**Figure 22B**).

The results obtained indicated that all the control strains, those containing no inactivation genes, displayed a reduction in susceptibility to rifampicin in the presence of red and white light. The first control was a clone carrying a mutation in the *rpoB* gene that showed an increase in rifampicin resistance from 5 µg/ml to 20 µg/ml in the presence of red light and to 15 µg/ml in the presence of white light. The remaining control strains included *E. coli* transformed with the low copy number plasmid, pQE (20-30 copies per cell) and with the high copy number vectors, pGEM3Zf(-) and pGEM-T-Easy (both containing 300-700 copies per cell). All three demonstrated a reduction in susceptibility to rifampicin under white light (3-fold) and under red light (4-fold). Thus, the slight increase in rifampicin resistance displayed in the absence of inactivation genes was not affected by the vectors' copy number. This apparent reduction in susceptibility was due to inactivation of the antibiotic by bleaching. The highest resistance was observed under red light, which is in accordance with rifampicin's absorbance spectrum. Its absorbance maximum is greatest in the longer red wavelengths (480-580 nm) and rifampicin appears red when in solution.

The activity of the Arr ADP-ribosyltransferase, or at least its phenotype of rifampicin resistance, was completely abolished by white, red and blue light. pGEM3Z-*Bst*49 displayed a 20-fold increase in susceptibility. An increase was also observed for the ORF mutants of the Arr enzyme. pMG4 showed a 10-fold increase whereas pMG1 and pMG2 displayed a 2.5-fold increase in susceptibility. Interestingly, pQE31-*Bst*49 was not affected by light. The resistance to rifampicin remained constant at 20 μg/ml under all four conditions. A possible explanation for this difference was that the initial level of resistance was so low that a further reduction may not have been detectable.

The gene responsible for inactivating rifampicin via glucosylation, carried by the shuttle plasmid pDA71, is referred to as pCL1 and when in the reverse orientation, pCL2. pCL1 showed a slight reduction in resistance in the presence of light from 400 μg/ml to 350 μg/ml whereas pCL2 remained unaffected. This increase in susceptibility was not as dramatic as that of the Arr ADP-ribosyltransferase. It was also not a function of wavelength as similar results were obtained for red, blue and white light. However, the two inactivation genes may not be directly comparable because they are cloned into different vectors.

Crude cell extracts of the ADP-ribosyltransferase and the glycosyltransferase that inactivate rifampicin were prepared, both in the presence and absence of light, to ascertain if the proteins were inactive or simply not synthesized. The results are illustrated in **Figures 23** and **25**.

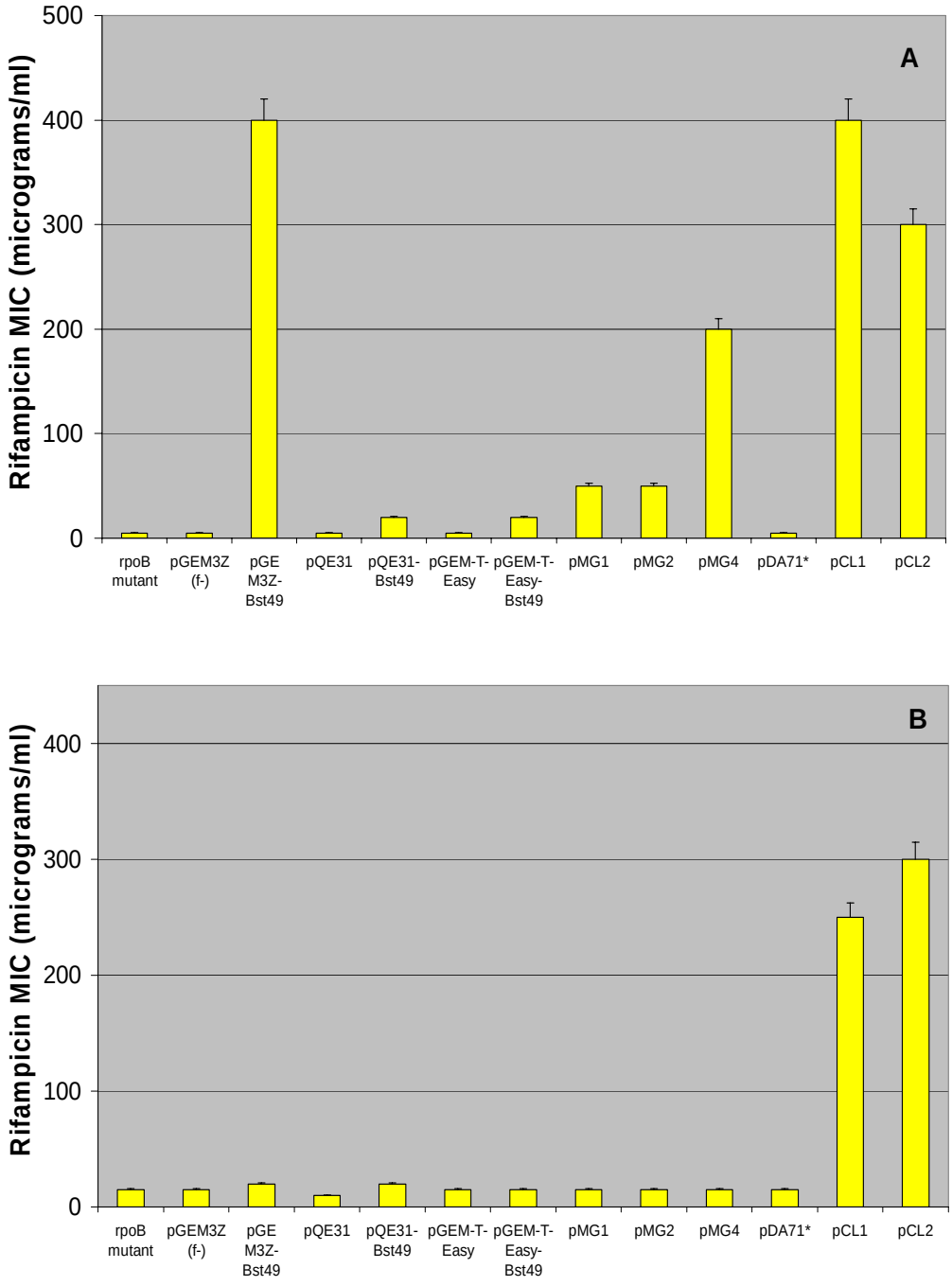


**Figure 21: Rifampicin MIC of glycosyltransferase, Arr ADP-ribosyltransferase and its mutants in *E. coli* MM294-4 cells in (A) the dark and (B) in the presence of white light at 650 lx.** Each set of experiments was repeated three times. The columns represent the means of results from all four experiments. Standard deviations of the means are indicated by error bars.

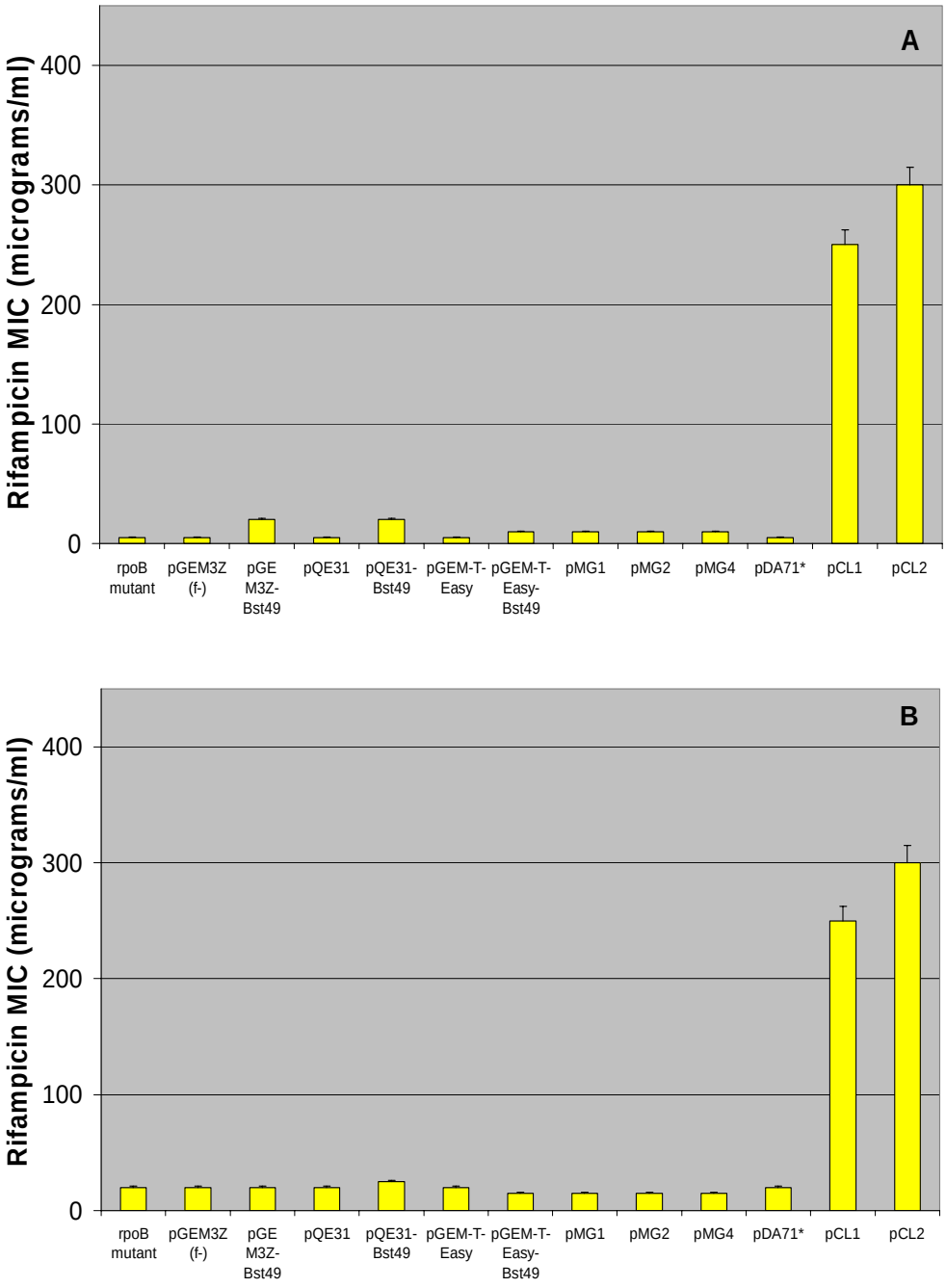


**Figure 22: Rifampicin MIC of glycosyltransferase, Arr ADP-ribosyltransferase and its mutants in *E. coli* MM294-4 cells in (A) blue and (B) red light at 650 lx.** Each set of experiments was repeated three times. The columns represent the means of results from all four experiments. Standard deviations of the means are indicated by error bars.

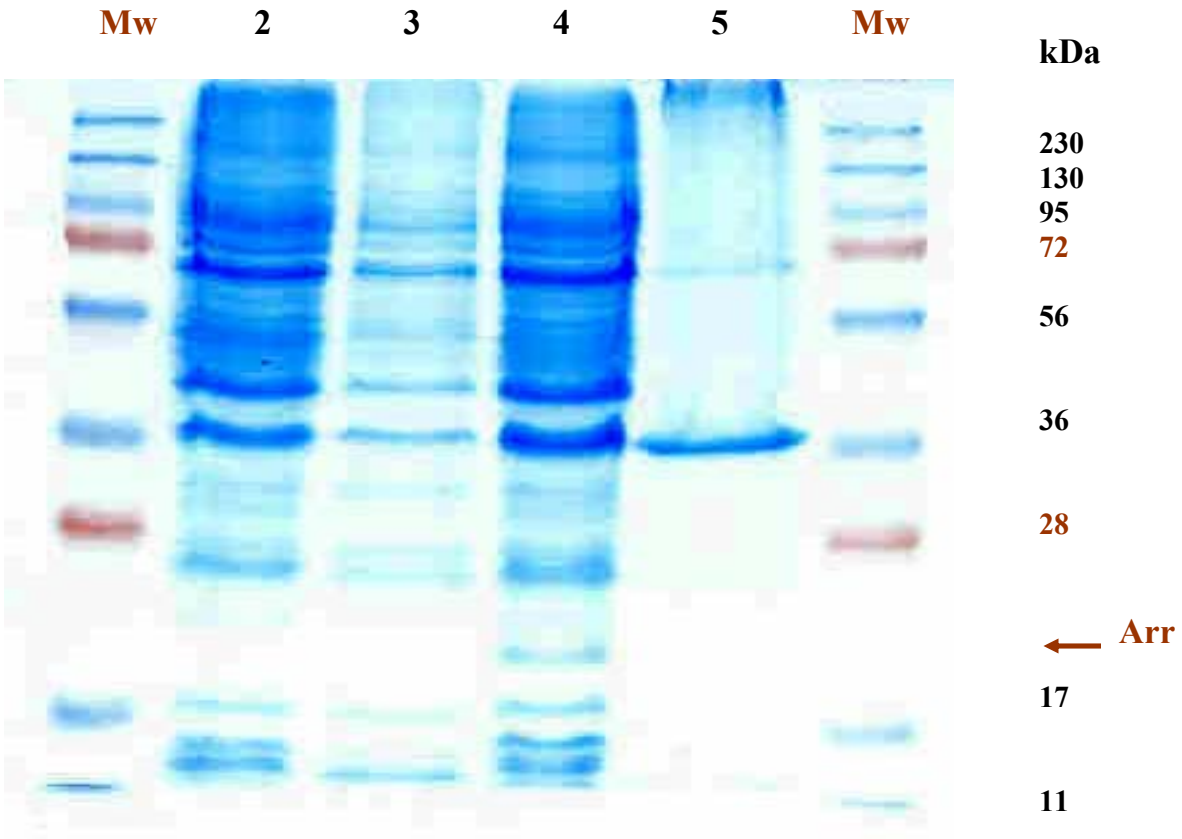


**Figure 23: Arr protein expression after being grown in the presence and absence of light.** Coomassie-stained SDS-PAGE mini gradient gel (4-12%) of crude cell extracts prepared from *E. coli* MM294-4 cells transformed with the following constructs: pET28 in the absence of light (2), pET28 in the presence of light (3), pET28-*Bst*49 in the absence of light (4), pET28-*Bst*49 in the presence of light (5). 20 µl of each fraction was loaded onto each lane. A band at ≈18 kDa (lanes 4) is indicated by the **red** arrow. This band is consistent with the predicted size of the Arr ADP-ribosyltransferase. Thus, the Arr enzyme was not synthesised in the presence of light.

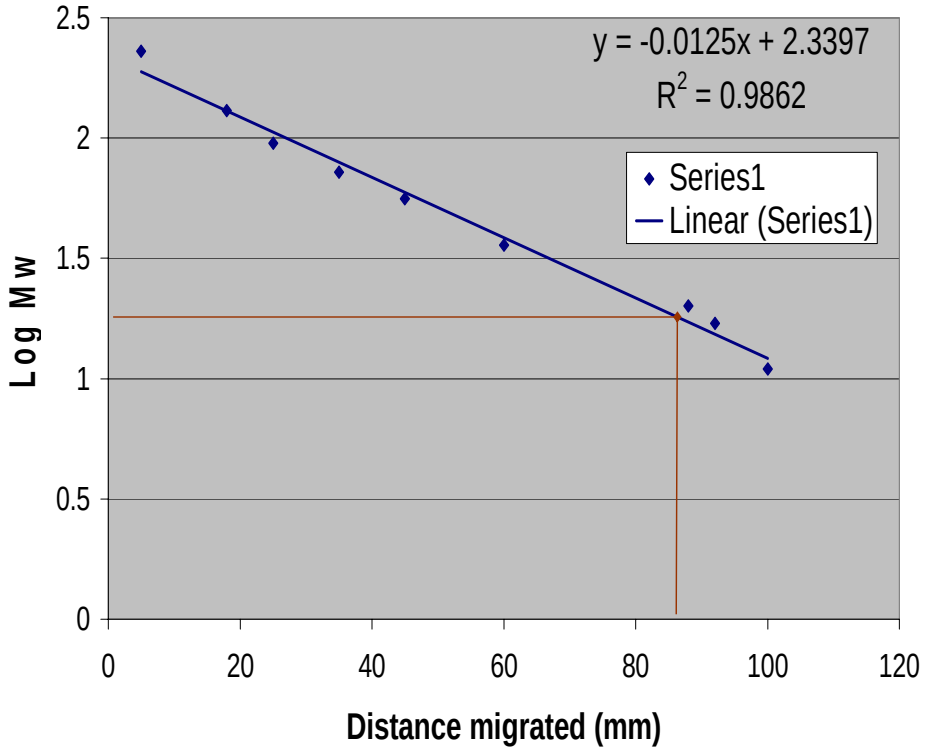


**Figure 24: Calibration curve for determining the molecular weight of the Arr ADP-ribosyltransferase, under varying light conditions.** The red lines converge at the data point (♦) where the log Mw for the band was extrapolated.

The relative Mw of the band was determined by comparing its mobility with those of the $M_w$ standards run on the same gel. By plotting a graph of distance travelled against the log $M_w$ for each of the nine standard proteins, a calibration curve was constructed (**Figure 24**). The electrophoretic mobility of the band was averaged to be 84 mm. The log $M_w$ was determined by the equation y = -0.0125x + 2.3397. This implied the size of the Arr enzyme to be about 19.4 kDa, which is consistent with its predicted size of 15.9 kDa given the error of measuring $M_w$ from SDS-PAGE gels. Fermentas pageruler prestained protein ladder plus (#SM1811) calibration kit for electrophoresis was utilised.

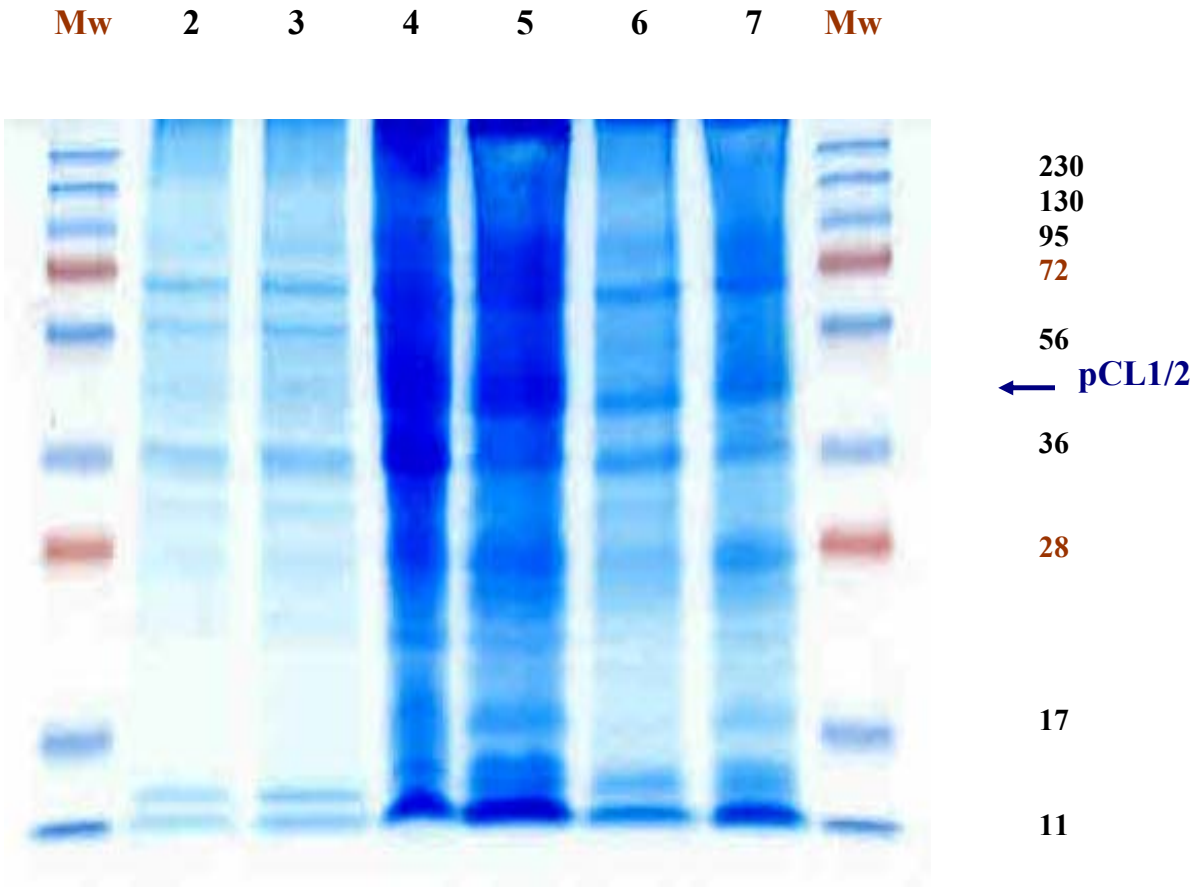


**Figure 25: Glycosyltransferase protein expression after being grown in the presence and absence of light.** Coomassie-stained SDS-PAGE mini gradient gel (4-12%) of crude cell extracts prepared from *E. coli* MM294-4 cells transformed with the following constructs: pDA71* in the presence of light (2), pDA71* in the absence of light (3), pCL2 in the presence of light (4), pCL2 in the absence of light (5), pCL1 in the presence of light (6), pCL1 in the absence of light (7). 20 µl of each fraction was loaded onto each lane. Bands at ≈46 kDa (4, 5, 6 and 7) are indicated by the **blue** arrow. These bands are consistent with the predicted size of the glycosyltransferase that inactivates rifampicin. Thus, the glycosyltransferase was synthesised in the presence of light.

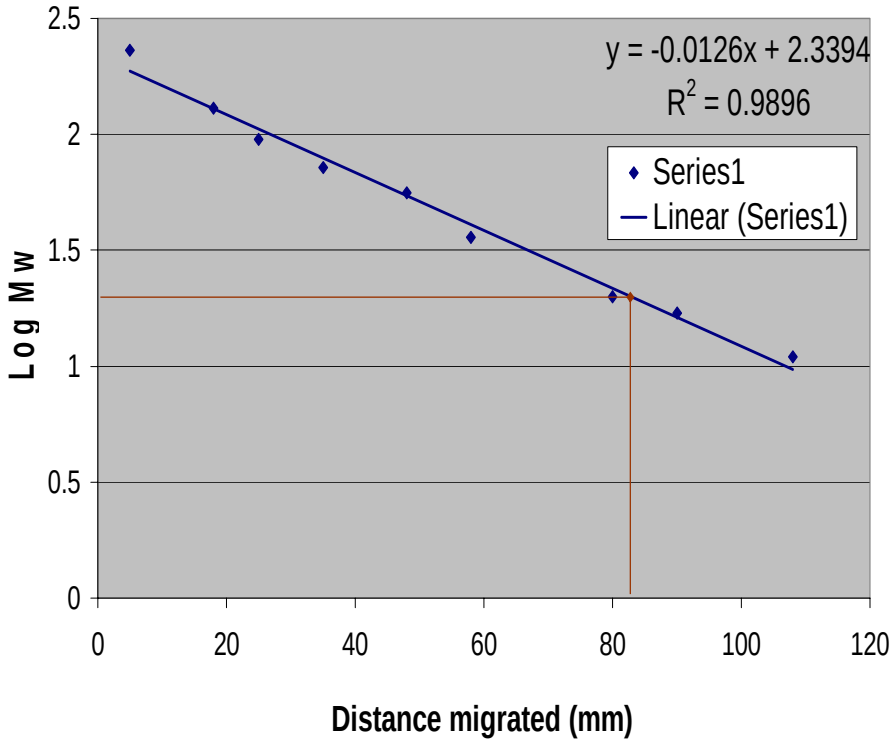


**Figure 26: Calibration curve for determining the molecular weight of the glycosyltransferase that inactivates rifampicin, under varying light conditions.** The blue lines converge at the data point (♦) where the log Mw for the four bands was extrapolated.

The relative Mw of the four bands was determined by comparing their mobilities with those of the $M_w$ standards run on the same gel. By plotting a graph of distance travelled against the log $M_w$ for each of the nine standard proteins, a calibration curve was constructed (**Figure 26**). The electrophoretic mobilities of the bands were averaged to be 58 mm. The log $M_w$ was determined by the equation y = -0.0126x + 2.3394. This implied the size of the glycosyltransferase to be about 40.6 kDa, which is consistent with its predicted size of 42.5 kDa given the error of measuring $M_w$ from SDS-PAGE gels. Fermentas pageruler prestained protein ladder plus (#SM1811) calibration kit for electrophoresis was utilised.

**4.4.5 *In vitro* enzymatic inactivation of rifampicin**

Inactivation of rifampicin by the ORF mutants was assessed by the *in vitro* plate assay method. *E. coli* MM294-4 cultures of the ORF mutants and a vector only control were grown in 10 ml LB supplemented with ampicillin (100 µg/ml) and rifampicin (10 µg/ml). These were incubated, shaking, at 37°C overnight. After the cells were pelleted by centrifugation at 15 000 rpm, the antibiotics were removed by washing twice with 2 ml of sonication buffer. Crude cell extracts were obtained by sonication for 10 seconds, repeating 3-4 times. The clarified supernatant was transferred to a sterile Eppendorf tube, to which rifampicin and the appropriate co-factor required for enzyme activity were added. The preferred ADP-ribose donor substrate of the Arr enzyme is nicotinamide adenine dinucleotide (NAD) or nicotinamide adenine dinucleotide, reduced (NADH). Each inactivation assay included only rifampicin, only co-factor and neither rifampicin nor co-factor controls. The reaction was stopped after the desired incubation time of 24 hrs at 37°C by denaturing the thermostable enzyme with Proteinase K (300 µg/ml) at 56°C for 15 min.

A rifampicin sensitive assay organism, *B. subtilis* 1A3-1, was diluted 1:100 and spread on a LB plate solidified with half the normal amount of agar containing 200 µg/ml of spectinomycin. 65 µl of the rifampicin-containing reaction mixture was then added to the wells made on the LB plates. These plates were incubated at 4°C for 4 hrs to allow for diffusion of the antibiotic. Following this, the plates were incubated for a further 4-5 hrs at 37°C. A measure of rifampicin inactivation was obtained from the size of the zones of inactivation that were visible on the plate when compared to the controls. The results are shown in **Table 19** below.

**Table 19:** *In vitro* enzymatic inactivation of rifampicin (10 µg/ml) by the ORF mutants

| Crude cell homogenates | Radius of zone of inhibition (mm) | | | |
|---|---|---|---|---|
| | **Control 1: Antibiotic only** | **Control 2: Buffer only** | **Control 3: Co-factor only** | **Inactivation assay reaction** |
| pGEM-T-Easy | 3 | 0 | 0 | 3 |
| pGEM-T-Easy-*Bst*49 | 0 | 0 | 0 | 3 |
| pMG1 | 0 | 0 | 0 | 7 |
| pMG2 | 0 | 0 | 0 | 7 |
| pMG4 | 0 | 0 | 0 | 15 |

The plate assay method demonstrated that cell extract transformed with pMG4 completely inactivated rifampicin in the presence of $NAD^+$ co-factor, which mediates enzyme activity. In contrast, *E. coli* cultures challenged with 10 µg/ml rifampicin and $NAD^+$ co-factor showed lowered activity. Radii of inhibition zones of 7 mm were observed, suggesting partial inactivation of rifampicin. These results were consistent with the MICs of each construct. The vector only control was included to confirm that the rifampicin inactivation phenotype was due to the cloned DNA fragments in pMG1, pMG2 and pMG4. The 3 mm inhibition radius was observed because of residual ampicillin to which *B. subtilis* 1A3-1 is susceptible. No zone of inhibition was detected when additional wash steps were performed during the assay.

### 4.5 Protein expression

The endogenous protein target of this ADP-ribosyltransferase has not yet been elucidated. Additionally, its cellular function remains unknown. Thus, biochemical characterisation and purification of the Arr ADP-ribosyltransferase and its mutants was vital. Complete biochemical analysis required copious amounts (milligrams) of protein. Such quantities were not available from its natural source, *M. smegmatis*. Since an active protein was produced in *E. coli* and because it is an easier organism to work with than either *Mycobacterium* or *Rhodococcus*, in terms of cloning and protein purification, an attempt at heterologous over-expression in this strain was made.

#### 4.5.1 Investigation of protein expression in pGEM-T-Easy-*Bst*49, pMG1, pMG2 and pMG4

Prior to cloning the *arr* gene and its mutants into an expression vector, their current levels of protein expression were determined. An induction study with these constructs was performed as they were cloned downstream from the *lac* promoter in pGEM-T-Easy. This promoter is repressed by the product of the *lacI* gene and is usually inducible with IPTG. However, SDS-PAGE analysis of protein extracts from pGEM-T-Easy-*Bst*49, pMG1, pMG2 and pMG4 indicated that the protein was expressed at such a low level that no band was visible at the 18 kilodalton region (**Figures 27** and **28**). Analysis of the predicted amino acid sequence of the *arr* ORF calculated a 15.9 kDa protein. Given the error of measuring $M_w$ from SDS-PAGE gels, an induced protein band would have been observable at ≈18 kDa. Additionally, induction with 1 mM IPTG had no effect on the amount of protein produced. This result could be explained by insufficient chromosomally encoded repressor protein to modulate transcription from this promoter as pGEM-T-Easy is a high copy number vector without a plasmid-borne *lacI* gene.

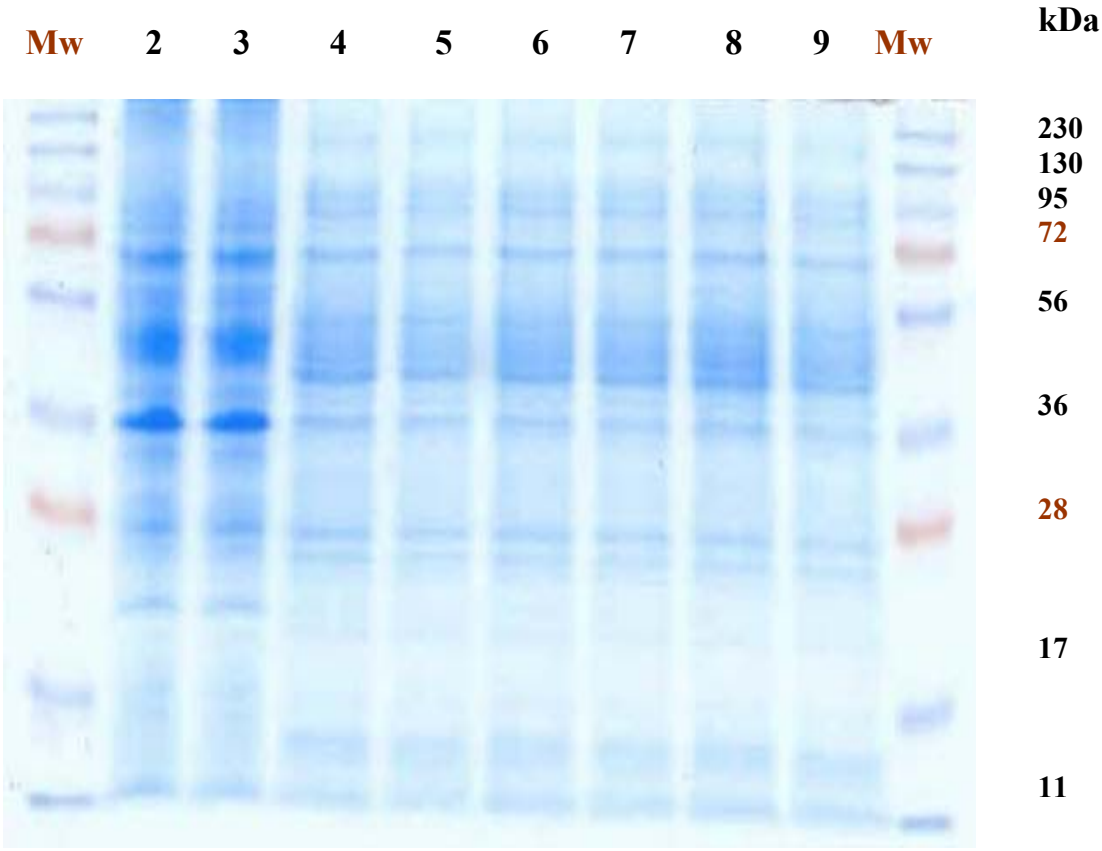


**Figure 27: Initial induction study showing expression levels of the Arr protein, pMG1 and pMG2 both in the presence and absence of IPTG.** Coomassie-stained SDS-PAGE mini gradient gel (4-12%) of crude cell extracts prepared from *E. coli* DH5α cells transformed with the following constructs: pGEM-T-Easy uninduced (2), pGEM-T-Easy induced (3), pGEM-T-Easy-*Bst*49 uninduced (4), pGEM-T-Easy-*Bst*49 induced (5), pMG1 uninduced (6), pMG1 induced (7), pMG2 uninduced (8) and pMG2 induced (lane 9). Samples were induced with 1 mM IPTG and 20 µl of each fraction was loaded onto each lane.

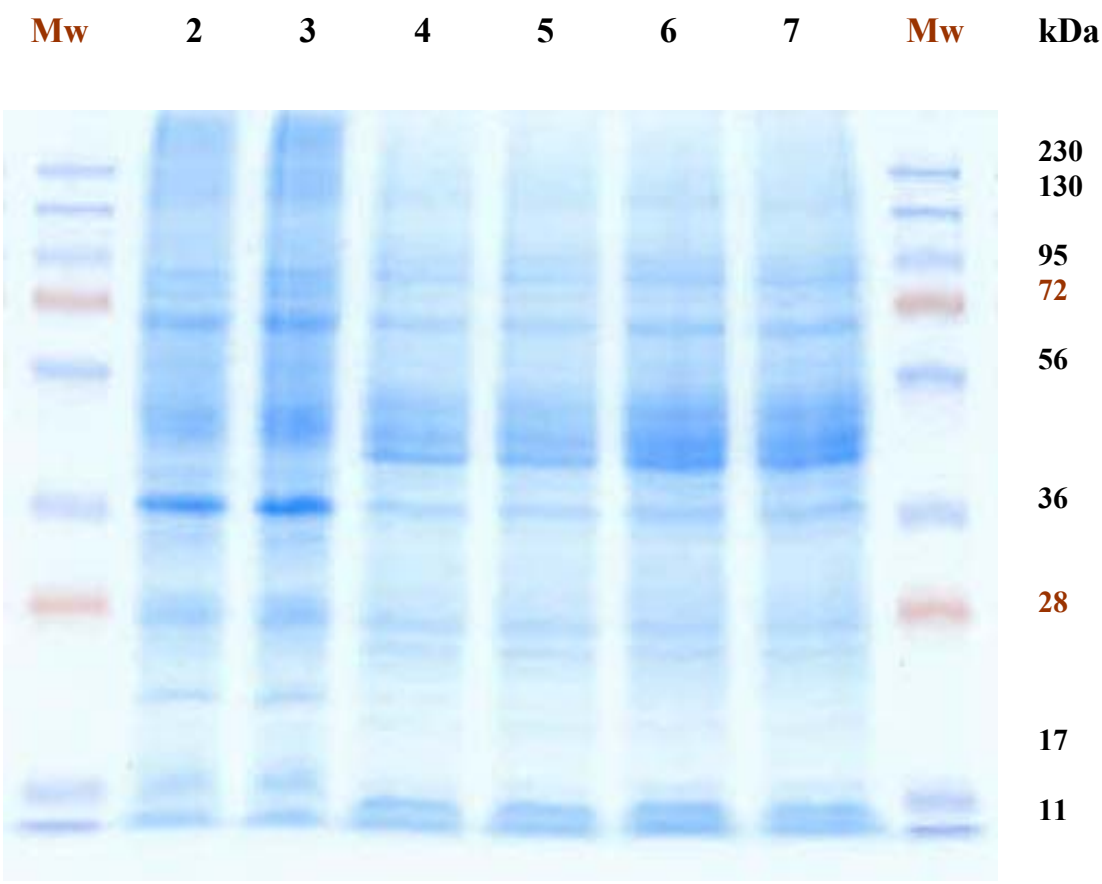


**Figure 28: Initial induction study showing expression levels of the Arr protein and pMG4, both in the presence and absence of IPTG.** Coomassie-stained SDS-PAGE mini gradient gel (4-12%) of crude cell extracts prepared from *E. coli* DH5α cells transformed with the following constructs: pGEM-T-Easy uninduced (2), pGEM-T-Easy induced (3), pGEM-T-Easy-*Bst*49 uninduced (4), pGEM-T-Easy-*Bst*49 induced (5), pMG4 uninduced (6) and pMG4 induced (7). Samples were induced with 1 mM IPTG and 20 µl of each fraction was loaded onto each lane.

**Figures 27** and **28** indicated that this expression system appeared not to be functional. One possible explanation was that the pGEM-T-Easy series of vectors have not been designed as expression vectors. A more successful alternative would be to utilise the pET series of expression vectors. These are specifically designed expression vectors with an inducible T7 promoter, which is recognised by *E. coli* RNA polymerase, for driving transcription of the inserted gene. Additionally, there is a T7 terminator region to prevent transcriptional read-through and a plasmid-borne *lacI*$^{q}$ gene to ensure efficient repression of transcription.

### 4.5.2 Cloning of the *arr* gene and its mutants into pET-28a(+)

The *arr* gene and its mutants were cloned into pET-28a(+). This vector was chosen as it offers the highest expression levels and the tightest control over basal expression in comparison to other vectors. Additionally, it has an N-terminal purification tag consisting of six consecutive histidine residues (6xHis tag). This tag is poorly immunogenic and at physiological pH (8.0) it is small, uncharged and it does not interfere with the structure and function of the over-expressed protein of interest within the cell.

The *arr* gene and its mutants were amplified by PCR. The four inserts were excised from a 0.8% agarose gel and purified. Both the inserts and vectors were then prepared by performing a double digestion with *Nde*I and *Xho*I. *Nde*I was purposely selected because it contains the start codon, ATG, in its recognition sequence. This minimised the probability of introducing a frameshift mutation. These double digestions were run on a 0.8% agarose gel to ensure restriction had occurred. Additionally, it allowed for the separation of the smaller fragment from the vector and the ratio of vector to insert concentration was determined. The four relevant inserts and the linearised vector were excised, purified and ligated. These ligations were transformed, via the $CaCl_2$ method, into *E. coli* Rosetta2(DE3)pLysS cells.

This strain was deliberately chosen as it enhances expression of proteins having codons rarely used in *E. coli*. More specifically, it supplies transfer RNAs (tRNAs) for seven rare codons: AUA, AGG, AGA, CUA, CCC, GGA and CGG. It is deficient in both *Ion* and *omp*T proteases and pLysS ensures more stringent control as it encodes T7 lysozyme, which is a natural inhibitor of T7 RNA polymerase. Transformants were selected for on LB-agar plates supplemented with 20 µg/ml kanamycin. Recombinant plasmids were confirmed by screening for the presence of inserts on a 0.8% agarose gel. These recombinants were sent for sequencing to verify the construction of the four in-frame fusion proteins, namely, pET28a-*Bst*49, pMG1a, pMG2a and pMG4a.

### 4.5.3 Determination of protein toxicity

A fundamental problem associated with the expression of recombinant proteins in growing cells is that energy and nutritional reserves are directed toward biomass production. Expression of the protein of interest is simultaneous with the expression of hundreds of host genes which compete for the transcription-translation machinery and metabolic resources. This metabolic stress may reduce the growth rate and viability of the host cell. Thus, a slower growth rate suggests that the gene may be toxic to the host cell. This results in the selection of deletion mutants which will invariably outgrow the original cell type. This reduces the yield and purity of the product. Conversely, a faster growth rate may indicate inefficient transcription or translation due to plasmid instability, ineffective induction or deletions in the control region. To judge the toxicity of the over-expressed Arr protein, cell growth before and after induction of expression was monitored. This was compared to the cell growth in the absence of IPTG. Controls included the growth rate of untransformed *E. coli* Rosetta2(DE3)pLysS cells (**Figure 29A**) and cells transformed with the vector only (**Figure 29B**). Growth curves for 100 ml cultures of pET28a-*Bst*49, pMG1a, pMG2a and pMG4a were established (**Figures 30A, 30B, 31A** and **31B**).

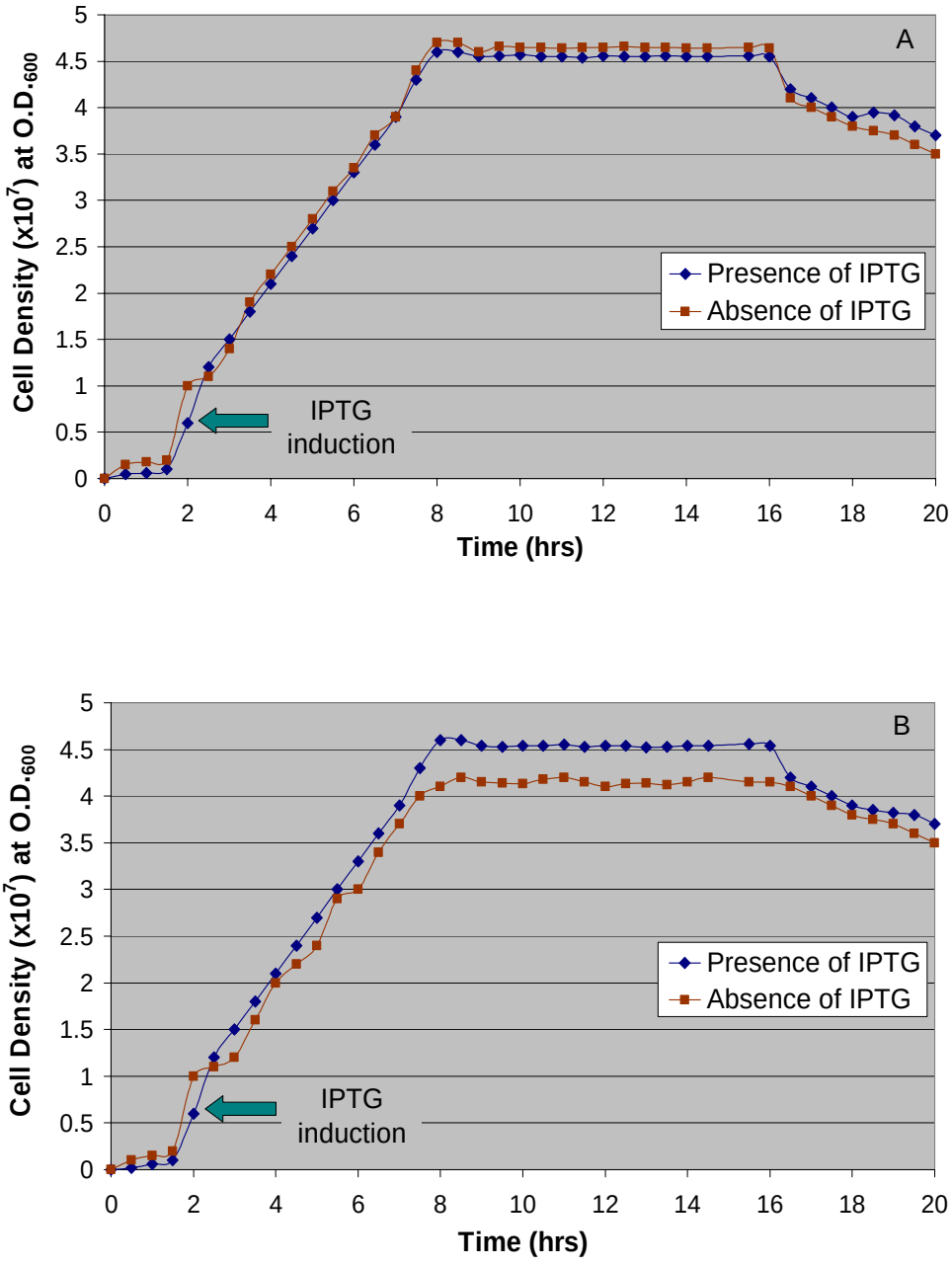


**Figure 29: Growth curve of (A) untransformed *E. coli* Rosetta2(DE3)pLysS cells and (B) *E. coli* Rosetta2(DE3)pLysS cells transformed with pET-28a(+) in LB medium in the presence (♦) and absence (■) of IPTG.** Absorbance readings were taken at 600 nm every 30 minutes.

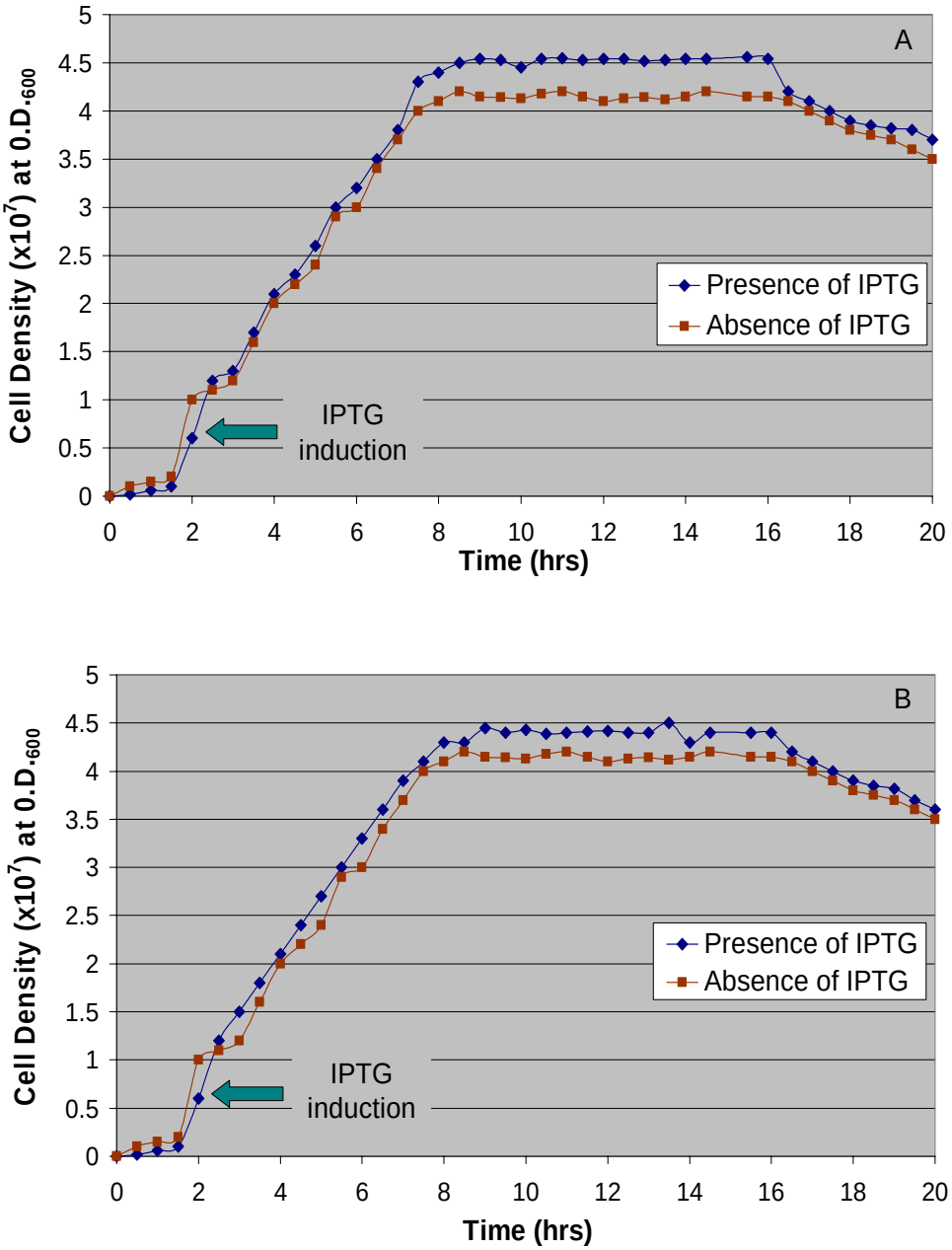


**Figure 30: Growth curve of *E. coli* Rosetta2(DE3)pLysS cells transformed with (A) pET28a-*Bst*49 and (B) pMG1a in LB medium in the presence (♦) and absence (■) of IPTG.** Absorbance readings were taken at 600 nm every 30 minutes. High readings were calculated by diluting the sample to enable photometric measurement in the linear range of 0.1-0.5 $O.D._{600}$.

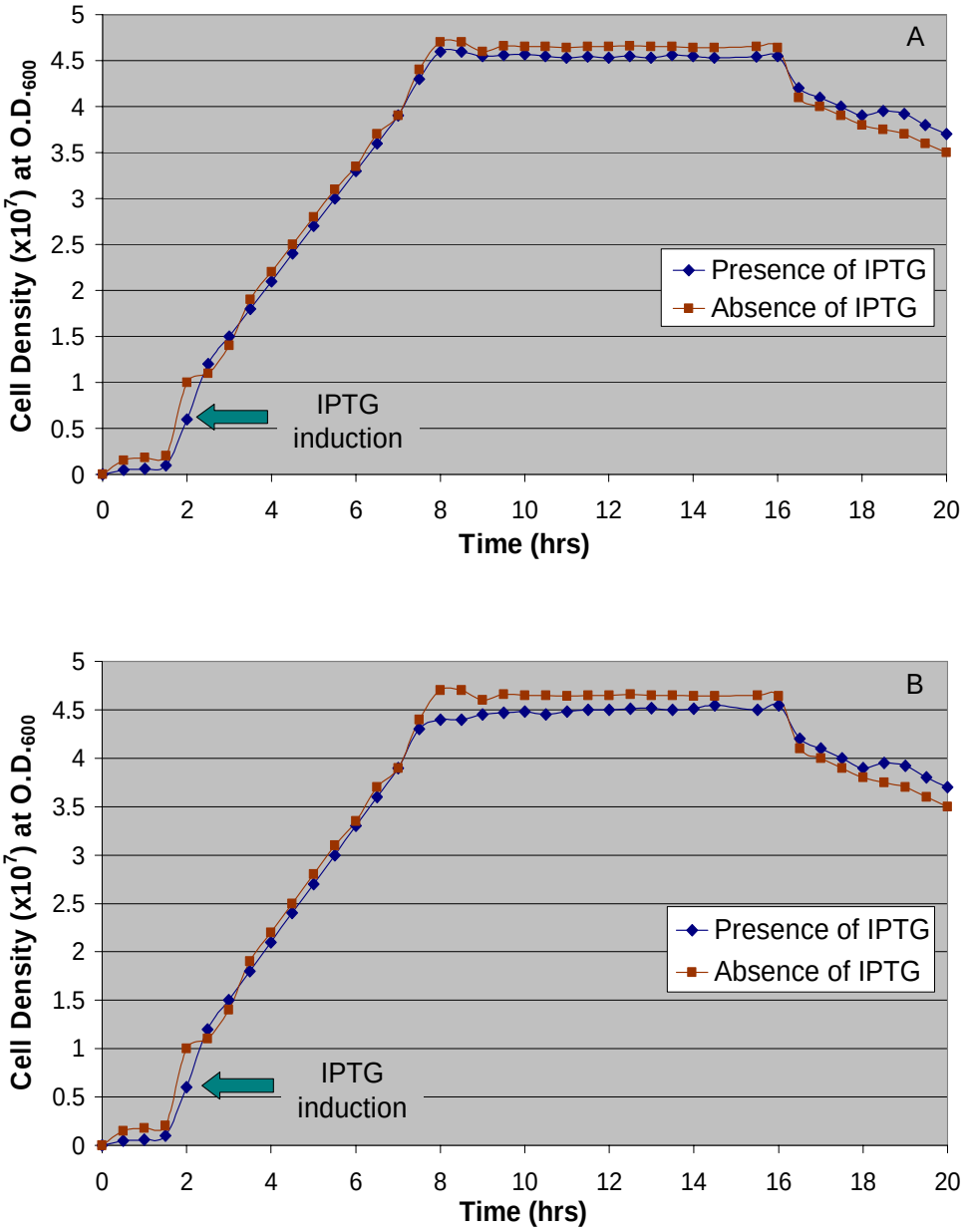


**Figure 31: Growth curve of *E. coli* Rosetta2(DE3)pLysS cells transformed with (A) pMG2a and (B) pMG4a in LB medium in the presence (♦) and absence (■) of IPTG.** Absorbance readings were taken at 600 nm every 30 minutes.

The growth curves established for each construct were analogous to their control, untransformed *E. coli* Rosetta2(DE3)pLysS cells. However, there was a slight variation in cell density in the absence or presence of IPTG. A higher cell density was observed in the presence of this inducer in **Figures 29B**, **30A** and **30B**, whereas more microbial growth was measured in the absence of IPTG in **Figures 31A** and **31B**. This suggested that the inducer was not responsible for this variation in cell growth. Presumably, a slightly larger colony was initially selected and this accounted for the greater number of cells present in the starting culture. Additionally, there was no disparity in growth rate before or after induction. This indicated that the over-expressed Arr ADP-ribosyltransferase and its mutants were not toxic to the host cell.

### 4.5.4 Determination of protein solubility

A primary consideration for recombinant protein expression and purification is the experimental purpose for which the protein will be utilised. For biochemical and structural studies, it is important to optimise conditions for the expression of soluble, functionally-active protein. Many polypeptide gene products expressed in *E. coli* accumulate as insoluble aggregates that lack functional activity. To establish whether the over-expressed Arr ADP-ribosyltransferase and its mutants were sequestered into seclusion bodies or not, both the insoluble (pellet) and soluble (supernatant) fractions were run on an SDS-PAGE gel. Both fractions are represented in **Figures 32** and **35** and **Figures 33** and **36** respectively.

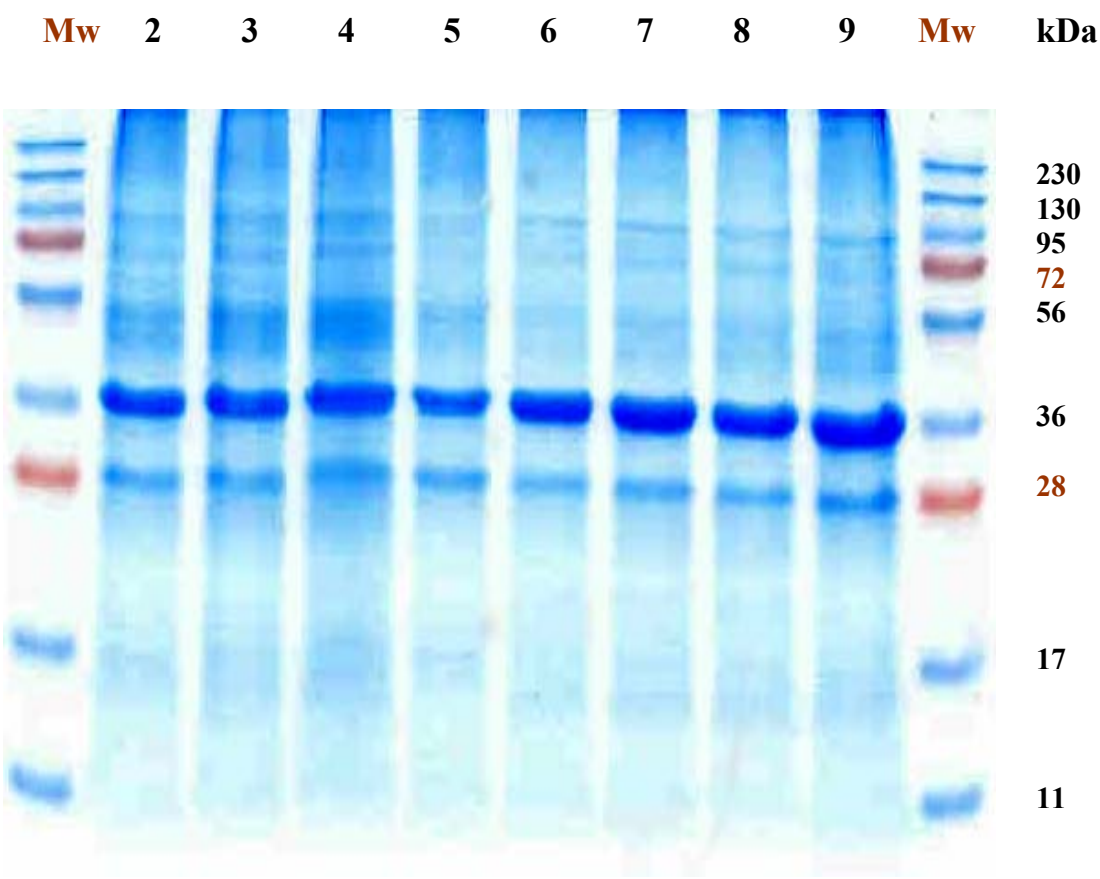


**Figure 32: Arr solubility determination illustrating the insoluble fraction under varying IPTG concentrations.** Coomassie-stained SDS-PAGE mini gradient gel (4-12%) of insoluble proteins from crude cell extracts prepared from *E. coli* Rosetta2(DE3)pLysS transformed with the following constructs: pET28a uninduced (2), pET28a 0.3 mM IPTG (3), pET28a 0.6 mM IPTG (4), pET28a 1.2 mM IPTG (5), pET28a-*Bst*49 uninduced (6), pET28a-*Bst*49 0.3 mM IPTG (7), pET28a-*Bst*49 0.6 M IPTG (8) and pET28a-*Bst*49 1.2 mM IPTG (9). 20 µl of each fraction was loaded onto each lane.

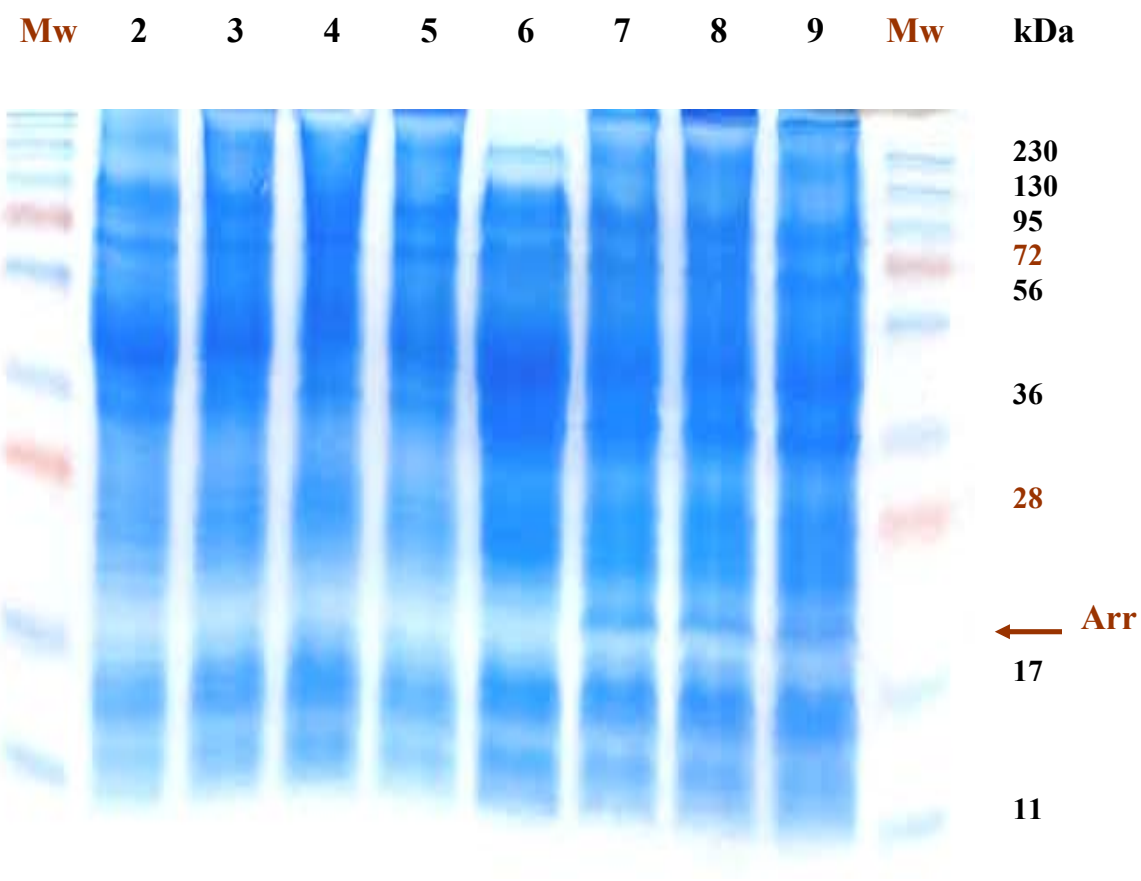


**Figure 33: Arr solubility determination illustrating the soluble fraction under varying IPTG concentrations.** Coomassie-stained SDS-PAGE mini gradient gel (4-12%) of soluble proteins from crude cell extracts prepared from *E. coli* Rosetta2(DE3)pLysS transformed with the following constructs: pET28a uninduced (2), pET28a 0.3 mM IPTG (3), pET28a 0.6 mM IPTG (4), pET28a 1.2 mM IPTG (5), pET28a-*Bst*49 uninduced (6), pET28a-*Bst*49 0.3 mM IPTG (7), pET28a-*Bst*49 0.6 mM IPTG (8) and pET28a-*Bst*49 1.2 mM IPTG 9). 20 µl of each fraction was loaded onto each lane. Induced bands at ≈18 kDa (7, 8 and 9) are indicated by the **red** arrow. These bands are consistent with the predicted size of the Arr ADP-ribosyltransferase.

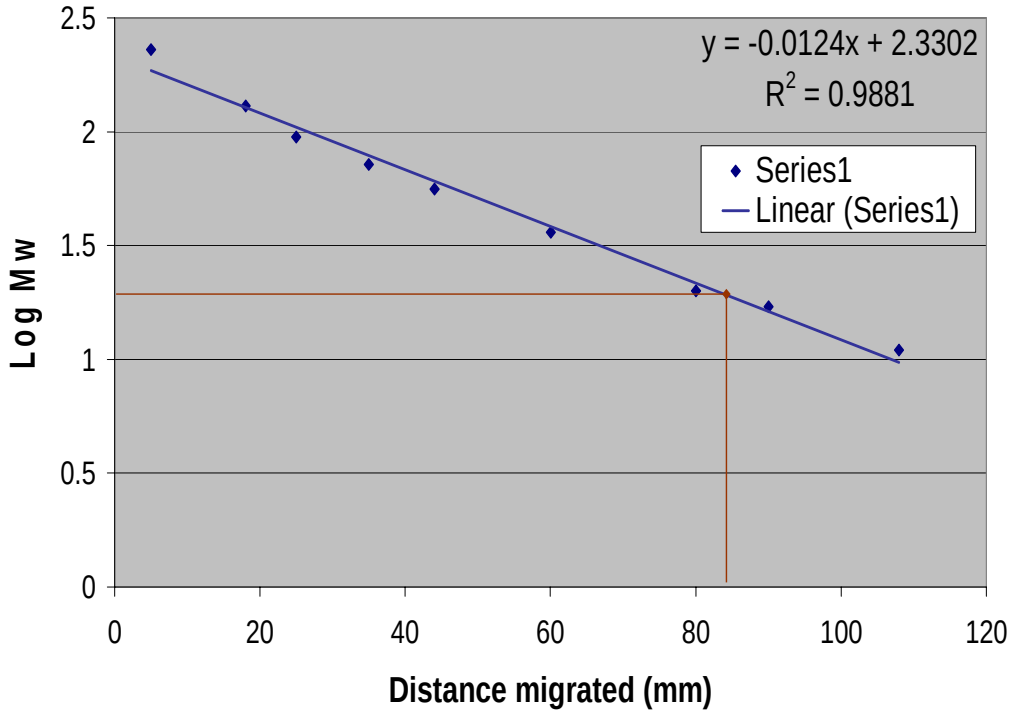


**Figure 34: Calibration curve for determining the molecular weight of the Arr ADP-ribosyltransferase, under varying IPTG concentrations.** The red lines converge at the data point (♦) where the log Mw for the three induced bands was extrapolated.

The relative Mw of the induced bands was determined by comparing their mobilities with those of the $M_w$ standards run on the same gel. By plotting a graph of distance travelled against the log $M_w$ for each of the nine standard proteins, a calibration curve was constructed (**Figure 34**). The electrophoretic mobilities of the three bands were averaged to be 84 mm. The log $M_w$ was determined by the equation y = -0.0124x + 2.3302. This implied the size of the Arr enzyme to be about 19.4 kDa, which is consistent with its predicted size of 15.9 kDa given the error of measuring $M_w$ from SDS-PAGE gels. Fermentas pageruler prestained protein ladder plus (#SM1811) calibration kit for electrophoresis was utilised.

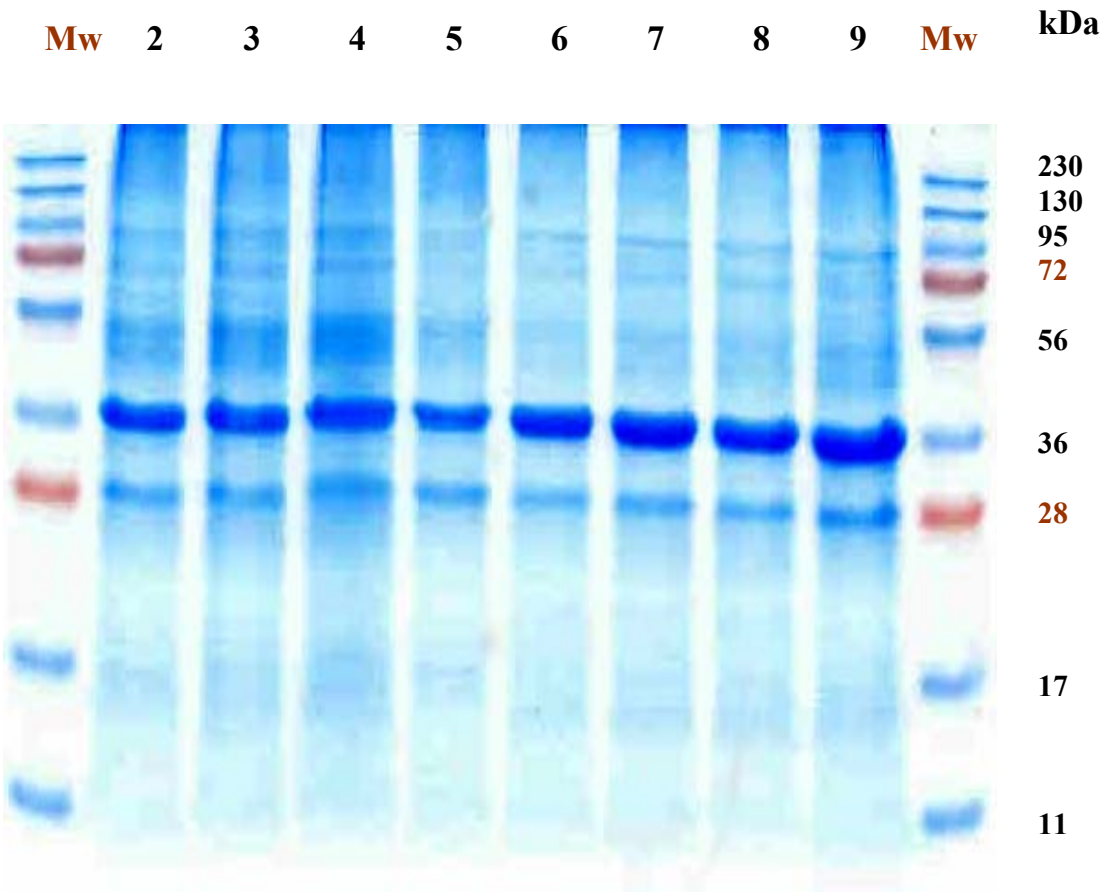


**Figure 35: Arr solubility determination illustrating the insoluble fraction under varying induction time.** Coomassie-stained SDS-PAGE mini gradient gel (4-12%) of insoluble proteins from crude cell extracts prepared from *E. coli* Rosetta2(DE3)pLysS transformed with the following constructs: pET28a 0 hr induction time (2), pET28a 1 hr induction time (3), pET28a 2 hrs induction time (4), pET28a 4 hrs induction time (5), pET28a-*Bst*49 0 hr induction time (6), pET28a-*Bst*49 1 hr induction time (7), pET28a-*Bst*49 2 hrs induction time (8) and pET28a-*Bst*49 4 hrs induction time (9). Samples were induced with 1 mM IPTG and 20 µl of each fraction was loaded onto each lane.

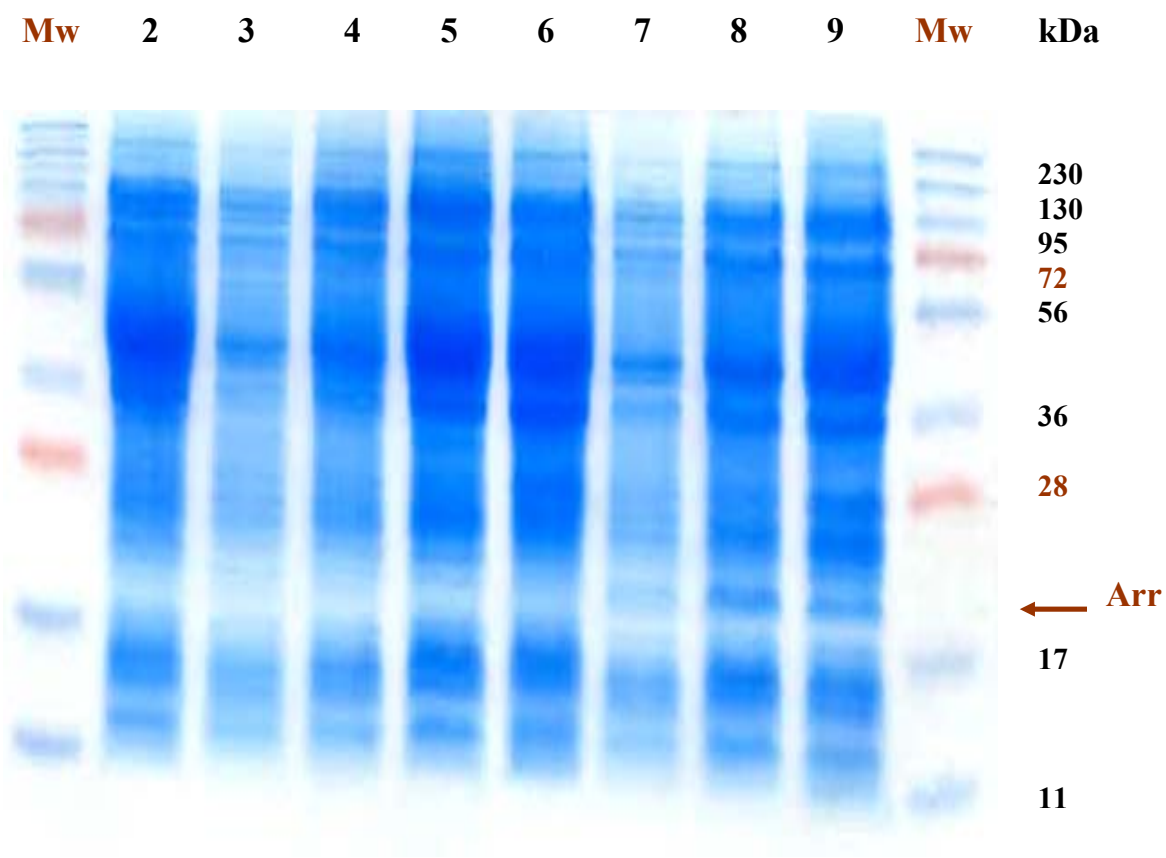


**Figure 36: Arr solubility determination illustrating the soluble fraction under varying induction time.** Coomassie-stained SDS-PAGE mini gradient gel (4-12%) of soluble proteins from crude cell extracts prepared from *E. coli* Rosetta2(DE3)pLysS transformed with the following constructs: pET28a 0 hr induction time (2), pET28a 1 hr induction time (3), pET28a 2 hrs induction time (4), pET28a 4 hrs induction time (5), pET28a-*Bst*49 0 hr induction time (6), pET28a-*Bst*49 1 hr induction time (7), pET28a-*Bst*49 2 hrs induction time (8) and pET28a-*Bst*49 4 hrs induction time (9). Samples were induced with 1 mM IPTG and 20 µl of each fraction was loaded onto each lane. Induced bands at ≈18 kDa (7, 8 and 9) are indicated by the **red** arrow. These bands are consistent with the predicted size of the Arr ADP-ribosyltransferase.

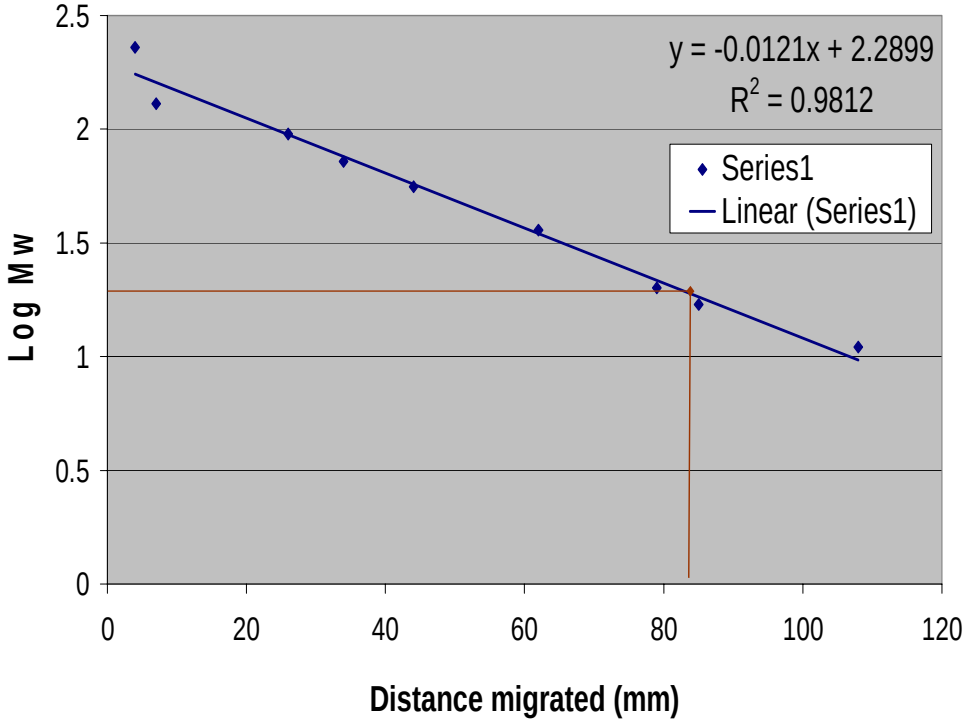


**Figure 37: Calibration curve for determining the molecular weight of the Arr ADP-ribosyltransferase, under varying induction time.** The red lines converge at the data point (♦) where the log Mw for the three induced bands was extrapolated.

The relative Mw of the induced bands was determined by comparing their mobilities with those of the $M_w$ standards run on the same gel. By plotting a graph of distance travelled against the log $M_w$ for each of the nine standard proteins, a calibration curve was constructed (**Figure 37**). The electrophoretic mobilities of the three bands were averaged to be 83 mm. The log $M_w$ was determined by the equation y = -0.0121x + 2.2899. This implied the size of the Arr enzyme to be about 19.3 kDa, which is consistent with its predicted size of 15.9 kDa given the error of measuring $M_w$ from SDS-PAGE gels. Fermentas pageruler prestained protein ladder plus (#SM1811) calibration kit for electrophoresis was utilised.

The above results indicated that the Arr ADP-ribosyltransferase was present in the soluble fraction of the crude cell extract (**Figures 33** and **36**). No induced bands of the correct size were visible in the insoluble fraction (**Figures 32** and **35**). However, an uninduced protein was observed. Soluble, functionally-active protein is easier to work with in comparison to seclusion bodies. Insoluble aggregates are problematic and need to be solubilised with strong denaturants such as guanidine hydrochloride or urea before further experimentation. These harsh conditions often result in alterations of the protein's structure and full activity is not always restored. These results indicated that no bands of the correct size were visible in the uninduced samples (**Figures 33** and **36**). This indicated that the presence of IPTG was required as an inducer for Arr expression. This was not the case with pGEM-T-Easy (**Figures 27** and **28**) where induction with IPTG had no effect on the amount of protein produced. This expression system appeared to be functional.

### 4.5.5 Determination of optimum expression conditions

pET28a(+) is a specifically designed expression vector that offers the highest induced expression levels and the tightest control over basal expression. However, conditions for optimal expression of individual proteins must be determined empirically. In order to maximise over-expression of this protein in *E. coli*, certain parameters needed to be varied. These parameters included IPTG concentration, induction time and temperature. IPTG is a sugar analogue that attaches to the *lac* repressor protein and inactivates it. Thus, RNAP is free to transcribe the sequence downstream from the *lac* promoter. Although IPTG initiates transcription while remaining intact, the optimal concentration of IPTG needs to be determined empirically as it varies for different proteins. **Figure 30A** indicated that the exponential phase of *E. coli* Rosetta2(DE3)pLysS cells, transformed with pET28a-*Bst*49, was reached after 2 hrs. This information was necessary for optimising the expression of the *arr* gene as the timing of IPTG induction is also critical. Furthermore, varying IPTG concentrations of 0.3, 0.6 and 0.9 mM were assessed (**Figure 33**).

Time is another important variable as intracellular protein content is often a balance between the amount of soluble protein in the cell, the formation of inclusion bodies and protein degradation. If there is insufficient time, the protein may not be synthesized to a high enough level. Conversely, if there is too much time, the protein may be degraded by proteases. Another possibility is the presence of too much protein which may be toxic to the host cell. Varying induction times of 1, 2 and 4 hrs were analysed (**Figure 36**). Temperature was not a determining factor as the Arr protein is very thermostable and therefore the experiments were carried out at 37˚C to suit the optimal growth temperature of *E. coli*.

The amount of protein produced under each condition was quantified by measuring the optical density of the corresponding band (**Table 20**). The values were obtained by using Quantity One® Software Version 4.6. This expression study indicated that all the conditions utilised resulted in the protein being expressed. However, the highest level of expression was observed when 0.6 mM IPTG was used. A slight difference was noted between the last two sets of conditions pertaining to induction time. Hence, an average of 3 hrs induction time was chosen for future work.

**Table 20:** Quantification of induced bands produced by pET28a-*Bst*49 under varying conditions of IPTG concentration and induction time

| **[IPTG] (mM)** | **Peak O.D.** | **Induction Time (hrs)** | **Peak O.D.** |
|---|---|---|---|
| Uninduced control | 0 | Uninduced Control | 0 |
| 0.3 | 0.06 | 1 | 0.04 |
| **0.6** | **0.08** | **2** | **0.13** |
| 1.2 | 0.07 | 4 | 0.12 |

### 4.5.6 Over-expression of the Arr enzyme and its mutants

The over-expression of the Arr enzyme and its mutants was successful when the optimum conditions were utilised. The results are indicated in **Figures 38** and **40** below. Induced bands of the correct size (**Figures 39** and **41**) were visible for all four constructs. This did not occur with a previous attempt that made use of a different expression vector (pQE) and host cell, *E. coli* DH5α (data not shown). The amount of each protein produced, before and after induction, was quantified by measuring the optical density of the corresponding band (**Table 21**). There was on average a five-fold increase in the amount of protein produced after induction. These values were obtained by using Quantity One® Software Version 4.6. This software was also used to calculate the Mw. The value obtained by the densitometer was compared to the one calculated from the calibration curve of the standard proteins. The values obtained correlated with one another. Thus, either or both methods could be used in the future.

**Table 21:** Quantification of induced bands produced by pET28a-*Bst*49 and its mutants under optimised conditions established for expression

| SDS-PAGE gel image | Protein | Peak O.D. (Before induction) | Peak O.D. (After induction) | Molecular weight (kDa) |
|---|---|---|---|---|
| **Figure 38** | pET28-*Bst*49 | 0.04 | 0.20 | 19.8 |
| | pMG1a | 0.06 | 0.44 | 18.6 |
| | pMG2a | 0.08 | 0.38 | 18.5 |
| **Figure 40** | pET28-*Bst*49 | 0.04 | 0.20 | 20.3 |
| | pMG4a | 0.04 | 0.20 | 18.7 |

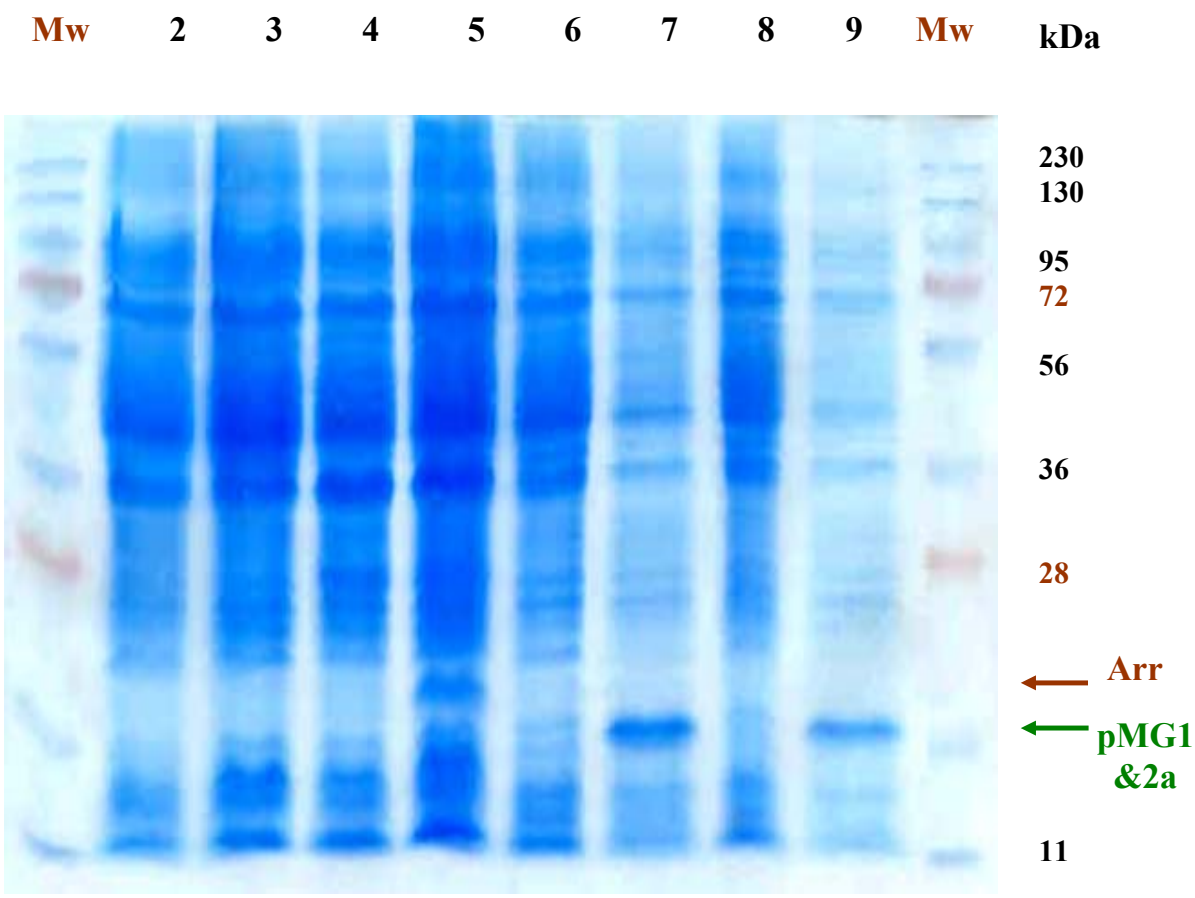


**Figure 38: Over-expression of pET28a-*Bst*49, pMG1a and pMG2a.** Coomassie-stained SDS-PAGE mini gradient gel (4-12%) of soluble proteins from crude cell extracts prepared from *E. coli* Rosetta2(DE3)pLysS cells transformed with the following constructs: pET28a uninduced (2), pET28a induced (3), pET28a-*Bst*49 uninduced (4), pET28a-*Bst*49 induced (5), pMG1a uninduced (6), pMG1a induced (7), pMG2a uninduced (8) and pMG2a induced (9). Samples were induced with 0.6 mM IPTG for 3 hrs. 20 µl of each fraction was loaded onto each lane. Induced bands at ≈18 kDa (5, 7 and 9) are indicated by the **red** and **green** arrows. These bands are consistent with the predicted size of the Arr ADP-ribosyltransferase and its mutants.

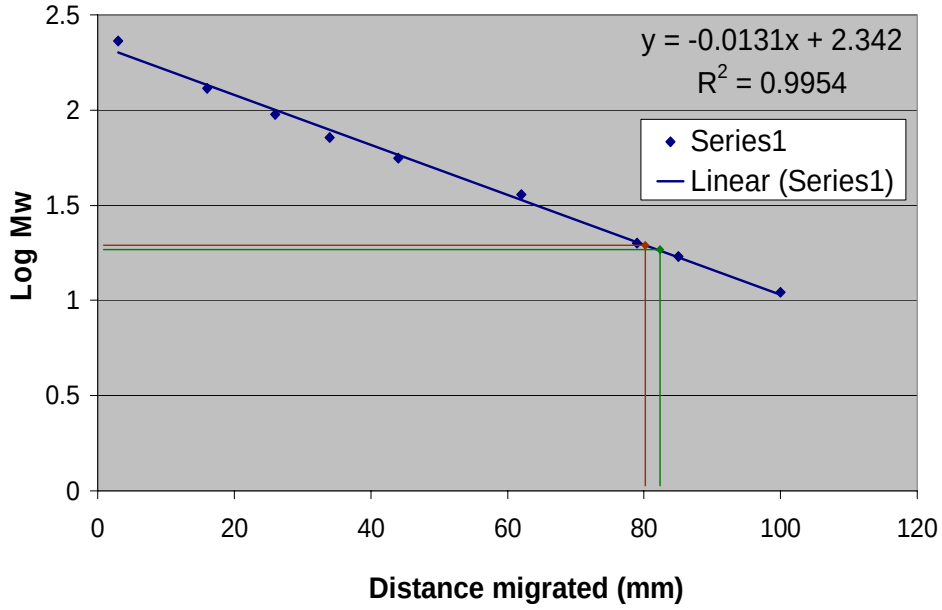


**Figure 39: Calibration curve for determining the molecular weight of pET28a-*Bst*49, pMG1a and pMG2a.** The red lines converge at the data point (♦) where the log Mw for pET28a-*Bst*49 was extrapolated whilst the green lines converge at another data point (♦) that represents the log Mw for pMG1a and pMG2a.

The relative Mw of the induced bands was determined by comparing their mobilities with those of the $M_w$ standards run on the same gel. By plotting a graph of distance travelled against the log $M_w$ for each of the nine standard proteins, a calibration curve was constructed (**Figure 39**). The electrophoretic mobility of pET28a-*Bst*49 was 80 mm whilst pMG1a and pMG2a travelled the same distance of 82 mm. The log $M_w$ was determined by the equation y = -0.0131x + 2.342. This implied the size of the Arr enzyme to be about 19.7 kDa, which is consistent with its predicted size of 15.9 kDa given the error of measuring $M_w$ from SDS-PAGE gels. Similarly, the size of pMG1a and pMG2a was calculated at 18.5 kDa. Fermentas pageruler prestained protein ladder plus (#SM1811) calibration kit for electrophoresis was utilised.

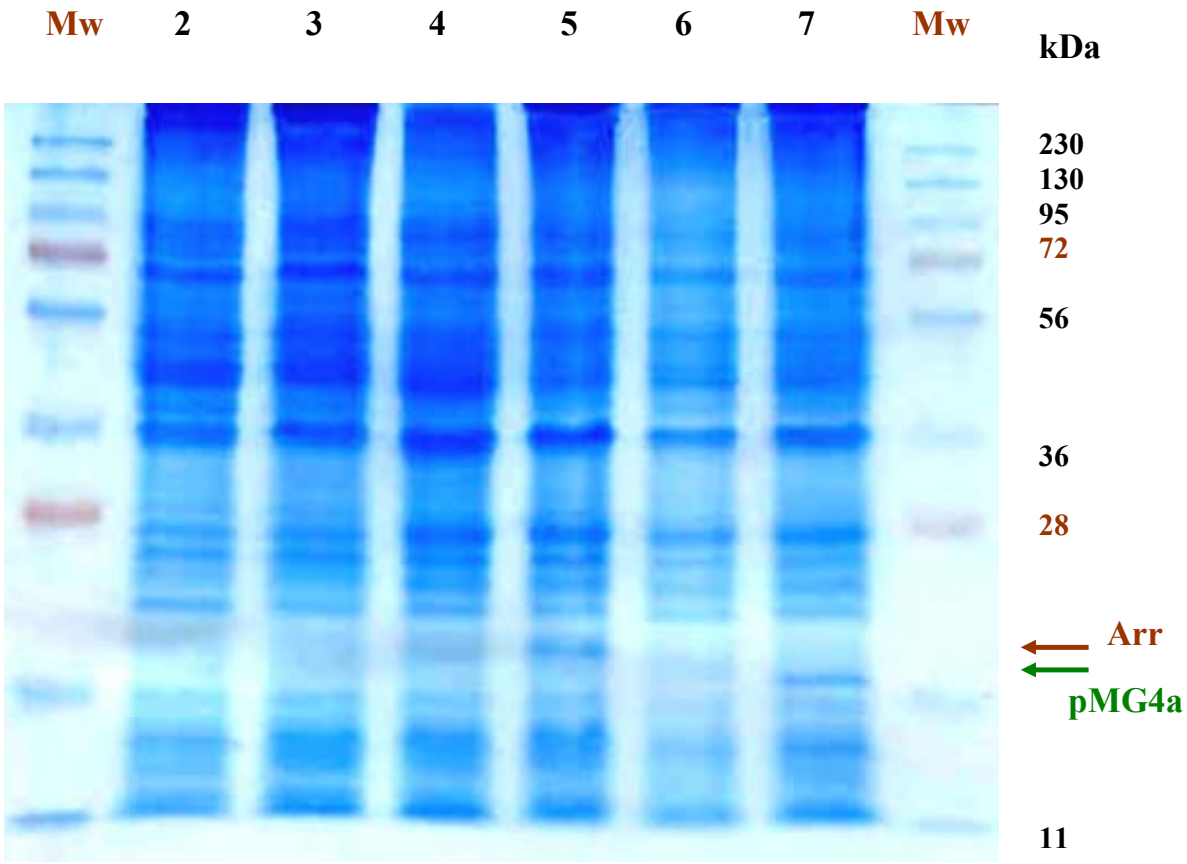


**Figure 40: Over-expression of pET28a-*Bst*49 and pMG4a.** Coomassie-stained SDS-PAGE mini gradient gel (4-12%) of soluble proteins from crude cell extracts prepared from *E. coli* Rosetta2(DE3)pLysS cells transformed with the following constructs: pET28a uninduced (2), pET28a induced (3), pET28a-*Bst*49 uninduced (4), pET28a-*Bst*49 induced (5), pMG4a uninduced (6) and pMG4a induced (7). Samples were induced with 0.6 mM IPTG for 3 hrs. 20 µl of each fraction was loaded onto each lane. Induced bands at ≈18 kDa (5 and 7) are indicated by the **red** and **green** arrows. These bands are consistent with the predicted size of the Arr ADP-ribosyltransferase and its mutant.

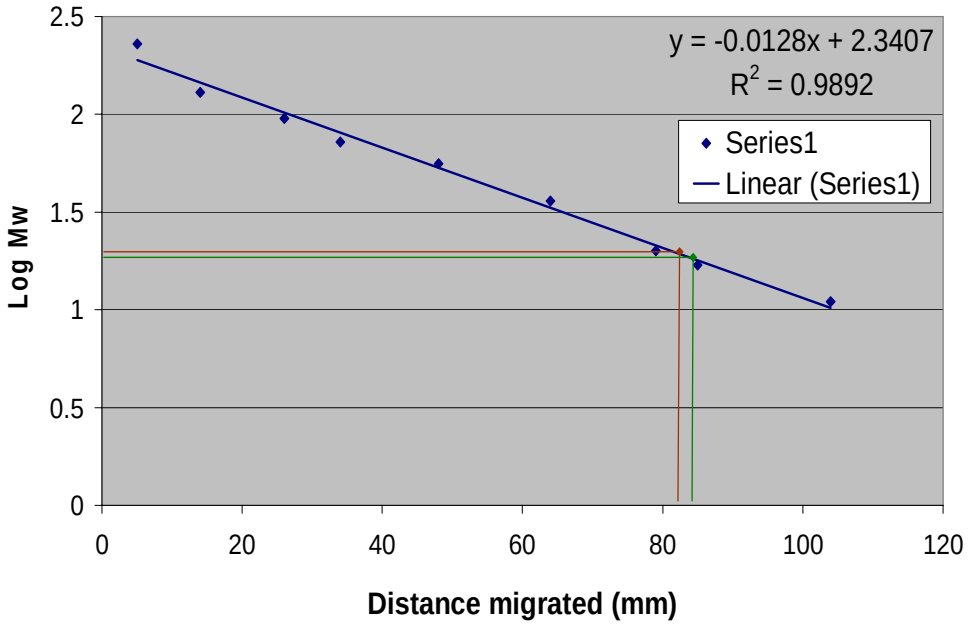


**Figure 41: Calibration curve for determining the molecular weight of pET28a-*Bst*49 and pMG4a.** The red lines converge at the data point (♦) where the log Mw for pET28a-*Bst*49 was extrapolated whilst the green lines converge at another data point (♦) that represents the log Mw for pMG4a.

The relative Mw of the induced bands was determined by comparing their mobilities with those of the $M_w$ standards run on the same gel. By plotting a graph of distance travelled against the log $M_w$ for each of the nine standard proteins, a calibration curve was constructed (**Figure 41**). The electrophoretic mobilities of pET28a-*Bst*49 and pMG4a were 82 and 84 mm respectively. The log $M_w$ was determined by the equation y = -0.0128x + 2.3407. This implied the size of the Arr enzyme to be about 19.5 kDa, which is consistent with its predicted size of 15.9 kDa given the error of measuring $M_w$ from SDS-PAGE gels. Similarly, the size of pMG4a was calculated at 18.4 kDa. Fermentas pageruler prestained protein ladder plus (#SM1811) calibration kit for electrophoresis was utilised.

### 4.6 Change in *E. coli* cell morphology due to over-expression of the *arr* gene and its mutants

Studies using Gram-positive bacteria have predicted that the *arr* gene product may be involved in cell wall biosynthesis, more specifically, in septum formation. When present in Gram-negative cells, a 100-fold reduction in CFU/ml was observed for a specific O.D. This implied that the cells were changing either by becoming more swollen or filamentous. Crystal violet-stained cultures of *E. coli* MM294-4 cells, transformed with the vector only, the unmutagenised *arr* gene, pMG1a, pMG2a and pMG4a were examined under the light microscope. Untransformed *E. coli* MM294-4 cells were included as a negative control.

Untransformed *E. coli* MM294-4 cells exhibited normal rod-shaped morphology as did those transformed with the vector only, pET28a (**Figures 42** and **43**). The unmutagenised *arr* gene demonstrated a filamentous morphology (**Figure 44**). This result was consistent with a lowered CFU/ml, suggesting an abnormality in cell wall biosynthesis. Filamentous growth occurs when cell division is inhibited. This is because *E. coli* MM294-4 cells are still able to grow but since they cannot divide, long filaments are formed. pMG4a also showed a filamentous morphology (**Figure 45**) whereas pMG1a and pMG2a displayed a mixture of morphologies (**Figures 46** and **47**). Normal rod-shaped, filamentous and other unusual morphologies were observed. pMG1a and pMG2a are more susceptible to rifampicin than pMG4a. Thus, the activity of the Arr ADP-ribosyltransferase with respect to rifampicin resistance and to the effect on the microbial cell wall may be distinguishable.

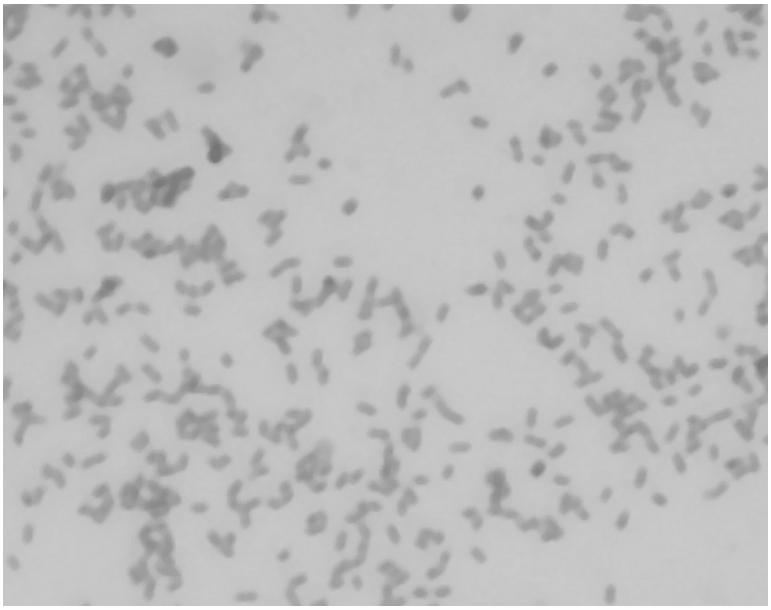

**Figure 42: Light microscopy of untransformed *E. coli* MM294-4 cells cultured in LB observed under oil immersion (x100).** Normal rod-shaped morphology was observed.

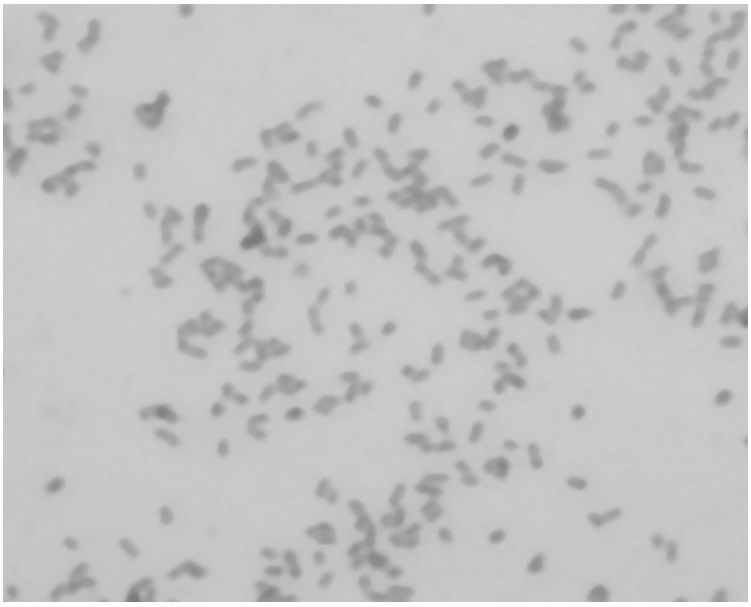

**Figure 43: Light microscopy of *E. coli* MM294-4 cells transformed with the vector only, pGEM-T-Easy, cultured in LB observed under oil immersion (x100).** Normal rod-shaped morphology was observed.

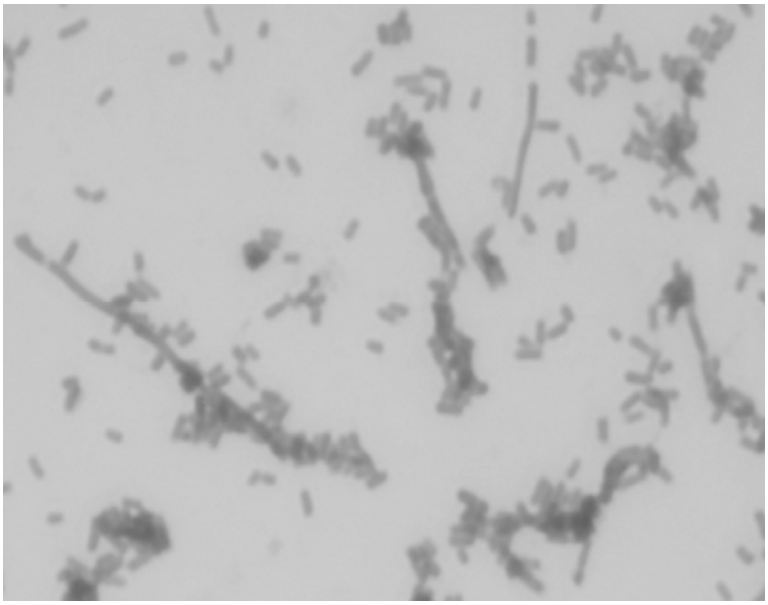

**Figure 44: Light microscopy of *E. coli* MM294-4 cells transformed with constructs containing the unmutagenised *arr* gene cultured in LB observed under oil immersion (x100).** Unusual filamentous morphologies were observed.

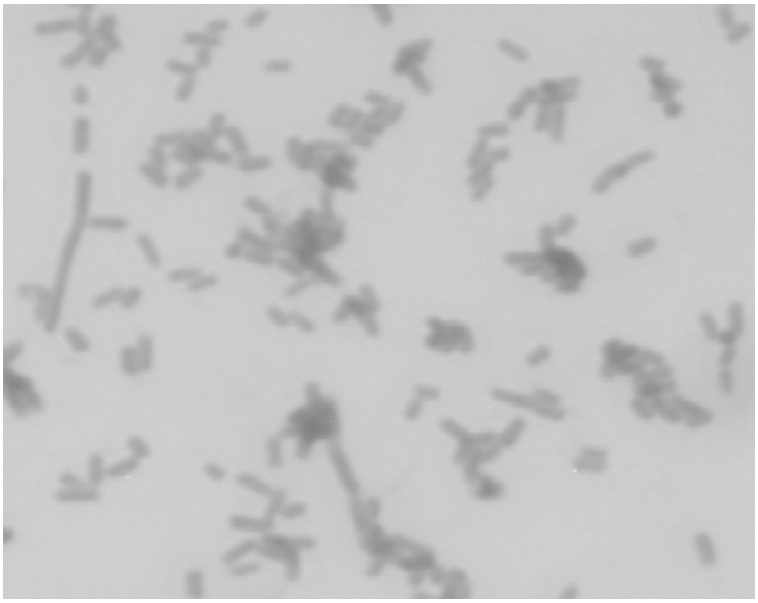

**Figure 45: Light microscopy of *E. coli* MM294-4 cells transformed with pMG4a cultured in LB observed under oil immersion (x100).** Unusual filamentous morphologies were observed.

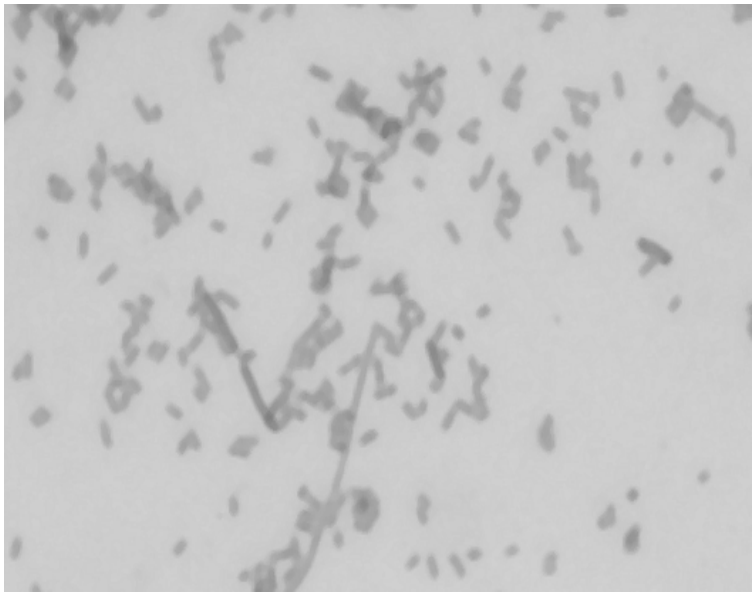

**Figure 46: Light microscopy of *E. coli* MM294-4 cells transformed with pMG1a cultured in LB observed under oil immersion (x100).** Normal rod-shaped, filamentous and other unusual morphologies were observed.

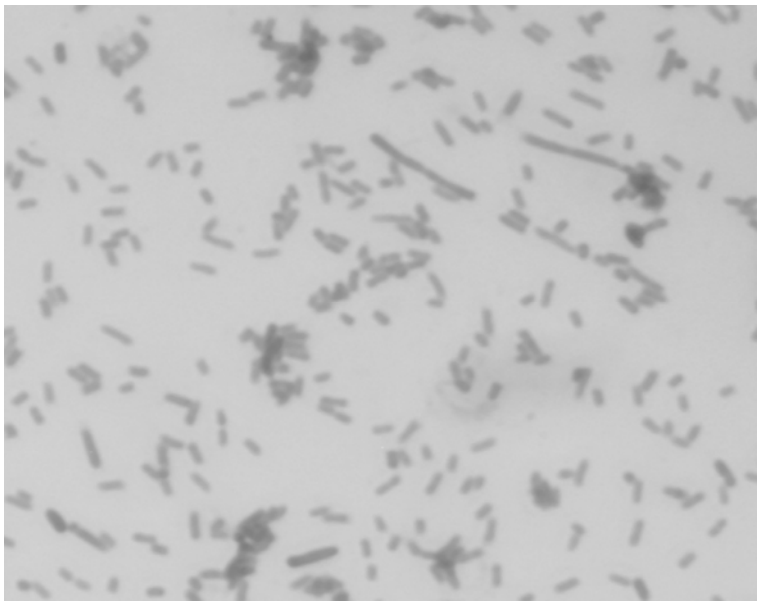

**Figure 47: Light microscopy of *E. coli* MM294-4 cells transformed with pMG2a cultured in LB observed under oil immersion (x100).** Normal rod-shaped, filamentous and other unusual morphologies were observed.

### 4.7 Protein purification

As previously mentioned, fusion proteins were constructed in an attempt to simplify their purification later. It was important to purify these over-expressed enzymes (pET28a-*Bst*49, pMG1a, pMG2a and pMG4a) from *E. coli* as this assisted in providing information pertaining to their chemical properties. Immobilized-metal affinity chromatography, with a nickel-nitrilotriacetic acid (Ni-NTA) matrix, was employed. NTA occupied four of the six ligand binding sites in the co-ordination sphere of the nickel ion, with two sites left vacant to interact with the 6xHis tag. Thus, the 6xHis-tagged proteins were bound tightly and problems such as low yields, impure products and metal-ion contamination were avoided.

#### 4.7.1. Protein purification under native conditions

Purification under native conditions was chosen as the proteins were located in the soluble fraction of the cell and biological activity needed to be retained. Native conditions made it more difficult to predict the amount of soluble protein present in the lysate. However, an expression level of <1% from the total protein preparation was determined. This indicated that the concentration of the 6xHis-tagged proteins was <1 mg/litre. To purify significant amounts of 6xHis-tagged proteins, 100 ml culture volumes were concentrated 100-fold by re-suspending the pellet in 1 ml lysis buffer.

There was a higher potential for binding of background contaminants under native than under denaturing conditions. This was reflected in the larger number of proteins that appeared in the first wash (**Figures 48**, **50**, **52** and **54**). Non-specific binding was reduced by including a low concentration of imidazole (10-20mM) in the lysis and wash buffers. The imidazole ring forms part of the structure of histidine. Imidazole itself bound to the nickel ions and disrupted the binding of dispersed histidine residues in unrelated, non-tagged background proteins.

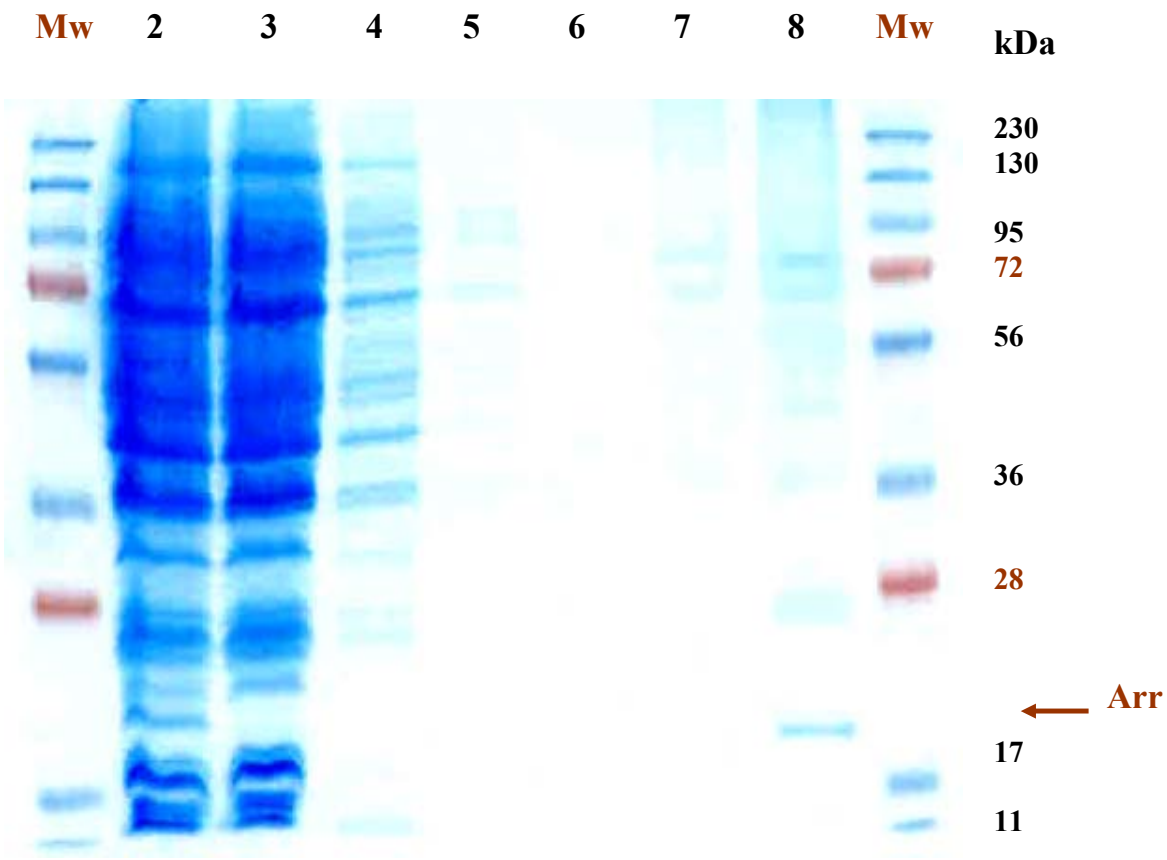


**Figure 48: Native purification of heterologously expressed pET28a-*Bst*49.** Following over-expression in *E. coli* Rosetta2(DE3)pLysS, 6xHis-tagged Arr ADP-ribosyltransferase was purified using Ni-NTA spin columns under native conditions (lysis and wash at 20 mM imidazole; elution at 200 mM imidazole). 20 µl of each 100 µl fraction was loaded onto each lane and run on a Coomassie-stained SDS-PAGE mini gradient gel (4-12%). Cell lysate (2), flow-through (3), wash step 1 (4), wash step 2 (5), wash step 3 (6), first eluate (7) and second eluate (8). Bands at ≈18 kDa (2 and 8) are indicated by the **red** arrow. These bands are consistent with the predicted size of the Arr ADP-ribosyltransferase.

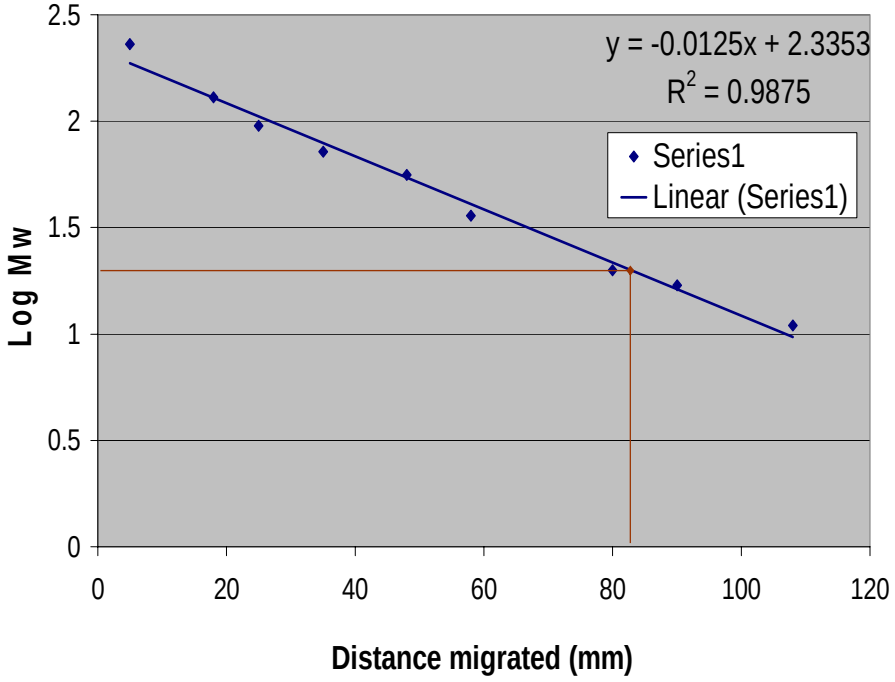


**Figure 49: Calibration curve for determining the molecular weight of purified pET28a-*Bst*49.** The red lines converge at the data point (♦) where the log Mw for purified pET28a-*Bst*49 was extrapolated.

The relative Mw of the induced bands was determined by comparing their mobilities with those of the $M_w$ standards run on the same gel. By plotting a graph of distance travelled against the log $M_w$ for each of the nine standard proteins, a calibration curve was constructed (**Figure 49**). The electrophoretic mobility of pET28a-*Bst*49 was 83 mm. The log $M_w$ was determined by the equation y = -0.0125x + 2.3353. This implied the size of the Arr enzyme to be about 19.8 kDa, which is consistent with its predicted size of 15.9 kDa given the error of measuring $M_w$ from SDS-PAGE gels. Fermentas pageruler prestained protein ladder plus (#SM1811) calibration kit for electrophoresis was utilised.

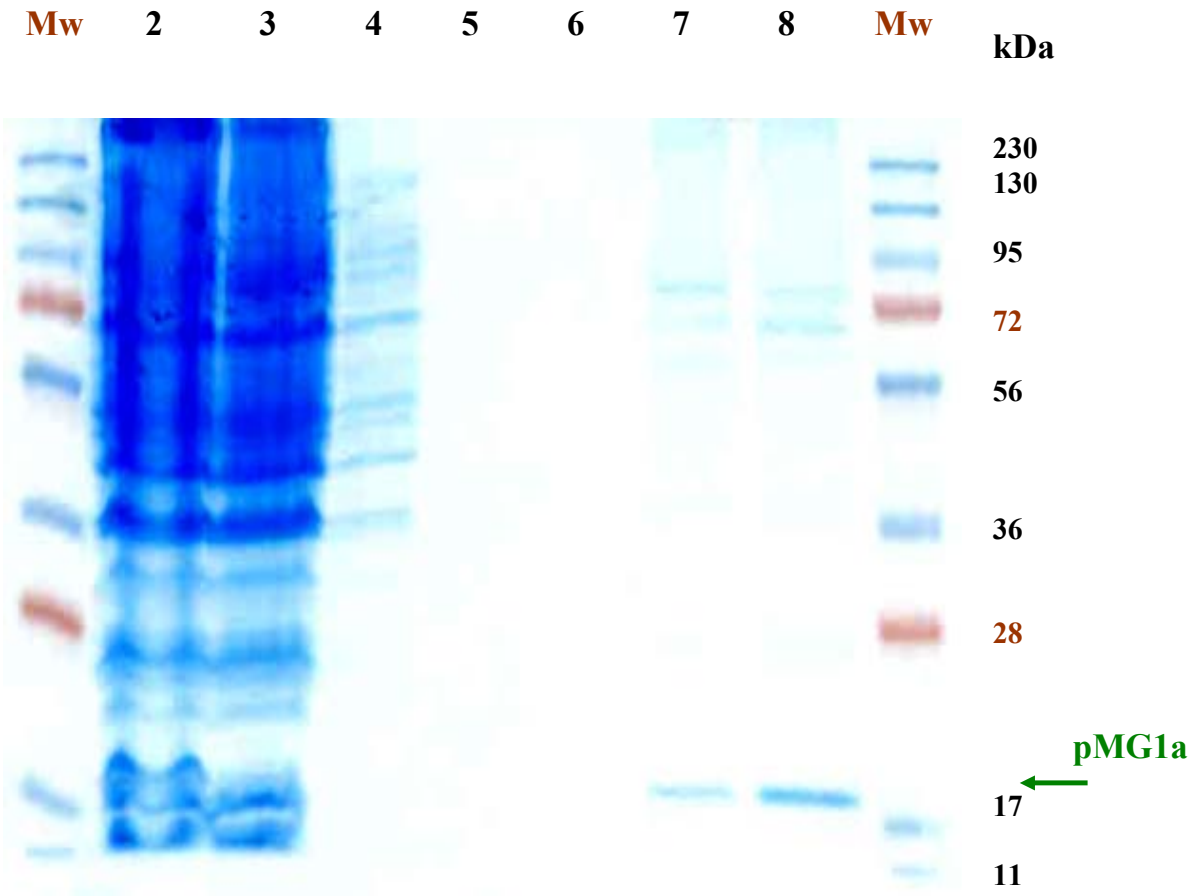


**Figure 50: Native purification of heterologously expressed pMG1a.** Following over-expression in *E. coli* Rosetta2(DE3)pLysS, 6xHis-tagged mutant Arr ADP-ribosyltransferase was purified using Ni-NTA spin columns under native conditions (lysis and wash at 20 mM imidazole; elution at 200 mM imidazole). 20 µl of each 100 µl fraction was loaded onto each lane and run on a Coomassie-stained SDS-PAGE mini gradient gel (4-12%). Cell lysate (2), flow-through (3), wash step 1 (4), wash step 2 (5), wash step 3 (6), first eluate (7) and second eluate (8). Bands at ≈18 kDa (2, 7 and 8) are indicated by the **green** arrow. These bands are consistent with the predicted size of the mutant Arr ADP-ribosyltransferase, pMG1a.

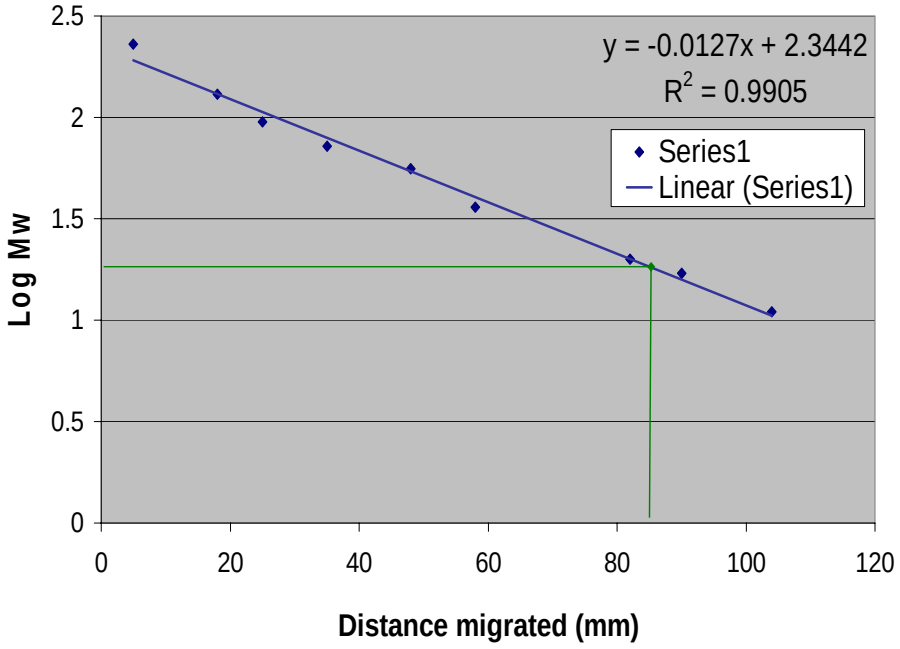


**Figure 51: Calibration curve for determining the molecular weight of purified pMG1a.** The green lines converge at the data point (♦) where the log Mw for purified pMG1a was extrapolated.

The relative Mw of the induced bands was determined by comparing their mobilities with those of the $M_w$ standards run on the same gel. By plotting a graph of distance travelled against the log $M_w$ for each of the nine standard proteins, a calibration curve was constructed (**Figure 51**). The electrophoretic mobility of pMG1a was 85 mm. The log $M_w$ was determined by the equation y = -0.0127x + 2.3442. This implied the size of the Arr enzyme to be about 18.4 kDa, which is consistent with its predicted size of 15.9 kDa given the error of measuring $M_w$ from SDS-PAGE gels. Fermentas pageruler prestained protein ladder plus (#SM1811) calibration kit for electrophoresis was utilised.

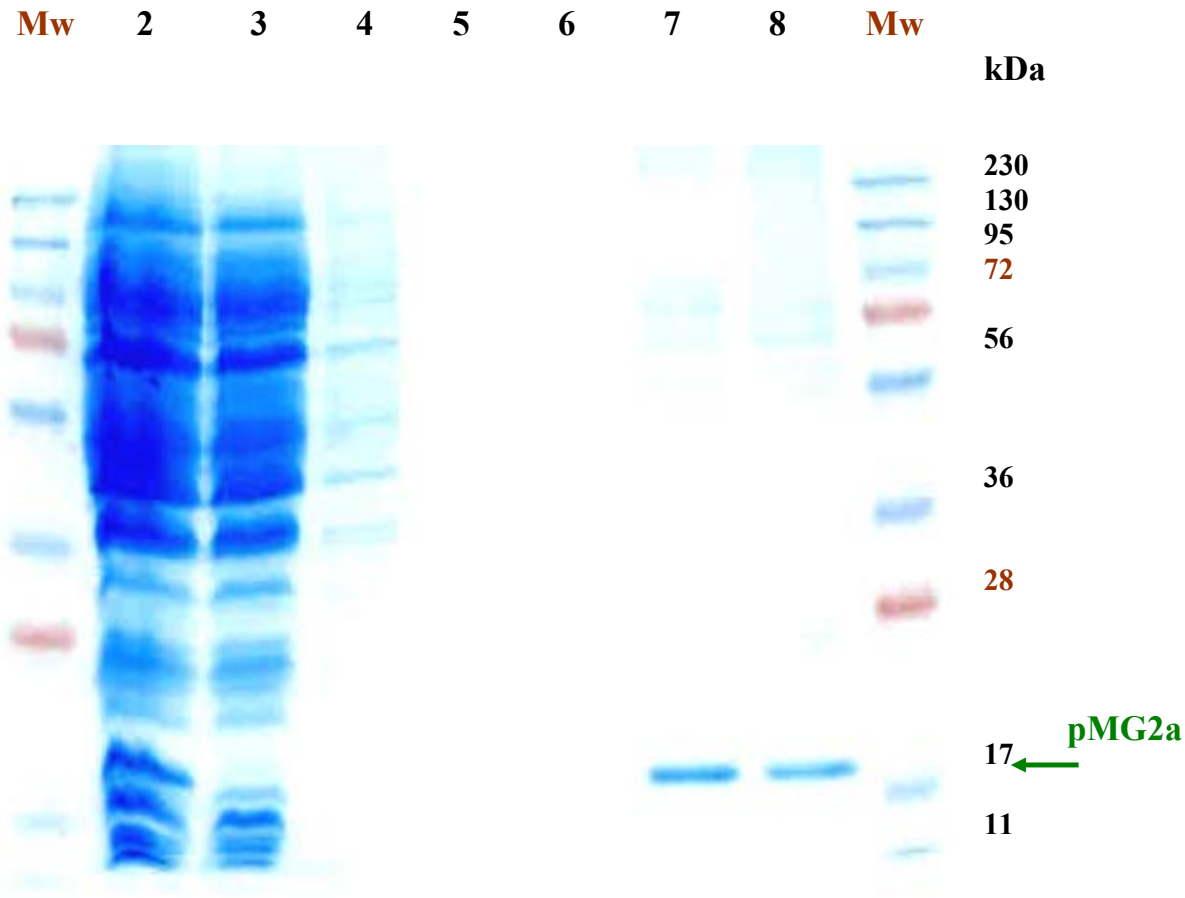


**Figure 52: Native purification of heterologously expressed pMG2a.** Following over-expression in *E. coli* Rosetta2(DE3)pLysS, 6xHis-tagged mutant Arr ADP-ribosyltransferase was purified using Ni-NTA spin columns under native conditions (lysis and wash at 20 mM imidazole; elution at 200 mM imidazole). 20 µl of each 100 µl fraction was loaded onto each lane and run on a Coomassie-stained SDS-PAGE mini gradient gel (4-12%). Cell lysate (2), flow-through (3), wash step 1 (4), wash step 2 (5), wash step 3 (6), first eluate (7) and second eluate (8). Bands at ≈18 kDa (2, 7 and 8) are indicated by the **green** arrow. These bands are consistent with the predicted size of the mutant Arr ADP-ribosyltransferase, pMG2a.

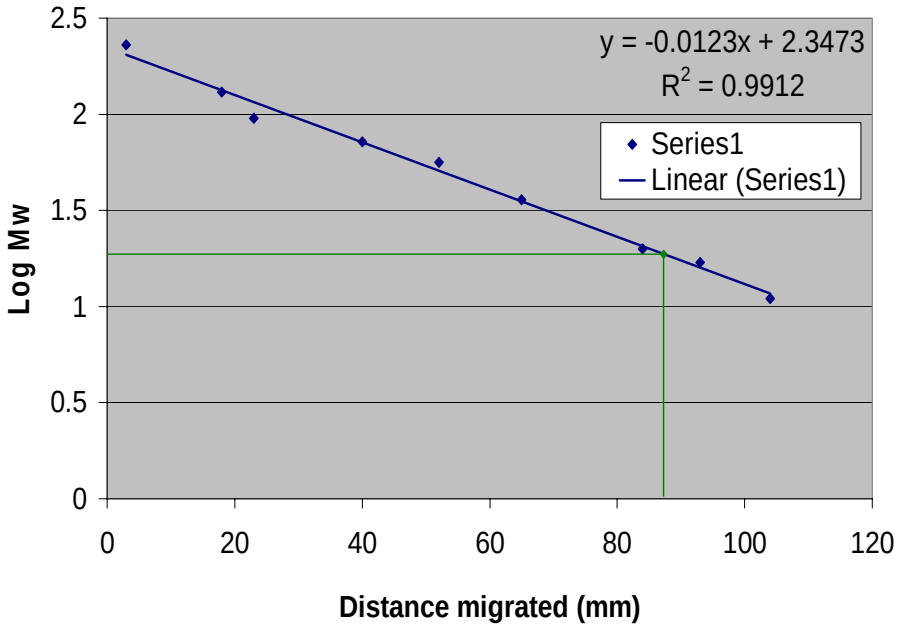


**Figure 53: Calibration curve for determining the molecular weight of purified pMG2a.** The green lines converge at the data point (♦) where the log Mw for purified pMG2a was extrapolated.

The relative Mw of the induced bands was determined by comparing their mobilities with those of the $M_w$ standards run on the same gel. By plotting a graph of distance travelled against the log $M_w$ for each of the nine standard proteins, a calibration curve was constructed (**Figure 53**). The electrophoretic mobility of pMG2a was 87 mm. The log $M_w$ was determined by the equation y = -0.0127x + 2.3442. This implied the size of the Arr enzyme to be about 18.9 kDa, which is consistent with its predicted size of 15.9 kDa given the error of measuring $M_w$ from SDS-PAGE gels. Fermentas pageruler prestained protein ladder plus (#SM1811) calibration kit for electrophoresis was utilised.

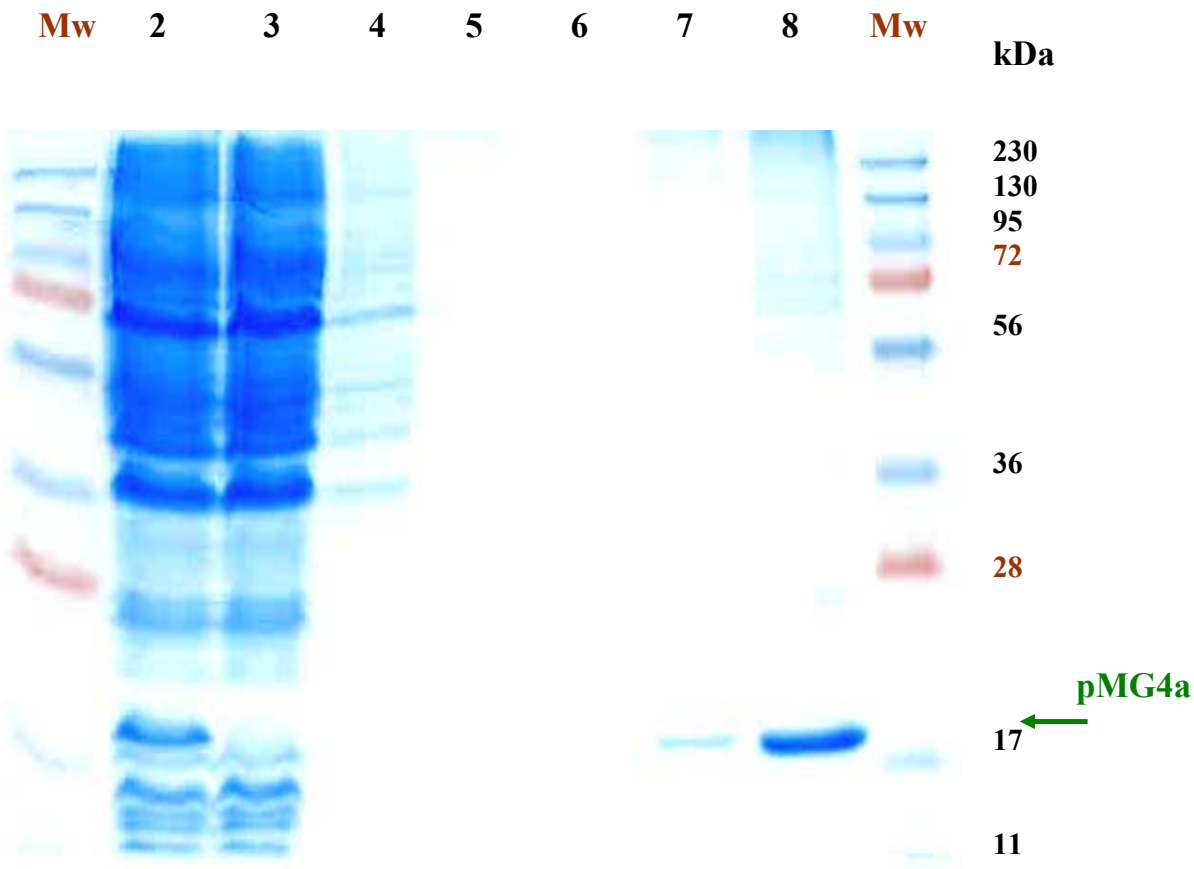


**Figure 54: Native purification of heterologously expressed pMG4a.** Following over-expression in *E. coli* Rosetta2(DE3)pLysS, 6xHis-tagged mutant Arr ADP-ribosyltransferase was purified using Ni-NTA spin columns under native conditions (lysis and wash at 20 mM imidazole; elution at 200 mM imidazole). 20 µl of each 100 µl fraction was loaded onto each lane and run on a Coomassie-stained SDS-PAGE mini gradient gel (4-12%). Cell lysate (2), flow-through (3), wash step 1 (4), wash step 2 (5), wash step 3 (6), first eluate (7) and second eluate (8). Bands at ≈18 kDa (lanes 2, 7 and 8) are indicated by the **green** arrow. These bands are consistent with the predicted size of the mutant Arr ADP-ribosyltransferase, pMG4a.

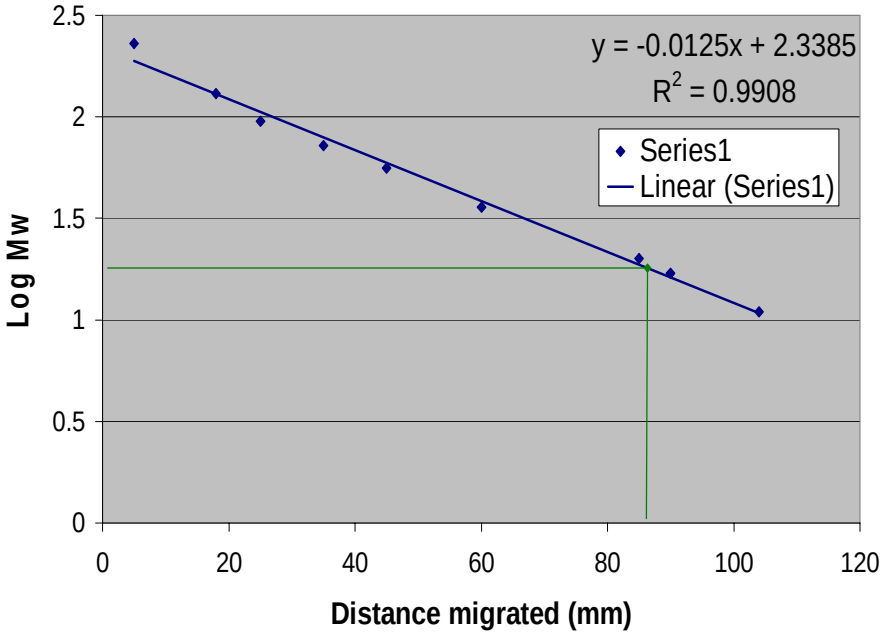


**Figure 55: Calibration curve for determining the molecular weight of purified pMG4a.** The green lines converge at the data point (♦) where the log Mw for purified pMG4a was extrapolated.

The relative Mw of the induced bands was determined by comparing their mobilities with those of the $M_w$ standards run on the same gel. By plotting a graph of distance travelled against the log $M_w$ for each of the nine standard proteins, a calibration curve was constructed (**Figure 55**). The electrophoretic mobility of pMG4a was 85 mm. The log $M_w$ was determined by the equation y = -0.0125x + 2.3385. This implied the size of the Arr enzyme to be about 18.4 kDa, which is consistent with its predicted size of 15.9 kDa given the error of measuring $M_w$ from SDS-PAGE gels. Fermentas pageruler prestained protein ladder plus (#SM1811) calibration kit for electrophoresis was utilised.

The histidine residues in the 6xHis-tag had a $pK_a$ of ≈6.0. When the pH was reduced to 4.5, the histidines became protonated. Under these conditions the 6xHis-tagged proteins could no longer bind to the nickel ions. Similarly, the increase in imidazole concentration (100 mM) prevented any binding. The proteins dissociated from the matrix because they could no longer compete for binding sites on the Ni-NTA resin. Thus, the purified proteins were eluted successfully and are visible in lanes 7 and 8 in **Figures 48**, **50**, **52** and **54**. The amount of purified protein was quantified by measuring the optical density of the corresponding band (**Table 22**). The values were obtained by using Quantity One® Software Version 4.6. Once these conditions had been established using small scale cultures, the experiments were scaled up in order to produce several milligrams (5-7 mg) of purified proteins for future work.

**Table 22:** Peak optical density of bands produced from purified pET28a-*Bst*49 and its mutants under native conditions

| Protein | Peak O.D. (Cell Lysate) | Peak O.D. (Eluate 1) | Peak O.D. (Eluate 2) | Molecular weight (kDa) | Concentration (mg/ml) |
|---|---|---|---|---|---|
| **pET28-*Bst*49** | 19.2 | 0 | 0.13 | 19.8 | 0.16 |
| **pMG1** | 19.2 | 0.12 | 0.22 | 18.6 | 0.32 |
| **pMG2** | 19.9 | 0.26 | 0.25 | 18.5 | 0.51 |
| **pMG4** | 19.3 | 0.12 | 0.38 | 18.7 | 0.48 |

# CHAPTER 5

# DISCUSSION

## 5.1 Evaluation of mutagenesis approaches: *in vivo* selection versus PCR-mediated *in vitro* mutagenesis

Rifampicin is a chemotherapeutic agent of choice to combat infections by pathogenic nocardioforms and *M. tuberculosis*. Soon after its introduction to clinical practice in 1972, resistant mutants were identified (Woodley *et al.,* 1972). Resistance has been primarily through target site alteration but in addition four inactivation mechanisms have been identified and include decomposition, ADP-ribosylation, glucosylation and phosphorylation. Rifampicin inactivation by ribosylation was the focus of this study as it functions in many mycobacterial pathogens. However, virtually nothing is known about the properties of this Arr ADP-ribosyltransferase. An approach to further characterise this enzyme by mutational analysis was made. The aim of this work was to obtain Arr mutants with alterations in the ORF which might provide information about the active site of this enzyme.

Two approaches were utilised to obtain these Arr ORF mutants, the first being *in vivo* selection. The mutants may arise from: chromosomal mutations in the host cell, mutations in the *rpo*B gene, reduced antimicrobial permeability or mutations associated with the plasmid. Once colonies that had arisen owing to plasmid-borne mutations were identified, it was necessary to differentiate among the three types of mutations that occurred. These involved alterations of the copy number or mutations associated with the promoter or the ORF. They are quite common and a large number have been well characterised. Ultimately, a single ORF mutant was identified from ≈80 plasmid-borne mutants, which were distinguished from an initial sample size of ≈600 rifampicin resistant mutants. Thus, a low success

rate of 0.17% was observed. An advantage of *in vivo* selection was its cost effectiveness.

The second approach of PCR-mediated *in vitro* mutagenesis proved more successful. Recombinant clones were selected on the basis of colour on indicator plates. These recombinants represented a mutant library that contained a population of mutants with different point mutations in the *arr* gene. Ten colonies were randomly chosen and sent for sequencing to confirm any nucleotide changes. Sequence analysis identified three of the ten clones as Arr ORF mutants. Thus, a 180-fold increase in success rate was observed in comparison to *in vivo* selection. The major advantage with this technique was its cost-effectiveness in terms of time. Another alternative was chemical mutagenesis. A disadvantage is contact with mutagens such as ethylmethanesulfonate (EMS), N-methyl-N′-nitro-N-nitrosoguanidine (NTG) or EtBr. This approach was not utilised because it had been previously investigated. PCR-mediated *in vitro* mutagenesis is similar to random chemical mutagenesis and *in vivo* selection, with the added benefit that the chosen primer pair provides a convenient way to target the random base pair mutations to a defined segment of DNA. It is site-directed as opposed to the other methods. Thus, it is more efficient, which is a determining factor for future work as MDR-TB and presently XDR-TB are a growing concern in the global community.

**5.2 Mutational analysis of the Arr ADP-ribosyltransferase**

Three mutated *arr* ORFs cloned into pGEM-T-Easy were studied. These constructs were pMG1a (obtained from *in vivo* selection), pMG2a and pMG4a (obtained from PCR-mediated *in vitro* mutagenesis). The amino acid substitution that occurred in each of these mutants was examined in terms of size and polarity. These are the chief contributing factors affecting protein folding both with regards to their own native conformations and to their aqueous environment. The implication of these structural changes on the functioning of the enzyme will then be considered.

### 5.2.1 Structural analysis of the *arr* gene in pMG1a

The *arr* gene in pMG1a had a single base pair change from cytosine to adenine at position 16 on the direct strand. This transversion resulted in a codon change from CCG to ACG and was predicted to cause an amino acid alteration from proline to threonine (**Figure 56**). The residue mass of proline is 97.1 D whereas threonine is 101.1 D. However, proline is non-polar and hydrophobic while threonine is polar, with an uncharged side chain, and hydrophilic. Additionally, proline is a cyclic amino acid that has conformational constraints imposed by the cyclic nature of its pyrrolidine side group. This is unique among the standard amino acids and it creates a tight bend, resulting in a change of direction within the polypeptide chain. In comparison, threonine has an open side chain. A greater torsion angle is present as the rotation around the α-carbon atom is increased. Consequently, the structure of the protein is more flexible. This amino acid substitution is classified as semi-conservative. However, a change in protein properties might be expected because packing of the polypeptide chain would be affected.

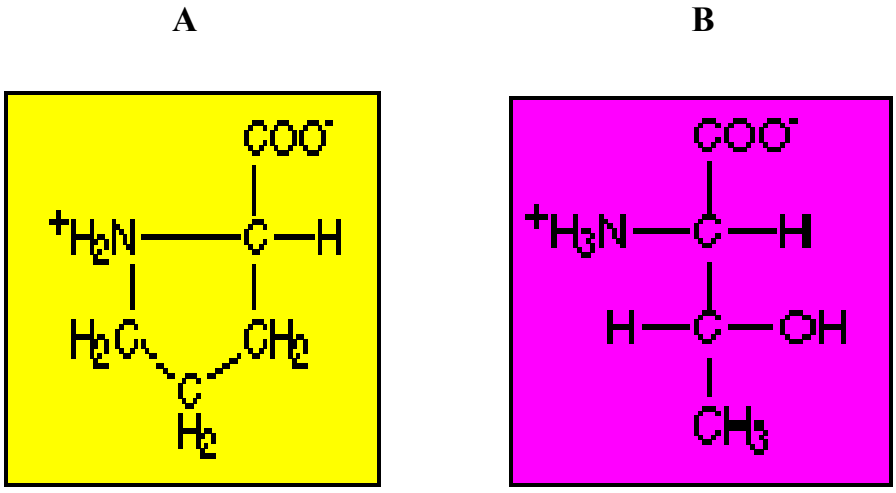


**Figure 56: Chemical structures of (A) proline and (B) threonine**

### 5.2.2 Structural analysis of the *arr* gene in pMG2a

A transition was detected in the *arr* gene in pMG2a. Consequently, a codon change from AAA to AGA at position 20 on the direct strand was observed. This was predicted to cause an amino acid alteration from lysine to arginine (**Figure 57**). Both amino acids are hydrophilic and polar, with positively charged side chains. The polarity of an amino acid's side chain determines its location within a protein. Non-polar amino acid residues are found in the interior. They form the hydrophobic core and are tightly packed and highly conserved. Uncharged, polar amino acids are found on the surface and in the interior of a protein. They satisfy the hydrogen bonding requirements of a polypeptide. These non-covalent interactions increase the protein's conformational stability. Charged, polar amino acids are situated on the surface. The above stimuli result in non-polar substances minimising contact with their aqueous environment. This is referred to as the hydrophobic effect that stimulates protein folding.

Arginine is larger than lysine with a residue mass of 156.2 D and 128.2 D respectively. Although similar in polarity, this difference in size will affect the protein's ability to fold into its native structure. Thus, this semi-conservative substitution may result in a moderate loss in function.

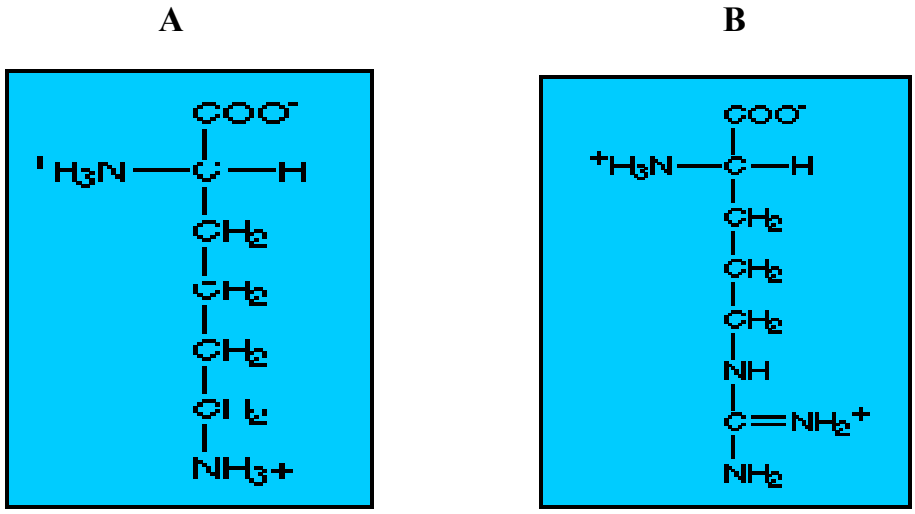


**Figure 57: Chemical structures of (A) lysine and (B) arginine**

### 5.2.3 Structural analysis of the *arr* gene in pMG4a

Two base pair changes were discovered in the *arr* gene in pMG4a. However, they were located in the same codon. Both were transversions and resulted in a codon change from GTC to TAC. This was predicted to cause an amino acid alteration from valine to tyrosine (**Figure 58**). This type of substitution had parallels to that of pMG1a. Valine is non-polar and hydrophobic while tyrosine is polar, with an uncharged side chain, and hydrophilic. However, these amino acids differ in size. The residue mass of valine is 99.1 D whereas tyrosine is 163.2 D. Although similar in polarity, this difference in size will affect the packing of the polypeptide into its native structure. Thus, this semi-conservative substitution was expected to result in a moderate loss in function.

**A** **B**

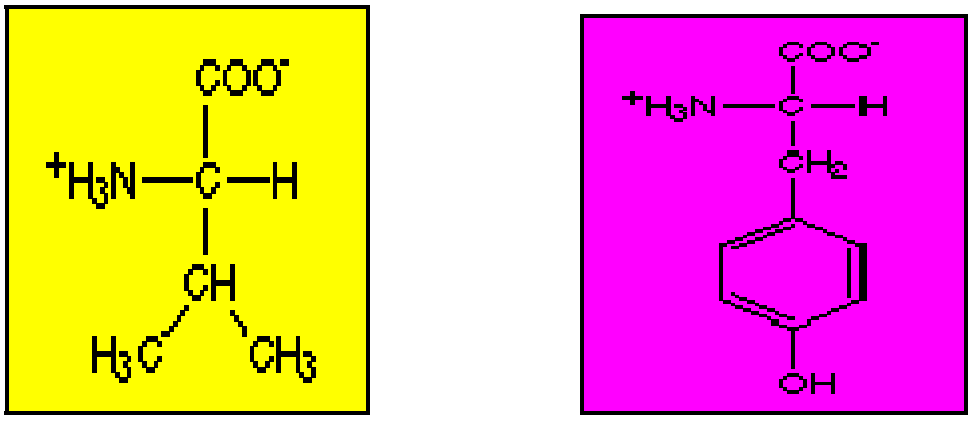


**Figure 58: Chemical structures of (A) valine and (B) tyrosine**

### 5.2.4 Implications of structural changes on Arr ADP-ribosyltransferase functioning

pMG1a and pMG2a conferred resistance to 50 µg/ml of rifampicin. They displayed a lowered activity of *in vitro* rifampicin inactivation. pMG4a conferred resistance to 200 µg/ml of rifampicin and it completely inactivated the drug in the presence of $NAD^+$. This difference in enzyme activity provided information about

the importance of those amino acids within the protein, particularly to its phenotype of rifampicin resistance. pMG1a and pMG2a showed a severe decrease in rifampicin resistance whereas only a slight decrease was observed in pMG4a. This implied that the position of the amino acid substitution was also significant as all the mutations were semi-conservative.

The substitutions for pMG1a and pMG2a occurred near the N-terminus while that of pMG4a was close to the protein's C-terminus. A possible explanation for the difference in rifampicin resistance could be that the amino acid substitutions located towards the N-terminus are closer to the enzyme's active site. A mutation here would have a greater impact on its ability to inactivate rifampicin than one situated by the C-terminus and closer to the enzyme's surface. The substitution in pMG4a did not affect its ability to inactivate rifampicin as severely as the substitutions in pMG1a and pMG2a. All the substitutions in the ORF mutants were classified as semi-conservative. This type of substitution is informative as the change in function can be related to the structural changes. This is not the case with radical substitutions where drastic alterations usually result in abolished activity.

### 5.3 Arr ADP-ribosyltransferases susceptibility to light

Individuals suffering from mycobacterial infections are often advised to increase their exposure to sunlight. This is due to the effects upon the patient's metabolism, for example elevating serum 25-hydroxy vitamin D (Davies *et al.,* 1987). Current chemotherapeutic treatments involve low-intensity laser radiation, which has been shown to enhance the efficacy of antibacterial agents (Maliev *et al.,* 1998). One of the most widely used chemotherapeutic agents to combat mycobacterial infections is rifampicin (Grosset, 1989). For this reason the relationship of light with regards to rifampicin inactivation genes was investigated.

Rifampicin resistance arising from the cloned ADP-ribosyltransferase and its mutants was greatly diminished (20-fold reduction) by light (Quan, 1997). I found there was no difference in the level of inhibition observed under white, red and blue light. A variation was only observed in the control samples containing no inactivation genes where bleaching, which is wavelength dependant, gave the impression of increased resistance to rifampicin. The glycosyltransferase, cloned from *N. brasiliensis* IFM 0236, displayed a slight decrease in resistance in the presence of white, red and blue light. However, when the gene was in the reverse orientation no effect was observed. The cloned *Rhodococcus equi* mono-oxygenase, which inactivates rifampicin by decomposition, was not inhibited by light. Thus, it is conceivable that sunlight is beneficial to individuals suffering from mycobacterial infections because it disables the bacterial response to antibiotic challenge in the case of ribosylative inactivation of rifampicin.

SDS-PAGE analysis of extracts from an *E. coli* transformant carrying the unmutagenised *arr* gene demonstrated that growth in the presence of light resulted in the complete disappearance of the band corresponding to the Arr ADP-ribosyltransferase (Quan, 1997). This also occurred when the *arr* gene was ligated into another vector, pET28a. The band corresponding to the glycosyltransferase was present, although slightly diminished. There was no difference in intensity of the band corresponding to the glycosyltransferase when it was expressed in the reverse orientation. This indicated that the Arr ADP-ribosyltransferase was photolabile whereas the glycosyltransferase was present in normal amounts but inactive in the presence of light.

The basis of Arr ADP-ribosyltransferases susceptibility to light remains unknown. An attempt to understand this inhibition was made by mutational analysis. *In vivo* selection was utilised to obtain light resistant mutants. Several attempts proved unsuccessful, suggesting that it may be impossible to acquire such mutants. Future work should explore this further.

## 5.4 Change in *E. coli* cell morphology due to over-expression of the *arr* gene and its mutants

Studies using Gram-positive bacteria have predicted that the *arr* gene product may be involved in cell wall biosynthesis; more specifically, in septum formation resulting in a change in cell morphology (Sugawara *et al.,* 2002). When the Arr ADP-ribosyltransferase was expressed at a high level in *E. coli* there was a 100-fold reduction in CFU/ml for a specific O.D. This was consistent with light microscope visualisations of *E. coli* cultures that revealed cells expressing the *arr* gene were filamentous whereas cells transformed with the vector only exhibited normal rod-shaped morphology (Puhača, 2003). Thus, a similar effect was observed in both Gram-positive and Gram-negative bacteria even though they differ in terms of cell wall structure and components.

Sugawara *et al.* (2002) demonstrated that four periplasmic proteins isolated from *Streptomyces coelicolor* shared the following consensus sequence Leu(or Ala)-Thr(or Ala)-Ala-Cys-Gly. Here, ribosylation occurred on the sulphur atom of the cysteine residue. This site of ADP-ribosylation is acknowledged as the location of lipoprotein modification needed for export of the proteins and their anchorage to the outer surface of the cytoplasmic membrane. Based on sequence data, all four proteins were functionally similar and participated in the regulation of transport of metabolites or nutrients through the membrane. Hence, one prediction for the Arr enzyme is that *in vivo* it possibly ribosylates target proteins on the thiol group of a cysteine residue and that it may resemble these isolated proteins as it is also an extra cellular protein.

Mutants with a lowered resistance to rifampicin exhibited normal rod-shaped, filamentous and other unusual morphologies. This indicated that the activity of the Arr ADP-ribosyltransferase with respect to rifampicin resistance and to the effect on the microbial cell wall may be distinguishable.

### 5.5. Over-expression, purification and biochemical characterisation of the Arr ADP-ribosyltransferase and its mutants

Previous attempts to over-express and purify the Arr ADP-ribosyltransferase had failed. This problem was overcome by changing the vector and host combination. Once this was completed, all of the aims of this MSc project were fulfilled. Future work involves the further biochemical characterisation of this enzyme and its mutants. This is of interest as it would elucidate the chemical properties of this protein. The pure enzyme can then be used to determine its substrate specificity as it appears not to be too specific in its choice of substrate, suggesting it may show activity against other antibiotics of clinical significance.

Biophysical measurements of wild-type and mutant Arr protein were made under the supervision of Dr. Gianfranco Risuleo (Rome, Italy). The eluted proteins were dissolved in a high ion strength buffer. This was a problem as only conductivity measurements could be performed because the high ion concentration inhibits the movement of charges on the protein's surface, which impairs the formation of a reliable representation of the dielectric response. Such conductivity measurements are less informative than dielectric relaxation measurements that provide data about a number of physico-chemical properties such as gyration radius, shape and dielectric constant. Consequently, the proteins were dialyzed against a series of low ion strength buffers (15mM $NH_4Cl$, 15mM NaCl and 10mM Tris-HCl pH7.5) to avoid shocking them from a high to low ion strength, possibly resulting in their precipitation out of solution. After the $O.D._{280}$ was determined, the first round of measurements was performed. This process was repeated two times until the protein concentration became too low for further analysis.

The results showed that wild-type Arr ADP-ribosyltransferase, pMG2a and pMG4a showed a comparable dielectric behaviour. In contrast, pMG1a had a significantly higher hydrodynamic radius and dipole movement indicating a dramatic change in conformation. These findings are encouraging and this procedure is confirmed as a tool for investigating the structure of proteins in

solution. Currently, the primary structure of the unmutagenised enzyme is being investigated by computational simulators to produce a fantasy structure.

The *in vivo* function of the *arr* gene remains unknown. This enzyme acts most efficaciously on semi-synthetic rifamycins rather than the secondary metabolites as they are synthesized by actinomycetes. This is evidenced by the higher levels of resistance to rifampicin when compared to the naturally produced rifamycin SV. Thus, it seems unlikely that this gene evolved solely to impart resistance against this antibiotic. It was proposed that this gene product and the other three rifampicin inactivating enzymes are involved in cell wall assembly. Consistent with this idea, glycosyltransferases are known to be involved in peptidoglycan biosynthesis and over-expression of the Arr enzyme results in altered cell morphology. Although ADP-ribosyltransferases show minimal sequence conservation, the Arr enzyme appears not to show any sequence conservation or similar secondary structure with other cloned and sequenced ADP-ribosylation enzymes. Hence, it may represent an entirely different class of ADP-ribosyltransferases.

Thus, with collaborative efforts between molecular biology and biochemistry the kinetic properties of the enzyme will be determined and its *in vivo* function elucidated. The three-dimensional structure will be established, allowing design of an inhibitor that can be chemically synthesised as part of drug improvement and development by rational design. This is a necessity as TB has reached epidemic proportions in Southern Africa and elsewhere.

# CHAPTER 6

# APPENDICES

## 6.1 APPENDIX A: MEDIA

**Table 1:** Composition of bacterial culture media

| Medium | Components | Components per litre (grams) |
|---|---|---|
| **LB** | Tryptone | 10 |
| | Yeast extract | 5 |
| | NaCl | 10 |
| **LB-agar** | Tryptone | 10 |
| | Yeast extract | 5 |
| | NaCl | 10 |
| | Agar: | |
| | for 1.5% LB agar | 15 |
| | for 0.75% LB agar | 7 |
| **SOC** | Tryptone | 20 |
| | Yeast extract | 5 |
| | NaCl | 0.5 |
| | Dissolve, then add: | |
| | 250 mM KCl | 10 ml |
| | 2 M $MgCl_2$ | 5 ml |
| | 1 M glucose | 20 ml |

## 6.2 APPENDIX B: SOLUTIONS

**Table 2:** Composition of solutions used for plasmid preparations from *E. coli*

| Solution | Composition of working solution |
|---|---|
| **Solution I** | 50 mM glucose<br>25 mM Tris-HCl<br>10 mM EDTA<br>pH 8.0 |
| **Solution II** | 0.2 M NaOH<br>1.0% SDS |
| **Solution III** | 5 M potassium acetate pH 4.8<br>88.5 ml $sdH_2O$<br>11.5 ml glacial acetic acid |
| **Ribonuclease** | 10 mg/ml solution in $sdH_20$, boiled at 95°C before use |
| **Deoxyribonuclease** | 10 mg/ml solution in $sdH_20$ |

**Table 3:** Composition of solutions for *E. coli* transformation

| Type of transformation procedure | Solution | Composition of working solution |
|---|---|---|
| ***E. coli* standard $CaCl_2$ transformation** | **$CaCl_2$ transformation buffer** | 20 mM Tris-HCl<br>100 mM $CaCl_2$<br>pH 7.6-8.0 |
| | **20% glucose** | 4g glucose<br>20 ml $sdH_2O$ |
| **High efficiency transformation protocol** | **TB buffer** | 10 mM HEPES<br>15 mM $CaCl_2$<br>250 mM KCl<br>55 mM $MnCl_2$ |
| | **SOB medium** | 2% Tryptone<br>0.5% Yeast Extract<br>0.05% NaCl<br>250 mM KCl<br>2 M $MgCl_2$ |

**Table 4:** Composition of agarose gel electrophoresis buffers for analysis of DNA

| Solution | Composition of working solution |
|---|---|
| **Agarose gels** | 0.8 g (0.4%), 1.6 g (0.8%) or 2.4 g (1.2%) agarose<br>20 ml 5x TBE<br>180 ml $sdH_20$ |
| **TE buffer** | 0.2 ml 0.5 M EDTA pH 8.0<br>1.0 ml 1M Tris-HCl pH 8.0 |
| **5x TBE** | 54.0 g Tris<br>27.5 g boric acid<br>20 ml 0.5 M EDTA pH 8.0 |
| **Bromophenol blue tracking dye** | 30% glycerol (w/v) in TE<br>0.025% bromophenol blue |
| **Running buffer (0.5x TBE)** | 25 ml 5x TBE<br>225 ml $sdH_20$<br>25 µl EtBr |

**Table 5:** Composition of SDS-PAGE solutions for analysis of proteins

| Solution | Composition of working solution (grams or millilitres) |
|---|---|
| **Acrylamide stock solution** | 30.0 g acrylamide<br>0.8 g N, N'methylenebisacrylamide<br>100 ml $sdH_2O$ |
| **Stacking gel (4%) buffer** | 30% acrylamide<br>1% bis<br>4x stacking buffer (0.5 M Tris pH 6.8)<br>10% SDS<br>10% APS<br>TEMED<br>$sdH_2O$ |
| **Separating gel (15%) buffer** | 30% acrylamide<br>1% bis-acrylamide<br>4x resolving buffer (1.5 M Tris pH 8.8)<br>10% SDS<br>10% APS<br>$sdH_2O$ |
| **10% Ammonium persulphate (APS)** | 0.44 mM APS<br>$sdH_2O$ to 1.0 ml |
| **10% Sodium dodecyl sulphate (SDS)** | 0.35 M SDS<br>$sdH_2O$ to 10 ml |

| | |
|---|---|
| **Electrophoresis buffer** | 25 mM Tris<br>0.2 M glycine (electrophoresis grade)<br>0.1% SDS<br>sd$H_2O$ to 5.0 L |
| **2x Sample loading buffer** | 0.5 M Tris-HCl pH 6.8<br>10% SDS<br>20% (v/v) glycerol<br>0.2 mM dithiothreitol (DTT)<br>0.3 mM bromophenol blue |

**Table 6:** Composition of Coomassie® staining solutions for analysis of proteins

| Solution | Composition of working solution |
|---|---|
| **Isopropanol fixing solution** | 25% (v/v) isopropanol<br>10% (v/v) acetic acid |
| **Coomassie staining solution** | 0.05% (w/v) Coomassie Brilliant Blue 2-250<br>40% (v/v) ethanol<br>10% (v/v) glacial acetic acid<br>50% (v/v) d$H_2O$ |
| **Destaining solution** | 40% (v/v) ethanol<br>10% (v/v) glacial acetic acid<br>50% (v/v) d$H_2O$ |

**Table 7:** Composition of solutions used for protein purification by metal affinity chromatography, specifically Ni-NTA, under native conditions

| Solution | Composition of working solution |
|---|---|
| **Lysis buffer** | 50 mM $NaH_2PO_4$<br>300 mM NaCl<br>10 mM imidazole |
| **Wash buffer** | 50 mM $NaH_2PO_4$<br>300 mM NaCl<br>20 mM imidazole |
| **Elution buffer** | 50 mM $NaH_2PO_4$<br>300 mM NaCl<br>250 mM imidazole |
| **Lysozyme** | 10 mg/ml solution in $sdH_2O$ |

**Table 8:** Composition of miscellaneous solutions

| Solution | Composition (grams or millilitres) |
|---|---|
| **0.5 M EDTA pH 8.0** | 18.6 g EDTA salt dehydrate<br>sd$H_20$ to 1 litre |
| **1 M Tris-HCl pH 8.0** | 15.8 g Tris-HCl<br>100 ml sd$H_2O$ |
| **Sodium Acetate pH 5.2** | 408 g NaAc.3 $H_20$<br>sd$H_20$ to 1 litre |
| **TE-saturated phenol** | 14 g phenol<br>10 ml TE buffer |
| **4mM Tris-HCl** | 0.012 g Tris-HCl<br>100 ml sd$H_20$ |
| **1 M IPTG** | 2 g in 8 ml sd$H_20$ |
| **1 M NaCl** | 5.8 g NaCl<br>100 ml sd$H_20$ |
| **Glycerol** | 3.4 ml glycerol<br>6.6 ml sd$H_20$ |

**Table 9:** Composition of inactivation assay solutions

| Solution | Composition of working solution |
|---|---|
| **Sonication buffer** | 2.0 ml 1 M Tris-HCl pH 7.2<br>100 µl 0.5 M EDTA<br>100 µl 1 M DTT<br>97.8 ml $dH_2O$ |
| **Co-factor NAD/NADH** | 1 mg/ml stock solution in $sdH_2O$ |
| **Proteinase K** | 5 mg/ml stock solution in $sdH_2O$<br>Final concentration of 300 µg/ml |

## 6.3 APPENDIX C: ANTIMICROBIAL AGENTS

| Agent | Stock concentration (mg/ml) | Solvent | Supplier |
|---|---|---|---|
| **Ampicillin** | 100 | 30% $sdH_2O$<br>70 % ethanol | Boehringer Mannheim |
| **Chloramphenicol** | 20 | ethanol | Boehringer Mannheim |
| **Kanamycin** | 10 | $sdH_2O$ | Sigma |
| **Nalidixic Acid** | 10 | 30% $sdH_2O$<br>70% ethanol | Sigma |
| **Rifampicin** | 10 | methanol | Sigma |
| **Spectinomycin** | 20 | ethanol | Sigma |
| **Streptomycin** | 20 | ethanol | Sigma |

## 6.4 APPENDIX D: PLASMIDS USED IN THIS WORK

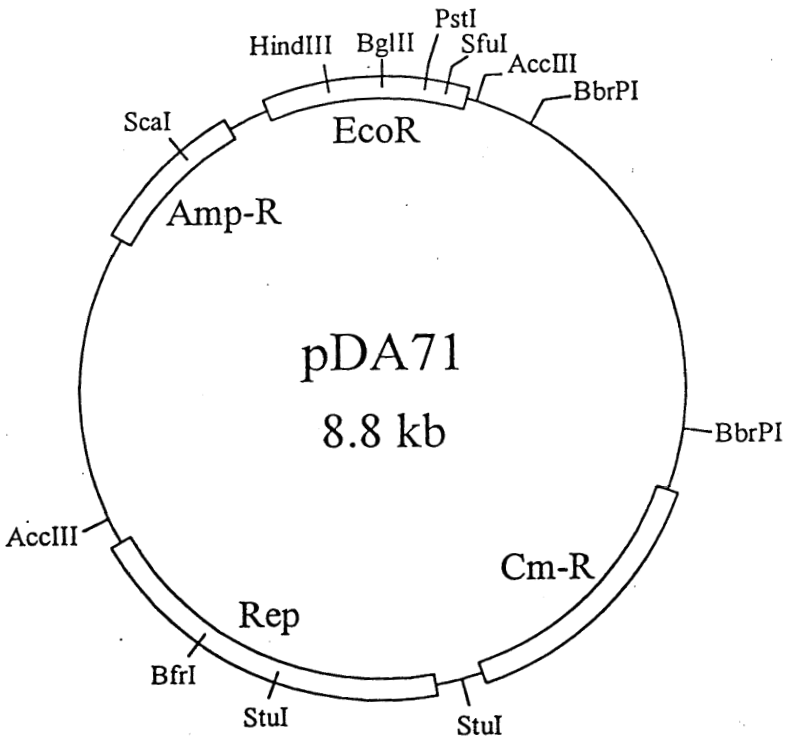


**Restriction map of pDA71** (adapted from http://seq.yeastgenome.org/vectordb/vector.html)

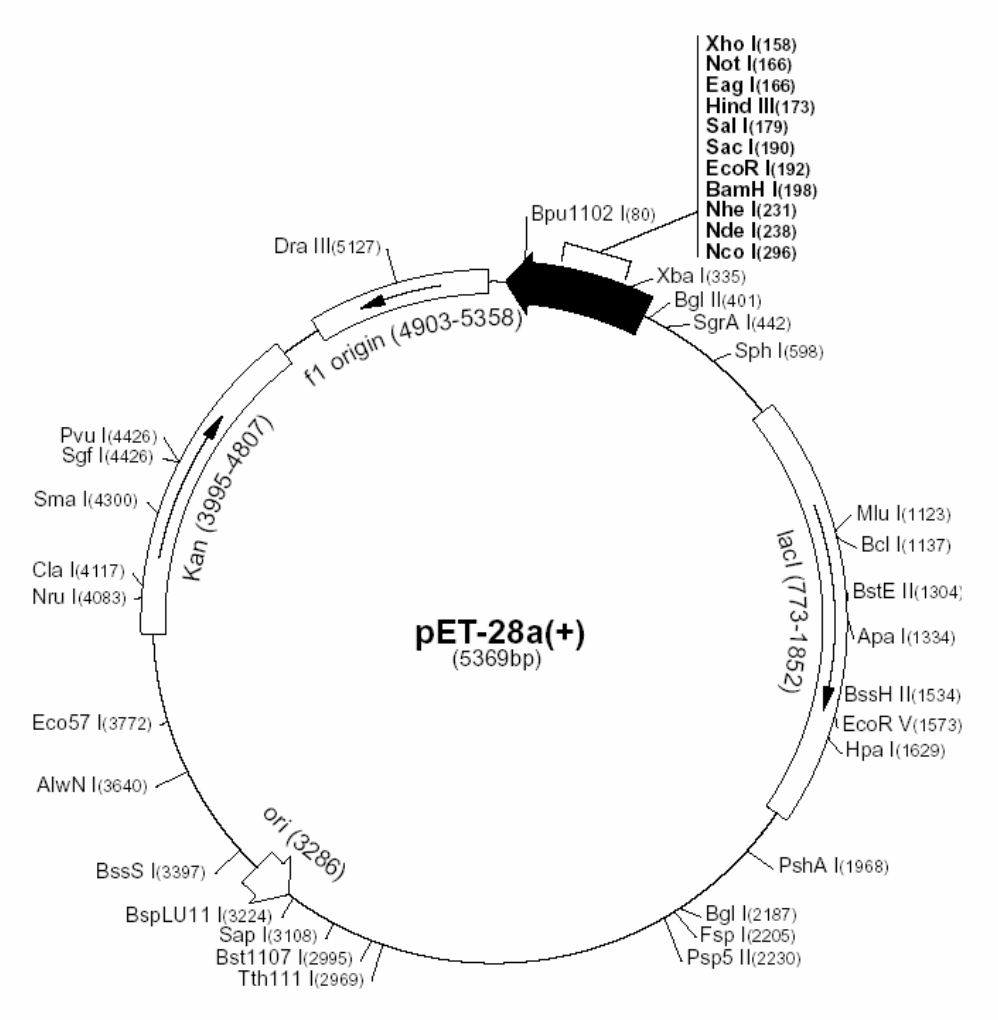


**pET-28a (+) Vector sequence reference points:**

| | |
|---|---|
| T7 promoter | 370-386 |
| T7 transcription start | 369 |
| His•Tag coding sequence | 270-287 |
| T7•Tag coding sequence | 207-239 |
| Multiple cloning sites (*Bam*HI - *Xho*I) | 158-203 |
| His•Tag coding sequence | 140-157 |
| T7 terminator | 26-72 |
| *lac*I coding sequence | 773-1852 |
| pBR322 origin | 3286 |
| Kan coding sequence | 3995-4807 |
| f1 origin | 4903-5358 |

**Restriction map of pET-28a(+)** (adapted from www.novagen.com)

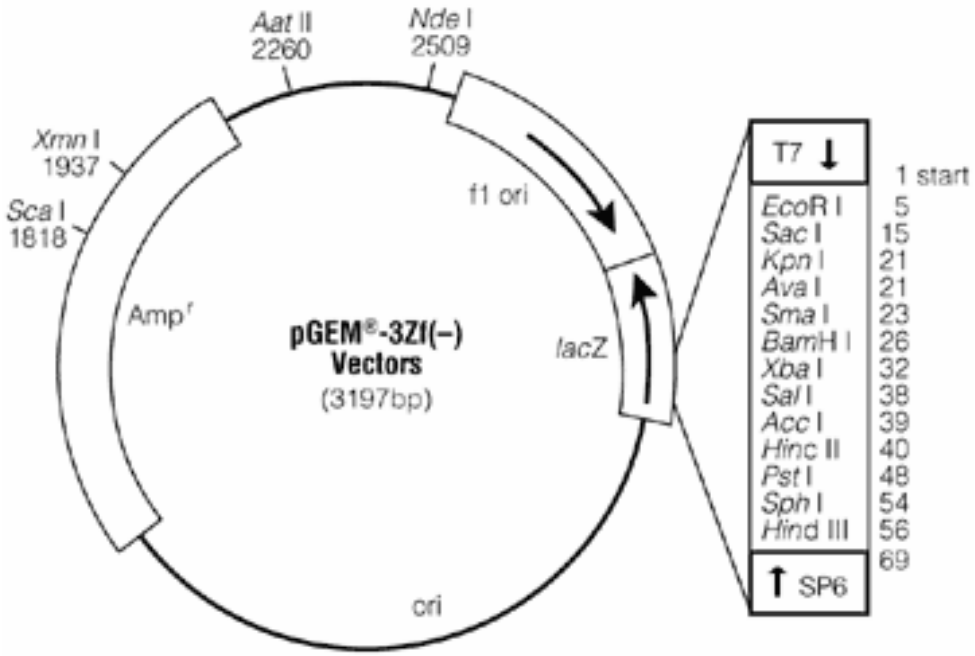


**pGEM®-3Zf(-) Vector sequence reference points:**

| | |
|---|---|
| T7 RNA polymerase transcription initiation site | 1 |
| SP6 RNA polymerase transcription initiation site | 69 |
| T7 RNA polymerase promoter (-17 to +3) | 3181-3183 |
| SP6 RNA polymerase promoter (-17 to +3) | 67-86 |
| Multiple cloning site | 5-61 |
| Phage f1 region | 2562-3017 |
| *lacZ* start codon | 108 |
| *lac* operon sequences | 3018-3178; 94-323 |
| β-lactamase coding region | 1265-2125 |
| Binding site of pUC/M13 forward sequencing primer | 3138-3154 |
| Binding site of pUC/M13 reverse sequencing primer | 104-120 |

**Restriction map of plasmid pGEM** (adapted from www.promega.com)

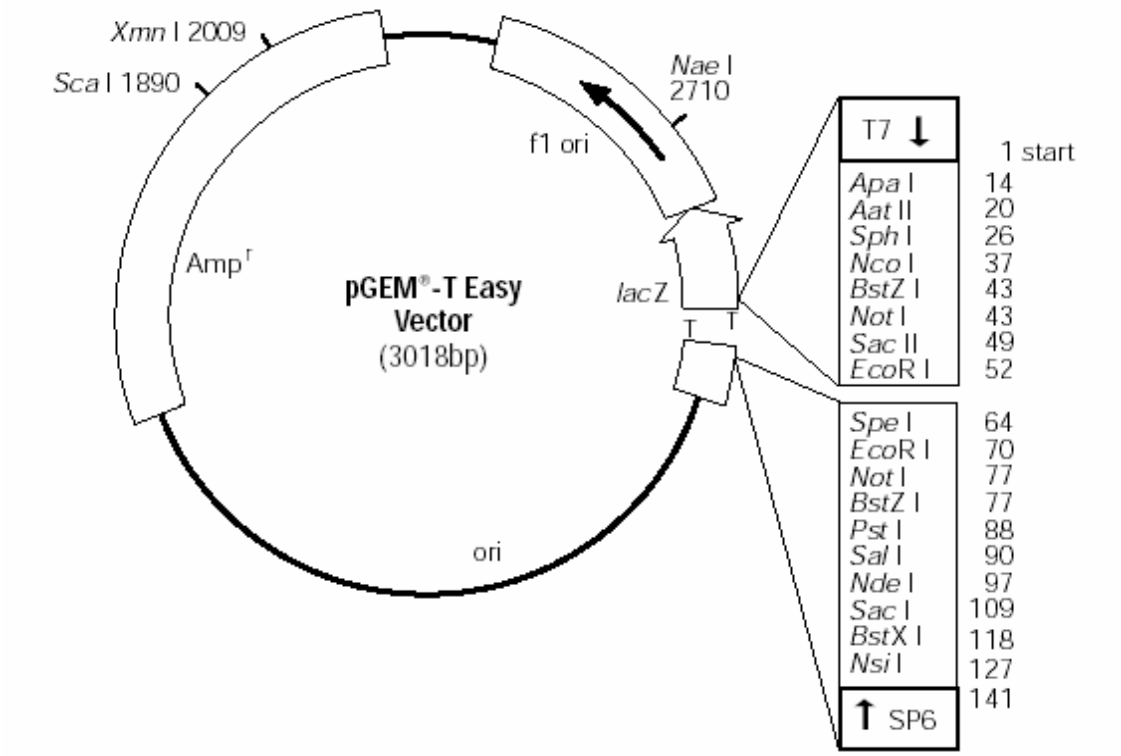


| **pGEM®-T Easy Vector Sequence reference points:** | |
|---|---|
| T7 RNA Polymerase transcription initiation site | 1 |
| SP6 RNA Polymerase transcription initiation site | 141 |
| T7 RNA Polymerase promoter | 3002-6 |
| SP6 RNA Polymerase promoter | 136-158 |
| multiple cloning site | 10-128 |
| *lac*Z start codon | 180 |
| *lac* operon sequences | 2839-2999, 166-395 |
| *lac* operator | 100-216 |
| β-lactamase coding region | 1337-2197 |
| phage f1 region | 2383-2838 |
| binding site of pUC/M13 Forward Sequencing Primer | 2959-2975 |
| binding site of pUC/M13 Reverse Sequencing Primer | 176-192 |

**Restriction map of plasmid pGEM-T-Easy** (adapted from www.promega.com, technical manual No. 042)

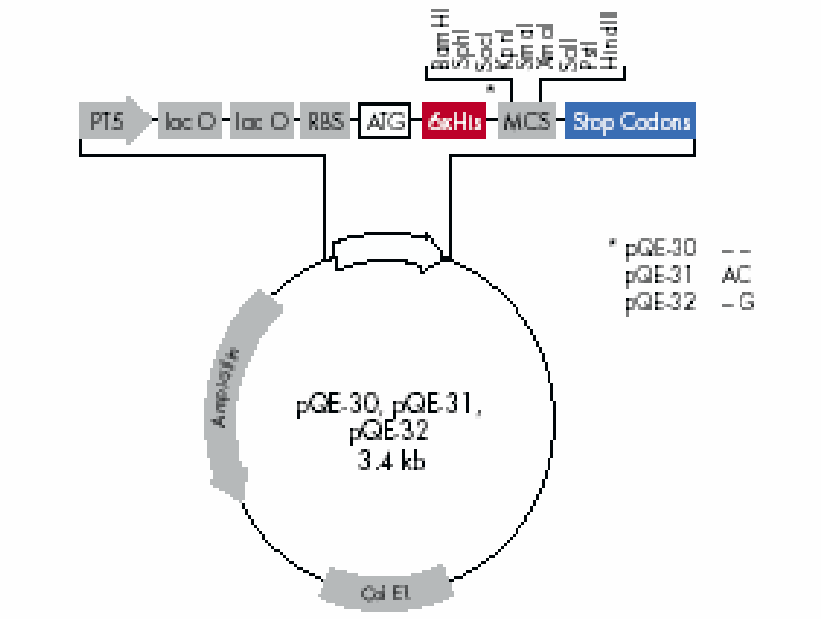


| Positions of elements in bases | pQE-30 | pQE-31 | pQE-32 |
|---|---|---|---|
| Vector size (bp) | 3461 | 3463 | 3462 |
| Start of numbering at *Xho*I (CTCGAG) | 1–6 | 1–6 | 1–6 |
| T5 promoter/lac operator element | 7–87 | 7–87 | 7–87 |
| T5 transcription start | 61 | 61 | 61 |
| 6xHis-tag coding sequence | 127–144 | 127–144 | 127–144 |
| Multiple cloning site | 145–192 | 147–194 | 146–193 |
| Lambda $t_0$ transcriptional termination region | 208–302 | 210–304 | 209–303 |
| *rrnB* T1 transcriptional termination region | 1064–1162 | 1066–1164 | 1065–1163 |
| ColE1 origin of replication | 1638 | 1640 | 1639 |
| β-lactamase coding sequence | 3256–2396 | 3258–2398 | 3257–2397 |

**Restriction map of plasmids pQE30/31/32** (adapted from www.qiagen.com,)

## 6.5 APPENDIX E: MOLECULAR WEIGHT MARKERS

### 6.5.1 DNA molecular weight markers

**Lambda DNA/HindIII Marker, 2 #SM0101/2/3**

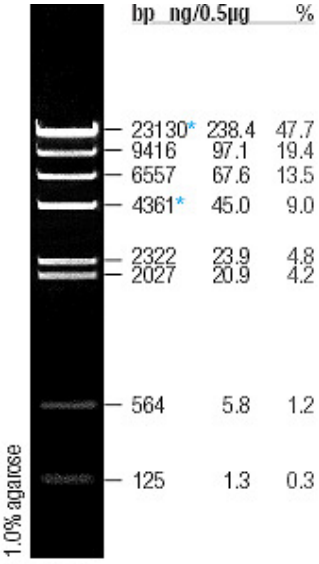


0.5µg/lane,
8cm length gel,
1X TAE, 7V/cm, 45min

**Range**
8 fragments (in bp): 23130*, 9416, 6557, 4361*, 2322, 2027, 564, 125.

**Lambda DNA/EcoRI+HindIII Marker, 3 #SM0191/2/3**

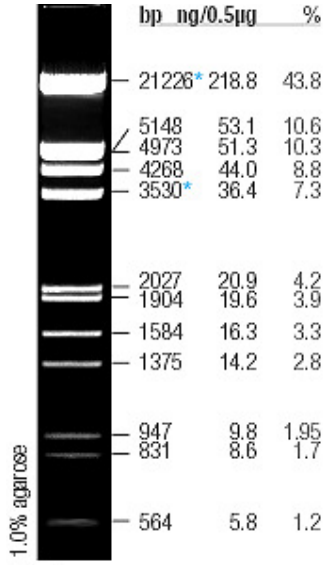


0.5µg/lane,
8cm length gel,
1X TAE, 7V/cm, 45min

**Range**
13 fragments (in bp): 21226*, 5148, 4973, 4268, 3530*, 2027, 1904, 1584, 1375, 947, 831, 564, 125 (it makes 0.3%).

**GeneRuler ™ DNA Ladder Mix, #SM0333**

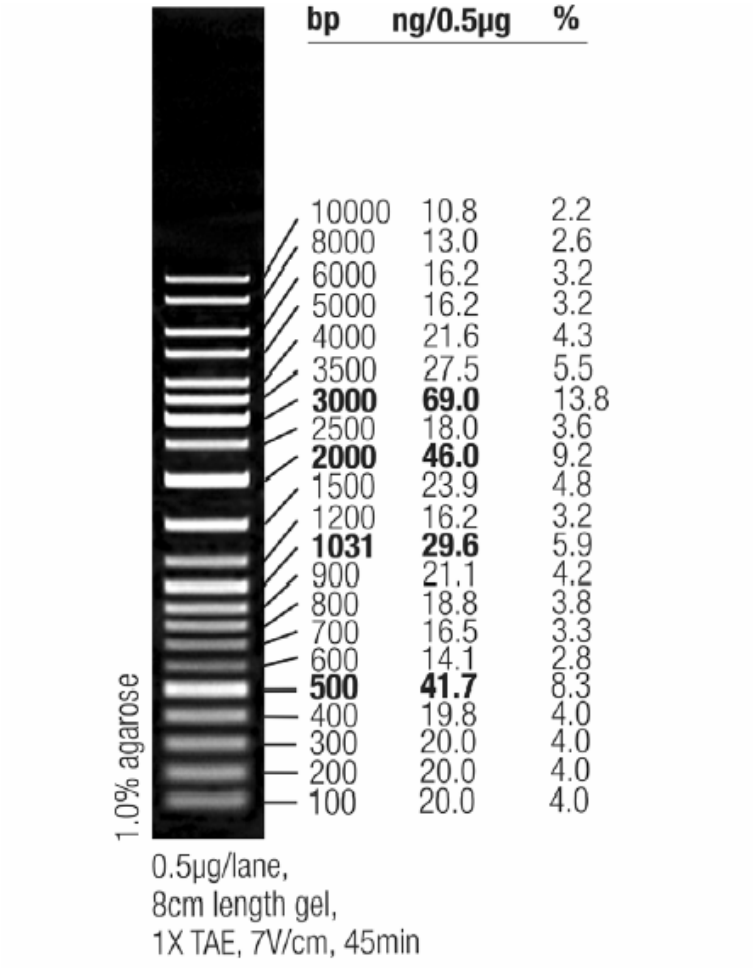

### 6.5.2 Protein Molecular weight marker

**PageRuler $^{TM}$ Prestained Protein Ladder Plus, (Fermentas #SM1811)**

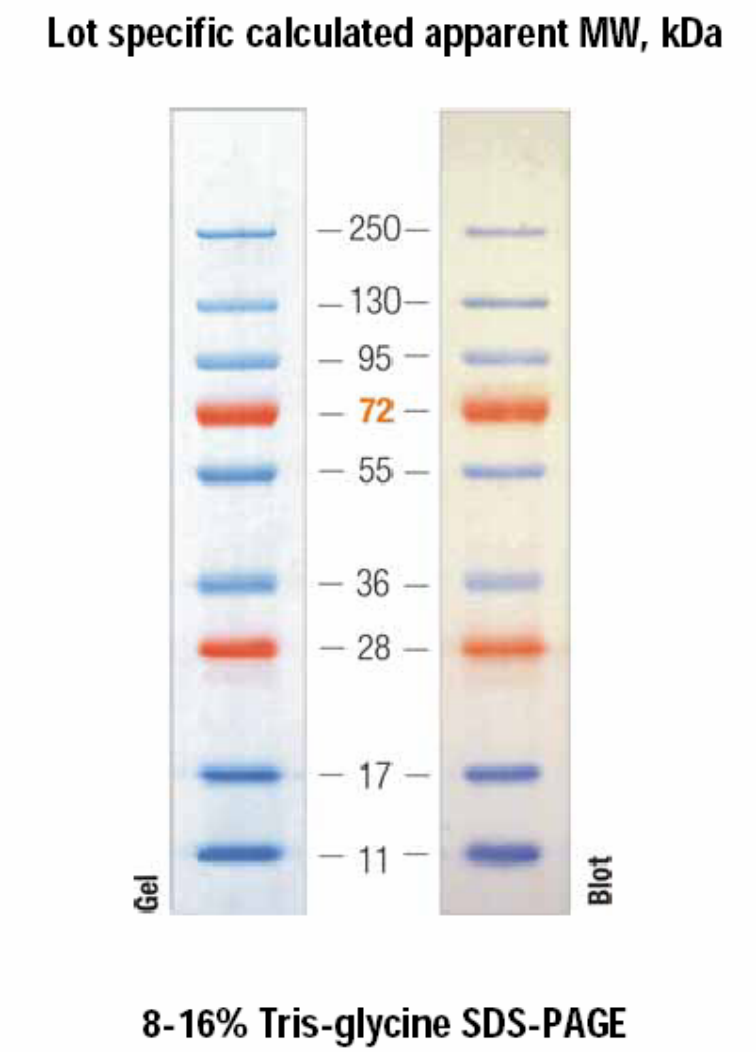

# CHAPTER 7

# REFERENCES


**Abadi, F.J.R., Carter, P.E., Cash, P. and Penington, T.H.** 1996. Rifampin resistance in *Neisseria meningitides* due to alteration in membrane permeability. *Antimicrob. Agents Chemother.* **40**: 645-651.

**Altschul., S.F., Gish, W., Miller, W., Myers, E.W., and Lipman, D.J.** (1990). Basic local alignment search tool. *J. Mol. Biol*. **215**: 403-410.

**Antosz, F.J.** 1992. Antibiotics (ansamacrolides), **2**: 926-961. *In* J.I. Kroschwitz and M Howe Grant (eds.), Encyclopaedia of Chemical Technology. John Wiley and Sons, New York.

**Barry, C.E. III, Lee, R.E., Mdluli, K., Sampson, A.E., Schroeder, B.G., Slayden, R.A. and Yuan, Y.** 1998. Mycolic acids: structure, biosynthesis and physiological functions. *Prog. Lipid Res.* **37**: 143-179.

**Birnboim, H.C. and Doly, J.** 1979. A rapid alkaline extraction procedure for screening recombinant plasmid DNA. *Nucl. Acid. Res*. **7:** 1513-1523.

**Bradford, M.M.** 1976. A rapid and sensitive method for the quantification of microgram quantities of protein utilizing the principle of protein-dye binding. *Anal. Biochem.* **72**: 248-254.

**Burgess, R.** 1969. Separation and characterisation of the subunits of ribonucleic acid polymerase. *J. Biol. Chem.* **244**: 6168-6176.

**Cadwell, R and Joyce, G.** 1991. Randomization of genes by PCR mutagenesis. *PCR Meth. Appl.* **2**: 28-33.

**Campbell, E.A., Korzheva, N., Mustaev, A., Murakami, K., Nair, S., Goldfarb, A. and Darst, S.A.** 2001. Structural mechanism for rifampicin inhibition of bacterial RNA polymerase. *Cell*. **104**: 901-912.

**Carter, P.E., Abadi, F.J.R., Yakubu, D.E., and Pennington, T.H.** 1994. Molecular characterisation of rifampin-resistant *Neisseria meningitides*. *Antimicrob. Agents Chemother.* **38**: 1256-1261.

**Dabbs E.R., Yazawa, K., Mikami, Y., Miyaji, M., Morisaki, N., Iwasaki, S., and Furihata, K.** 1995. Ribosylation by mycobacterial strains as a new mechanism of rifampin inactivation. *Antimicrob. Agents Chemother*. **39**: 1007-1009.

**Dabbs, E.R.** 2004. A review of rifampicin inactivation mechanisms in bacteria. Chiba University Annual Report of the Research Centre for Pathogenic Fungi and Microbial Toxicoses **8**: 51-58.

**Dabbs, E.R. and Quan, S.** 2000. Light inhibits rifampicin inactivation and reduces rifampicin resistance due to a cloned mycobacterial ADP-ribosylation gene. *FEMS Microbiol. Lett.* **182:** 105-109.

**Embley, T.M., and Stackebrandt, E.** 1994. The molecular phylogeny and systematics of the actinomycetes. *Annu. Rev. Microbiol*. **48**: 257-289.

**Ezekiel, D.H., and Hutchins, J.E.** 1968. Mutations affecting RNAP associated with rifampicin resistance in *Escherichia coli*. *Nature*. **220**: 276–277.

**Finnerty, W.R.** 1992. The biology and genetics of the genus *Rhodococcus*. *Annu. Rev. Microbiol.* **46**: 193-218.

**Goodfellow, M. and Cross, T.** 1984. Classification, pp. 7-164. *In* M. Goodfellow, M. Modarski, S.T. Williams (eds.), The Biology of the Actinomycetes. Academic Press, London.

**Gottlieb, D.** 1973. General consideration of the actinomycetales, pp. 1-5. *In* G. Sykes (Ed.), Actinomycetales: characteristics and practical importance. Academic Press, London.

**Gregersen, T.** 1978. Rapid method for distinction of gram-negative from gram-positive bacteria. *Eur. J. Appl. Microbiol. Biotechnol.* **5:** 123-127.

**Grosset, J.H.** (1989). Present status for chemotherapy for tuberculosis. *Rev. Infect. Dis.* **11**, 5347-5352.

**Hartmann, G., Honikel, K.O., Knusel, F., and Nuesch, J.** 1967. The specific inhibition of the DNA-directed RNA synthesis by rifamycin. *Biochim. Biophys. Acta* **145**: 843–844.

**Honore, N. and Cole, S.T.** 1993. Molecular basis of rifampicin resistance in *Mycobacterium leprae*. *Antimicrob. Agents Chemother.* **37**: 414-418.

**Hui, J., Gordon, N. and Kajioka, R.** 1977. Permeability barrier to rifampin in mycobacteria. *Antimicrob. Agents Chemother*. **11**: 773-779.

**Imai, T., Quan, S., Mikami, Y., Yazawa, K., Dabbs, E.R., Morisaki, N., Iwasaki, S., Hashimoto, Y. and Furihata, K**. 1999. ADP-ribosylation as an intermediate in inactivation of rifampicin by a mycobacterial gene. *Antimicrob. Agents Chemother*. **43**: 181-184.

**Imai, T., Watanabe, K., Mikami, Y., Yazawa, K., Ando, K., Nagata, Y., Morisaki, N., Hashimoto, Y., and Dabbs, E.R.** 1999. Identification and

characterisation of a new intermediate in the ribosylative inactivation of rifampicin by *Mycobacterium smegmatis*. *Microb. Drug Res*. **5**: 259-264.

**Inoue, H., Nojima, H. and Okayama, H.** 1990. High efficiency transformation of *Escherichia coli* with plasmids. *Gene.* **96**: 23-28.

**Jin, D.J. and Gross, C.A.** 1988. Mapping and sequencing of mutations in *Escherichia coli rpoB* gene that leads to rifampicin resistance. *J. Mol. Biol.* **202**: 45-58.

**Kapusnik, J.E., Parenti, F. and Sandee, M.A.** 1984. The use of rifampicin in staphylococcal infections - A review. *J. Antimicrob. Chemother*. **13**: 61-66.

**Krueger, K.M. and Barbieri, J.T.** 1995. The family of bacterial ADP-ribosylating exotoxins. *Clin. Microbiol. Rev.* **8**: 34-47.

**Laemmli, U.K.** 1970. Cleavage of structural proteins during the assembly of the head of bacteriophage T4. *Nature* **227**: 680-685.

**Lancini, G. and Zanichelli, W.** 1977. Structure-activity relationships in rifamycins, pp.531-600. *In* D. Perlam (Ed.), Structure-activity relationships among the semi-synthetic antibiotics. Academic Press, New York.

**Lancini, G.C.** 1983. Ansamycins, pp. 198-212. *In* Biochemistry and genetic regulation of commercially important antibiotics. Addison-Wesley Publishing.

**Lechevalier, H.A. and Lechevalier, M.P.** 1970. Chemical composition as criterion in the classification of aerobic actinomycetes. *Int. J. Syst. Bacteriol*. **20**: 435-443.

**Leung, D., Chen, E. and Goeddel, D.** 1989. A method for random mutagenesis of a defined DNA segment using a modified polymerase chain reaction. *Technique*. **1**: 11-15.

**Lucas, S.B., Hounnou, A., Peacock, C., Beaumel, A., Kadio, A. and De Cock, K.M.** 1994. Nocardiosis in HIV-positive patients: an autopsy study in West Africa. *Tuber. Lung Dis*. **75**: 301-307.

**Maliev, B.M., Ergorova, I.L., Sorokina, I.A., Tarnueva, O.K., and Ermakova, G.I.** 1998. Laser technologies in treatment of patients with pulmonary tuberculosis. *Probl. Tuberk.* **3**: 38041.

**Nicholls, A., Sharp, K.A. and Honig, B.** 1991. Protein folding and association: insights from the interfacial and thermodynamic properties of hydrocarbons, proteins structure. *Funct. Genet.* **11**: 281-296.

**Nikaido, H.** 1996. Multidrug efflux pumps of Gram-negative bacteria. *J. Bacteriol.* **178**: 5853-5859.

**O'Hara, K., Kawabe, T., Taniguchi, K., Ohnuma, M., Nakagawa, M., Naitou, Y. and Sawai, T.** 1997. A new simple assay for determining aminoglycoside inactivation in intact cells of *Pseudomonas aeruginosa*. *Microbios.* **90**: 177-186.

**Okusu, H.D. and Nikaido, H.** 1996. AcrAB efflux pump plays a major role in the antibiotic resistance phenotype of *Escherichia coli* multiple-antibiotic-resistance (Mar) mutants. *J. Bacteriol.* **178**: 306-308.

**Prelog, V. and Oppolzer.** 1973. Ansamycine, eine neuartige klasse von mikrobiellen stoffwechselprodukten. *Helv. Chim. Acta*. **56**: 1179-1187.

**Puhača, S.** (2003). Purification and molecular characterisation of the ADP-ribosyltransferase responsible for ribosylative inactivation of rifampicin. Masters Dissertation. University of the Witwatersrand.

**Putman, M., Van Veen, H.W. and Konings, W.N.** 2000. Molecular properties of bacterial multidrug transporters. *Microbiol. Mol. Biol. Rev.* **64**: 672-693.

**Quan, S.** 1997. Cloning and characterisation of rifampicin inactivation genes from *Mycobacterium* and closely related organisms. PhD Thesis. University of the Witwatersrand.

**Quan, S., Venter, H. and Dabbs, E.R.** 1997. Ribosylative inactivation of rifampin by *Mycobacterium smegmatis* is a principal contributor to its low susceptibility to this antibiotic. *Antimicrob. Agents Chemother.* **41**: 2456-2460.

**Sánchez, L., Pan, W., Vinas, M. and Nikaido, H.** 1997. The *acrAB* homolog of *Haemophilus influenza* codes for a functional multidrug efflux pump. *J. Bacteriol.* **179**: 6855-6857.

**Sanger, F., Nicklen, S., and Coulson, A.R.** 1977. DNA sequencing with chain-terminating inhibitors. *Proc. Natl. Acad. Sci*. **74**: 5463-5467.

**Sealey, P.G. and Southern, E.M.** 1982. Gel electrophoresis of DNA, pp. 39-76. *In* D., Rickwood and B.D. Hames (eds), Gel Electrophoresis of Nucleic Acids: *A practical approach*. IRL Press, Oxford.

**Sensi, P**. 1983. History of the development of rifampicin. *Rev. Infect. Dis.* **5**: S402-S406.

**Sensi, P., Greco, A.M. and Ballotta, R.** 1960. Isolation and properties of rifomycin B and rifomycin complex. *Antibiot. Annu*. **7**: 262-271.

**Sippel, A. and Hartmann, G.** 1970. Rifampicin resistance of RNA polymerase in the binary complex with DNA. *Eur. J. Biochem.* **16**: 152-157.

**Spangler, B.D.** 1992. Structure and function of cholera toxin and the related *E. coli* heat-labile enterotoxin. *Microbiol. Rev.* **56**: 622-647.

**Stackebrandt, E., Smida, J. and Collins, M.D.** 1988. Evidence of phylogenetic heterogeneity within the genus *Rhodococcus*: revival of the genus *Gordona* (Tsukamura). *J. Gen. Appl. Microbiol.* **34**: 341-348.

**Sugawara, K., Dohmae, N., Kasai, K., Saido-Sakanaka, H., Okamoto, S., Takio, K and Ochi, K.** 2002. Isolation and identification of novel ADP-ribosylated proteins from *Streptomyces coelicolor* A3(2). *Biosci. Biotechnol. Biochem*. **66**: 2292-2296.

**Šuput, J., Lechevalier, M.P. and Lechevalier, H.A.** 1967. Chemical composition of variants of aerobic actinomycetes. *Appl. Microb*. **15**: 1356-1361.

**Tanaka, Y., Yazawa, K., Dabbs, E.R., Nishikawa K., Komaki H., Mikami Y., Miyaji M., Morisaki N, and Iwasaki S.** 1996. Different rifampicin inactivation mechanisms in *Nocardia* and related taxa. *Microb. Immunol*. **40**: 1-4.

**Tautz, D. and Renz, M.** 1983. An optimized freeze-squeeze method for the recovery of DNA fragments from agarose gels. *Anal. Biochem*. **132**: 14-19.

**Telenti, A., Imboden, P., Marchesi, F., Lowrie, D., Cole, S.T., Colston, L., Matter, K., Schoolfer, K. and Bodmer, T.** 1993a. Detection of rifampicin-resistant mutations in *Mycobacterium tuberculosis*. *Lancet* **341**: 647-650.

**Ueda, K. and Hayaishi, O.** 1985. ADP-ribosylation. *Annu. Rev. Biochem*. **54**: 73-100.

**Weaver, R.F.** 1999. *Molecular Biology*. 1st ed. WCB/McGraw-Hill, London. pp. 64-66.

**Wehrli, W. and Staehelin, M.** 1971. Actions of rifamycins. *Bacteriol. Rev*. **35**: 290-309.

**Woodley, C.L., Kilburn, J.O., David, H.L. and Silcox, V.A.** 1972. Susceptibility of mycobacteria to rifampin. *Antimicrob. Agents Chemother*. **2**: 245-249.

**Zillig, W., Fuchs, E., Palm, P., Rabussay, D. and Zechel, K.** 1970. On the different subunits of DNA dependent RNA polymerase from *E. coli* and their role in the complex function of the enzyme, pp. 151-157. *In* Proc. 1st Int. Lepetit Colloq. RNA Polymerase transcript. North Holland Publishing Co., Amsterdam.

**Zuckerlandl, E. and Pauling, L.** 1965. Molecules as documents of evolutionary history. *J. Theor. Biol*. **8**: 357-366.